Supramolecular Assemblies of Carbon Nanomaterials with Photochromic Molecules for Sustainable Molecular Electronics

A Thesis submitted

in partial fulfillment for the Degree of

Doctor of Philosophy

By

Devi Renuka K

SC13D012

Department of Chemistry

INDIAN INSTITUTE OF SPACE SCIENCE AND TECHNOLOGY

THIRUVANANTHAPURAM

June 2019

To

My Amma, Achan & Husband……..

CERTIFICATE

This is to certify that the thesis entitled **Supramolecular Assemblies of Carbon Nanomaterials with Photochromic Molecules for Sustainable Molecular Electronics** submitted by **Devi Renuka K** to the Indian Institute of Space Science and Technology Thiruvananthapuram, in partial fulfilment for the award of the degree of **Doctor of Philosophy** is a *bona fide* record of research work carried out by him under our supervision. The contents of this Thesis, in full or in parts, have not been submitted to any other Institution or University for the award of any degree or diploma.

Prof. Kuruvilla Joseph
Supervisor
Dean Student Activities, IIST
Senior Professor
Department of Chemistry

Dr. Mahesh.S

Co-Superviser

Scientist

Polymers and Special

Chemical Division

VSSCThiruvananthapuram

2018

Counter signature of the HOD with seal

DECLARATION

I declare that this thesis entitled **Supramolecular Assemblies of Carbon Nanomaterials with Photochromic Molecules for Sustainable Molecular Electronics** submitted in partial fulfilment of the degree of **Doctor of Philosophy** is a record of original work carried out by me under the joint supervision of Prof.Kuruvilla Joseph and Dr.Mahesh S, and has not formed the basis for the award of any other degree or diploma, in this or any other Institution or University. In keeping with the ethical practice of reporting scientific information, due acknowledgments have been made wherever the finding of others have been cited.

Devi Renuka K

SC13D012

Thiruvananthapuram-695 547

June 2019

ACKNOWLEDGEMENTS

Only the grace of god almighty enabled me to step into IIST, an esteemed institution of India under ISRO to do research. Little did I realize the bliss bestowed upon me when I cleared the interview. Now that I have reached the end of my journey I have to look back with gratitude and acknowledge the help and encouragement extended to me from various quarters.

There is a wide gulf between a regular academic course and the field of research. I was quite baffled when I put my first step in the meandering route of research. It was the strong support and the direction given by my guide Dr.S.Mahesh that initiated and kept me moving in the right direction. I had not to grope further in a darkness because my guide stood fast with me like a beacon of light right from the point of selecting a topic for research, he was there advising me, guiding me and instilling confidence in me to go ahead. Wholeheartedly I acknowledge my indebtedness to him and place on record the yeoman help received from him for completing the project. He was such a wonderful guide, guard and companion.

No less is the protection extended to me by Prof. Kuruvila Joseph. In his characteristic way, he was there as a pillar of support and source of inspiration. At every station of my research, he helped me by his deep insight and long experience and kept me away from committing even a silly inadvertent oversight or error. I could be on the right track of success because of the steadfast support of the two luminaries. I also acknowledge the goodwill of the Director of IIST, Dr.V K Dadhwal and Former Director Dr.K.S.Dasgupta.

The key role played by the doctoral committee (DC) in the field of research is an accepted reality. The doctoral committee put the research in the right track by giving directions at every stage. In my case also the positive role of the doctoral committee contributed a lot to a fruitful research. The members with their long experience, involvement and dedication in research served as pole stars directing my progress of research in the right and steadfast direction without even a small drift. Prof. Nirmala Rachel James (Chairman and Former HOD Chemistry) IIST, Dr Benny K. George VSSC Trivandrum, Dr Reji Varghese IISER Trivandrum, Dr M. L. P. Reddy NIIST Trivandrum,

Dr K. G. Sreejalekshmi IIST, Dr Seena B Avionics department IIST who constituted the DC strained every nerve to make my research perfect. I acknowledge my everlasting indebtedness to each and every one of them. Dr K. Prabhakaran, HOD Chemistry and other faculties of the chemistry department, Dr Jobin Cyriac, Dr K. Y. Sandhya, Dr Gomathi N, Dr J. Mary Gladis, and Dr Jinesh (Department of Physics) evinced a keen interest in my research work and could be banked upon at every point of time.

Bureaucratic hurdles often hamper smooth research in many premier institutions in India but I am very happy to place on record the exception of IIST in this respect. I thank all the office staff, hostel staff and security personal for their caring support. Mr Sreekumar, Mrs Bindu P. C, Mrs Bindu J M, Miss Rehna, Miss Jayasree L., Miss Jayasree R., Mr Dileep, Mr Loveson, Miss Remya, Mr Muralidharan Nair, Miss Ratna Bhai, and Miss Amertha Selvi were there always with me.

In the course of my research, I had to make use of the facility of the other premier institutions. They include, NIIST Thiruvananthapuram, CUSAT Cochin, IISER Thiruvananthapuram, Sree Chitra institute Thiruvananthapuram, Kerala University Thiruvananthapuram and M. G. University Kottayam. I was given all help and guidance in these establishments. Both the academic community and the administrative personal ensured that I had an atmosphere suited to my requirements for doing various tests, characterization etc with complete satisfaction. I would like to make specific mention of Dr A. Ajayaghosh, Dr K Narayanan Unni, Dr Bhoge Gowde, Dr J D Sudha, Dr Luxmi Verma, Mr Satyajith Das, Mr Shyju Parameswaran, Dr Rahul Dev Mukhopadhay, Dr Ramakrishnan Rajaram, Mr Aadharsh for their help and support.

Lakshmi Chechi who was a project fellow working with Dr S. Mahesh was the first one to introduce me to my the lab work. She always patronized me with her sisterly care and affection and made me feel at home. Dr Sarah, Dr Raneesh, Dr Mukhtar, Dr Manjunath, Dr Rakesh, Dr Sujith, Miss Reshma, Mrs Aswathi, Miss Neema, Mrs Haritha, Mr Yogesh, Mr Praveen, Mr sanu, Mr Deeraj, Miss Saisree, Miss Arya, Miss Varsha, Miss Ann Mary, Miss Sreekala, Dr Roymon Joseph, Dr Linsha V and Mr.Preetham Hazra with their love, support and guidance individually and collectively made my work smooth and light. Mrs Reshmi, Mrs Karthika, Mrs Meegle and myself started research work in the institute together. We had a wonderful and passionate relationship throughout the five years spend together. Mr Najeeb P. K. from the senior batch was my close buddy during all the time. I would like to thank Miss Geethu Venugopal, former internship student for linting her support in my research work.

I would like to thank all my teachers and friends from ST.Thomas' College Thrissur. I thank my favourite teacher and role model Prof.K.L.Joy, for always inspiring me to do bigger things. I fondly remember all my school teachers and childhood friends for their support.

My parents and relatives were always there with prayers for my success. My father Damodaran P, a retired professor of English went meticulously through my script to make the presentation coherent and exact. My husband Dr Sreekuttan M. Unni working with CSIR as scientist took pains to see that the presentation is factually and technically perfect. I don't have enough words to thank my mother Sudhalekshmi. She is my strength and without her nothing is possible for me. I thank my elder sister Devi Radhika for her love and phycological support. Advaith the nine-year-old son of my elder sister, in his characteristic playful mood could always be banked upon for relief at tense moment. I am also greatly indebted to my husband's family for their support.

(Devi Renuka K)

ABSTRACT

The growing field of electronics always inspired the scientists to go for new materials and technology. In the past, the electronic industry depended mainly on inorganic materials especially metals for the fabrication of devices. The complete dependence over the metals led to the increase in energy consumption for the construction of devices and their functioning. Most important drawback associated with the gadgets and devices based on metals is the difficulty in their disposal. The excessive accumulation of damaged devices became hazardous to the environment. This made the scientists to explore organic molecules for the electronic development. The organic electronic materials failed to perform at conditions of high temperature, heat etc. The invention of carbon nanomaterials made the electronic industry to rely on them as they can withstand drastic conditions. The concept of smart materials based on carbon nanomaterials which can respond to external stimuli like pH, light, heat, redox potential inspired the scientists to make such stimuli responsive electronic devices. The hybrid materials developed by coupling photochromic molecules, a class of organic molecules which respond to the stimulus light coupled with carbon nanomaterials became the centre of attraction in the optically responsive smart materials.

The increased environmental issues shifted the focus of material researchers across the globe to go for sustainable/green materials. This led to the rise of a new path in the electronic industry termed ‘sustainable molecular electronics. This area involves the use of bioresources for the production of materials which are eco-friendlier for the device fabrication and gadgets. This thesis focuses on the development of such materials for the construction of molecular electronic switches.

The photochromic azobenzene molecules are derived from cardanol a well-known bioresource material obtained from cashew nut shell liquid. The azobenzene molecules are then coupled with various carbon nanomaterials to develop molecular switches. The different carbon nanomaterials selected are zero-dimensional

graphene quantum dot, one-dimensional carbon nanotube, two-dimensional graphene oxide and three-dimensional single-walled carbon nanohorn.

The graphene quantum dots (GQDs) is derived from a bioresource material honey. The GQDs show a green fluorescence. The GQDs are then coupled with photochromic azobenzene system DOAZOC1 derived from cardanol. The two-component system then selectively screened the presence of a harmful carbamate pesticide carbofuran. The entire process resulted in a fluorescence switch GQD-DOAZOC1-Carbofuran. This fluorescence switch is then employed for developing three molecular devices: molecular fluorescent probe, molecular logic gate and molecular keypad lock.

The DOAZOC1 molecule is further coupled with acid-functionalized multi-walled carbon nanotube. Two different kinds of hybrids are prepared. The first one is the covalent hybrid, where the components are connected through anhydride linkage. The second one is the non-covalent hybrid formed through supramolecular interactions like hydrogen bonding and π-π stacking. Both the hybrids function as photo-tunable conductance switches.

Another azobenzene molecule AZOC2 is prepared from cardanol. This bulkier molecule is then coupled with reduced graphene oxide, a two-dimensional planar carbon nanomaterial to prepare both covalent and non-covalent hybrids. Here the hybrids exhibited photoswitching of conductance. The photomodulated conductance switches are again developed by coupling single-walled carbon nanohorn with DOAZOC1 molecule through covalent and non-covalent mode of functionalization. The mechanism of this conductance modulation in all the hybrids developed is investigated. The photo-isomersation ability of azobenzene molecules present in the hybrids are found to be responsible for the photoswitching of conductance in them. The non-covalent approach is observed as the better method of functionalization.

The present study therefore focuses on the development of fluorescence switch and conductance switch from bioresource based materials. We hope that the thesis will form a foundation to explore more ‘sustainable molecular electronic devices’.

Table of Contents

LIST OF SCHEMES

LIST OF TABLES

LIST OF FIGURES

ABBREVIATIONS

Ag/AgCl	Silver/Silver chloride
AFM	Atomic force microscopy
ATRP	Atom transfer radical process
AZNME	(E)-N,N-dimethyl-4-(*p*-tolyldiazenyl)aniline
AZOC1	4-[(4-cardanyl)azo]benzoic acid
AZOC2	4,4'((1E,1'E)-(((((4-methyl-1,3-phenylene)bis(azanediyl))bis(carbonyl))bis(oxy))bis(2-(pentadeca-1,3,5,7,9,11,13-heptayn-1-yl)-4,1-phenylene))bis(diazene-2,1-diyl)dibenzoicacid compound with dihydrogen (1:26)
AzoPU	Azopolyurethane
CIE	Commision International de I'Eclairage
CNPs	Carbon nanoparticles
CNSL	Cashewnut shell liquid
CNT	Carbon nanotube
CS	Cationic chitosan
^{13}C NMR	Carbon-13 Nuclear Magnetic Resonance
1D	One-dimensional
2D	Two-dimensional
3D	Three-dimensional
DBTDL	Dibutyl tin dilaurate
DE	Diffraction efficiency
DFT	Density functional theory
DLL	Dash-line lithographic method
DPNME	(E)-N,N-dimethyl-1,4-(*p*-pyrrolidinofullerenediazenyl)aniline
DR1	Disperse Red 1
DR1-A	Anthracene functionalized DR1

DR1-P	Pyrene tethered DR1
DR1-U	Untethered DR1
DMF	Dimethyl formamide
DO3	Disperse orange 3
DOAZOC1(1)	4-[4-dodecyloxycarbonyloxy-2-pentadecylphenylazo]benzoic acid
EDAX	Energy dispersive X-ray spectroscopy
EDLC	Electrochemical double layer capacitor
ESR	Electron Spin Resonance
FET	Field Effect Transistor
FTIR	Fourier Transform Infrared
FTNMR	Fourier Transform Nuclear Magnetic Resonance
FWCNT	Few-walled carbon nanotube
FWHM	Full-Width-Half-Maximum
GQDs	Graphene quantum dots
GO	Graphite Oxide
HDI	Hexamethylene diisocyanate
HNO_3	Nitric acid
H_2SO_4	Sulphuric acid
H_2O_2	Hydrogen peroxide
^1H NMR	Proton Nuclear Magnetic Resonance
HRMS-ESI	High resolution electrospray ionization mass spectrometry
HRMS-FAB	High resolution mass spectrometry with Fast Atom Bombardment
HRTEM	High-resolution transmission electron microscopy
ITO	Indium tin oxide
KCl	Potassium chloride
LB	Langmuir-Blodgett
LBL	Layer by layer assembly
LED	Light emitting diodes
MO	Methyl orange

mSAM	Mixed self-assembled monolayer
MWCNT	Multi-walled carbon nanotube
MWCNT-1	Covalent hybrid MWCNT-DOAZOC1
1.MWCNT	Non-covalent hybrid MWCNT-DOAZOC1
NIR	Near infrared
NMFP	N-methylfulleropyrrolidine
NPAP	4-(4-nitrophenyl)azophenol
OLED	Organic light emitting diodes
PCL	Polycaprolactone
PET	Photo-induced electron transfer
PL	Photoluminescence
PMMA	Polymethyl methacrylate
PMMMAZO	Poly{6-[4-(4-methoxyphenylazo)phenoxy}hexyl methacrylate
PSS	Photostationary State
PTF	Photothermal fuel
RB flask	Round bottom flask
RhB	Rhodamine B
RGO	Reduced graphene oxide
RGO-AZOC2-C	Covalent RGO-AZOC2
RGO-AZOC2-NC	Non-covalent RGO-AZOC2
SAED	Selected-area electron-diffraction
SEM	Scanning electron microscopy
SHG	Second harmonic generation
SPMA	Spiropyran ether methacrylate
SRG	Surface Relief Grating
STEM	Scanning transmission electron microscope
SWCNH	Single-walled carbon nanohorn
SWCNH-F	Functionalized single-walled carbon nanohorn
SWCNT	Single-walled carbon nanotube
TDI	2,4-Toluene diisocyanate
TGA	Thermogravimetric Analysis

TLC	Thin layer chromatography
TM	Transition metals
TMS	Tetramethylsilane
UV-Vis	Ultraviolet-visible
XPS	X-ray Photoelectron spectroscopy
XRD	X-ray diffraction

NOTATIONS

φ	Quantum yield
ε	Molar absorption coefficient
A	Absorbance
I	Intensity
V	Voltage
λ	Wavelength
τ	Lifetime
T	Temperature
t	Time
K	Rate constant
F	Fluorescence intensity
C	Concentration

Chapter 1: Introduction

Carbon Nanomaterials, Photochromic Molecules and Their Hybrids: An Overview

This chapter focuses on recent progress in the field of molecular electronic materials based on the coupling of photochromic azobenzene molecule with different carbon nanomaterials. The emergence of sustainable molecular electronics is also discussed. Further this chapter includes a brief description of important photochromic molecules, the advantage of light as an external stimulus and the superiority of azobenzenes over other photochromic molecules. The covalent and non-covalent methods for coupling the carbon nanomaterials with azobenzene molecules are included the discussion. Both these are included the discussion. Different hybrid materials developed by coupling azobenzene molecules with carbon nanomaterials for various applications are also subjected to study. The scope and main objectives of the thesis are enumerated in the end section of the chapter.

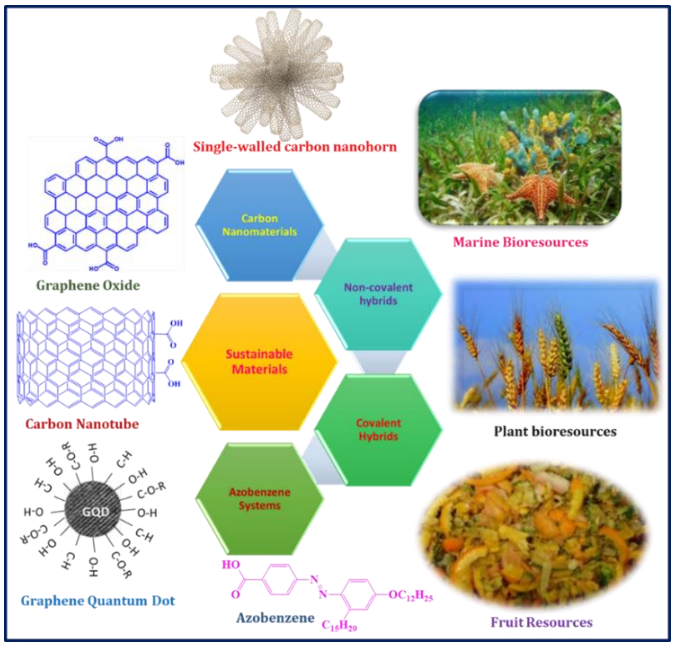

1.1. Evolution of sustainable molecular electronics

The modern life is obsessed with the use of high-end technology in all fields. The process of urbanization resulted in a global economy for the electronic devices. Recently the focus of electronic industry has been shifted from inorganic/silicon-based technology to organic/carbon-based technology. There are two main reasons behind this change. Production as well as disposal of the inorganic electronic material require large quantum of energy. The other factor is the high cost involved in the process (Gutowski et al. 2009; Allwood et al. 2011). The environmental issues also play a keyrole. The high energy changes and the hazardous chemical processes associated with inorganic electronics is a strong deterant. As a result, the thrust is shifted to the use of environmentally friendly material for the production of electronic devices. All these factors resulted in the rapid growth of organic/carbon-based technologies. The organic/carbon based material have an edge over the electronic devices in terms of flexibility, miniaturization of size, thickness etc (Ante et al. 2012; Zhang et al. 2012).

The scientists and engineers vie with one another for the betterment of technology in all fields especially in the field of consumer products. The aim is to decrease the cost of production and make the process of disposal easy. Here comes the importance of the so called ***'Sustainable Molecular Electronics'***. This is an area of hot pursuit creating a boost in the research scenario connected with electronic materials. According to a report made by G.Brundtland " Sustainable development is the development that meets the needs of the present without compromising the ability of future generations to meet their own needs"

(Brundtland 1987; WCED 1987). So the sustainable electronics correlates with different kinds of sustainability like environmental, social and most importantly technological (Figure 1.1).

Figure 1.1: Representative image for sustainable/green electronics. Reproduced with permission from Ref [106] Copyright © 2014 The Royal Society of Chemistry.

The sustainable electronics points towards the building of a technological world which not only uses ecofriendly/natural resources for the synthesis of materials but also aims at following a green protocol regarding the manufacturing process, way of disposal etc. Researchers also focus on many "Off The Grid" sustainable devices so that it can benefit the marginalized part of the society which is totally away from the current technological developments. Lack of resources and lack of enough knowledge make the advantages of modern developments inaccessible to a large segment of the society, especially that of the lower strata. The sustainable electronics led to a revolution in terms of the modernization of technology to tap different bioresources to produce materials with innovative

functionalities. The incorporation of sustainable materials in the field of electronic goods also ensure a steady supply of devices over a long period of time (Zhang et al. 2012).

Recently a perspective by Derek R Lovely (Lovley 2017) has discussed the future of 'green electronics' by "e-biologics", a technology that deals with biologically produced electronic materials and related biomimetics. The work exclusively discusses the role of microbes in fabricating electronic devices (Table 1.1). Similarly there is a review article by Mihai Irimia Vladu (Irimia-Vladu 2014) discussing recent developments in the electronic industry mainly based on biodegradable and biocompatible materials.

			Potential advantages over abiotic materials			
			Reduction in:			
Material	Fabrication method	Potential applications	Energy[a]	Harsh chemicals[b]	Toxic waste	Flexibility in product design[c]
Metal/metalloid precipitates	Microbially mediated precipitation of soluble forms of metals/metalloids	Nanowires, transistors, capacitors	+	+		
Protein scaffolds for metals	*In vitro* assembly of peptides	Nanowires, capacitors	+	+		+
Lipid-cytochrome filaments	Outer membrane extensions dried and chemically fixed	Nanowires, transistors	+		+	
Electrically conductive pili	Microbial expression from native or synthetic PilA monomer gene	Nanowire electrical connections, conductive composite materials, nanosensors, transistors, capacitors	+	+	+	+
Self-assembling conductive protein wires	*In vitro* assembly of peptides	Nanowire electrical connections, conductive composite materials, nanosensors, transistors, capacitors	+	+	+	+
Living biofilms	Cell growth	Conductive "polymers" and circuits with potential for self-repair, sensors, biological computers	+	+	+	+

Table 1.1: e-Biologic types, fabrication methods, potential applications, and potential advantages over abiotic materials. Reused with permission from Ref [154] Copyright © 2017 Lovely, mBio, American Society for Microbiology.

Thus, sustainable molecular electronics aims at the development of a greener technology for the fabrication of devices. The sustainability covers the entire process taking place during the development of the device right from the source of production, substrate used, methodology and application.

1.2. Photochromic molecules in molecular electronics

1.2.1. Photochromic molecules

The development of multifunctional materials which respond to external stimuli is an attractive paradigm in organic electronics Among the different stimuli like pH, redox potential, heat, the stimulus light stands apart (Figure 1.2) (Yerushalmi et al. 2005). Because it is a cleaner energy source and can be applied to materials in any state. Light has high spatio-temporal resolution and a particular wavelength of light can be selected to photoexcite a single molecule or the entire system. Unlike the chemical or thermal processes light can drastically alter the electronic configuration in a short span of time. This limits the changes to molecular level.

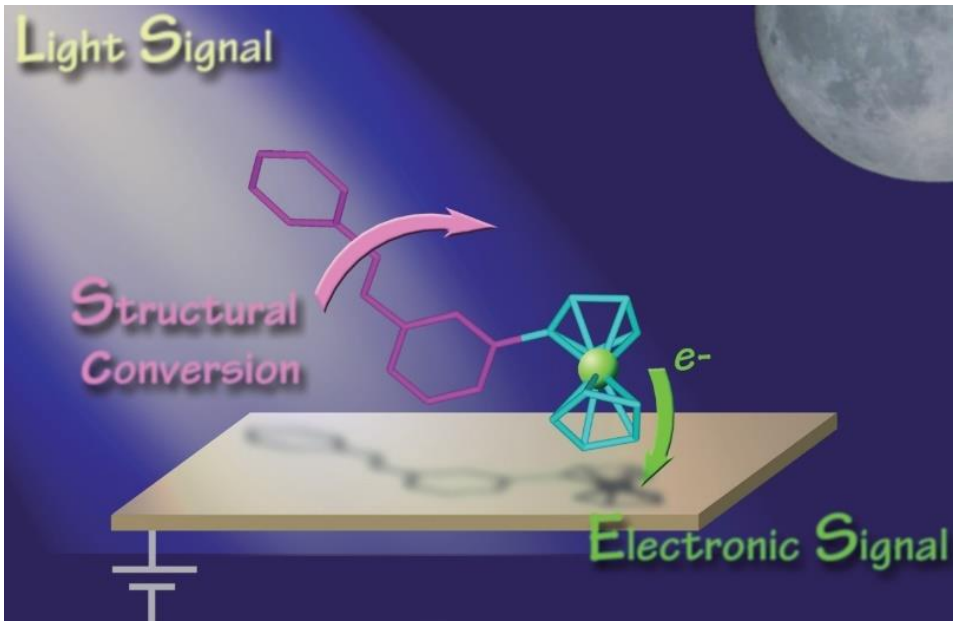

Figure 1.2: Representative image for light as external stimulus in organic electronics. Reproduced with permission from Ref [135] Copyright © 2008 The Royal Society of Chemistry.

Photochromic molecules are those class of organic molecules which undergo reversible transformation between two isomers under the influence of light (Pardo et al. 2011; Stranius et al. 2017; Wang et al. 2018). The diarylethenes, spiropyrans, azobenzenes, fulgides, norboradienes etc are some of the important members of photochromic molecules (Figure 1.3 a) to e)). On a broader basis photochromic are divided into two classes namely P-type and T-type. The P-type photochromic molecules undergo reversible transformation between two states, only when exposed to light. But T-type molecules once converted to an isomeric form can revert back to the original state under optic and thermal condition (Dürr et al. 2003; Sliwa et al. 2005). A second form of classification less in vogue is based on the type of molecular reaction involved. A unimolecular reaction it is a positive photochromism; a bimolecular reaction is termed as negative or inverse photochromism. (McArdle et al. 1983).

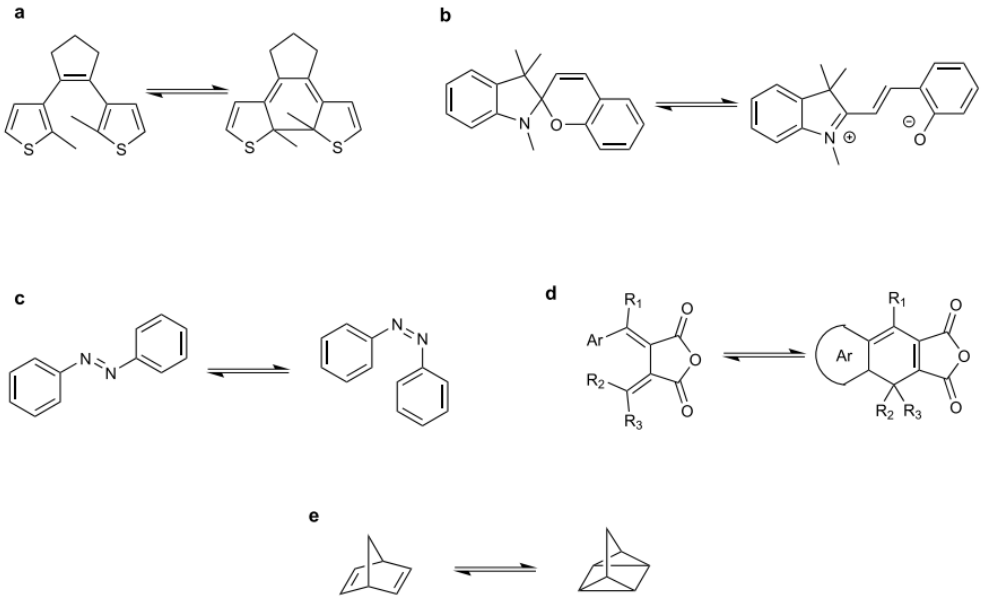

Figure 1.3: The important members of photochromic Molecules: a) Diarylethene (dithienylethene), b) Spiropyran/ merocyanine, c) Azobenzene, d) Fulgide (Here Ar=2,5-dimethylfuran-3-yl, R_1=methyl, and R_2 and R_3 are both part of an adamantane unit), and e) Norbornadiene/quadricyclaneazobenzene. Reused with permission from Ref [243], copyright, Nature publishing group-2016.

A third type of classification is based on the chemical processes involved. There are five groups based on i) pericyclic reactions ii) *cis/trans* (E/Z) isomerisations iii) Intramolecular hydrogen transfer iv) intramolecular group transfer v) dissociation processes and vi) oxidation-reduction process (Bouas-Laurent et al. 2001). The most popular photochromic molecules azobenzenes, diarylethenes, spiropyrans and stilbenes are discussed below.

1.2.1.1. Azobenzenes

The photochromic azobenzenes are commonly termed as "molecular photon engines". The azobenzene systems are those photo-responsive cores in which an azo group (-N=N-) is linked between two phenyl groups. Azobenzene molecules exist in two isomeric forms *trans* and *cis* showing distinct absorption spectra, steric structures and dipole moments. By the proper tuning of the wavelength region of the light applied it is easy to control the interconversion between the *trans* and *cis* isomers (Dürr et al. 2003; Song et al. 2004).

The azobenzenes show strong absorption in the UV-Visible spectrum due to the presence of π-conjugation in its structure. The region where π-conjugation absorption band appears is tunable by the alteration of substitutional patterns of the two phenyl rings in it. The main energetic electronic states or bands shown by azobenzene systems are n→π* and π→π*. The n→π* transition usually occurs at wavelength greater than 400 nm and shows blue shift with increasing polarity of the solvents (Griffiths 1972). The π→π* band appears between 300-400 nm. The azobenzenes also exhibit a σ-σ* transition in the range of 200-300 nm. The

absorption bands are strongly affected by the environment as well as the nature of groups on the phenyl rings (Ji et al. 2004). Depending on the relative energies of n→π* and π→π* bands azobenzenes can be classified into three classes (Rau 1990):

i) Azobenzene type: They have properties similar to the unsubstituted azobenzenes ((Ph–N=N–Ph). The π→π* band is very intense and is in the UV region. The n→π* is weaker and is in the visible region (yellow colour).

ii) Aminoazobenzene type: This class has π→π* and n→π* bands overlapping in the UV-visible region. Here the azocompounds have electron-donating moieties (X) either at ortho or para positions (o- or p-(X)–C_6H_4–N=N–Ar) (orange colour).

iii) Pseudo-stilbene type: This class contains donor substituents (X) and electron acceptors (Y) at the 4 and 4' positions respectively (push/pull system) [(X)–C_6H_4–N=N–C_6H_4–(Y)] The absorption band corresponding to π→π* transition is red-shifted, changing the appearance order with respect to the band n→π*. (red colour).

The most important feature of azomoieties is their capacity to undergo photo-induced molecular motion by reversibly addressing the molecular conformation between *trans* (E) and *cis* (Z) under illumination with light. Four types of mechanisms are proposed for the E-Z conversion of azobenzene systems. None of them is conclusively finalized, but continues to be under intensive investigation right from the moment of their proposal. The mechanisms are (1) rotation through the N=N bond. This mechanism involve the rupture of π-bond and free rotation around N-N bond. This leads to changes in C-N-N-C dihedral angle,

but fixes the N-N-C angle at ~120° (Magee et al. 1941). (2) inversion through the surface of one N=N–C bond angle with an increase in value to 180°. The C-N=N-C angle is at 0° and this mechanism involves the appearance of a transition state where an azonitrogen atom is present in the sp hybridized state (Curtin et al. 1966). (3) concerted-inversion of the N=N–C bond angle. Its value increases to 180° and involve a linear transition state. (4) inversion assisted rotation which results in larger variations in the C-N=N-C- angle along with less but prominent changes in the N=N-C angle. It is assumed that the isomerization from $S_0 \rightarrow S_1$ state ($n \rightarrow \pi^*$) occurs mainly through the rotation and that of high excited states and vibrational levels $S_0 \rightarrow S_2$ ($\pi \rightarrow \pi^*$) through the inversion and concerted inversion mechanisms (Figure 1.4) (Bandara et al. 2012).

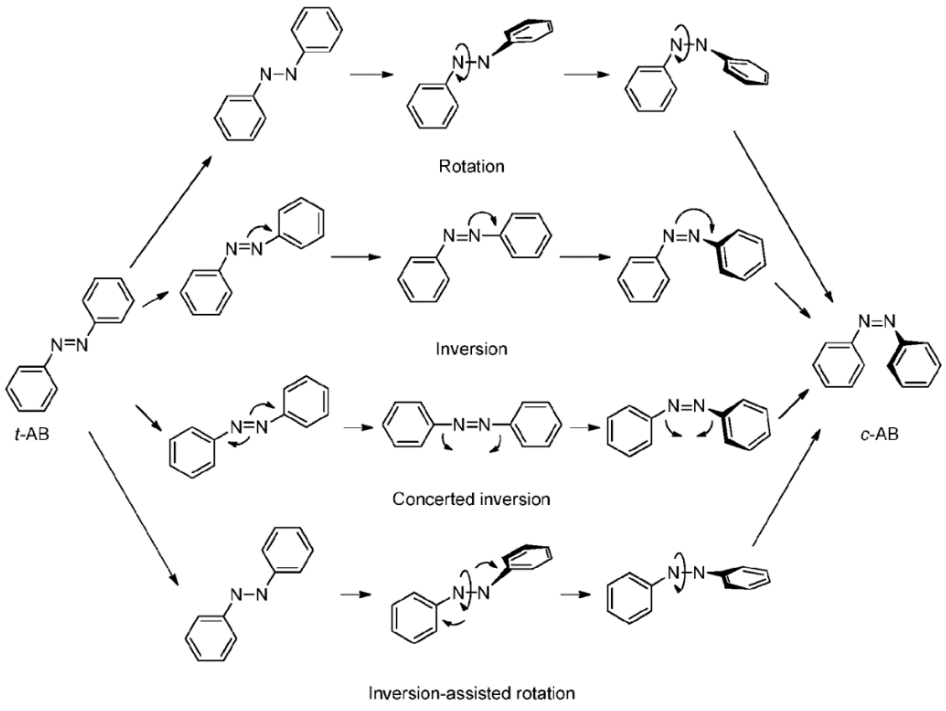

Figure 1.4: The proposed mechanism for the different types of mechanism for the photo-isomerisation of azobenzene. Reprinted with permission from Ref [16] Copyright © 2012 The Royal Society of Chemistry

The *cis* and *trans* isomers of azobenzene systems differ in many properties.

i) Absorption Spectra: In the absorption spectra the *trans* isomer shows a high intense π→π* band and a very weak n→π* band. The n→π* transition is weak because it is forbidden by the symmetry rules. In contrast the *cis* isomer shows a less intense π→π* band and a strong n→π*, since the transition is allowed transition in the cis isomer (Beveridge et al. 1966).

ii) Dipole moment: The *cis* isomer generally possesses a higher dipole-moment than the *trans* isomer (Hartley et al. 1939).

iii) Redox potential: The *trans* isomer has low redox potential than the *cis* isomer. The *trans* isomer is planar in structure so electron localization is more which reduces its redox potential (Gupta et al. 1988).

The azobenzene systems possess excellent tunable property due to the photo-isomerisation capacity in response to light as the external stimulus. These properties made them explorable to an enormous range of applications like molecular switches (Mativetsky et al. 2008), liquid crystals (Yu et al. 2004), actuators (Kumar et al. 2016) and sensors (Joshi et al. 2014).

1.2.1.2. Diarylethenes

Diarylethenes form another interesting class of photochromic molecules which belong to the P-type. They are derivatives of stilbene, where the phenyl rings are replaced by thiophene or furan or other five membered heterocyclic rings with low aromatic stabilization energy. In response to light the molecules exist in open and closed forms (Figure 1.5). Diarylethene systems can be switched between the two isomeric forms electrochemically. This differentiates them from other

photochromic molecules (Oudar 1977). Both isomers are thermally stable and the open/coloured to can be switched to closed/decoloured through multiple cycles of more than 10000 times with a speed range of picosecond. The quantum yield is around one and majority of diarylethene molecules undergo photochromic reactions in the single crystalline phase (Irie et al. 2014).

The diarylethene molecules possess interesting properties which make them excellent candidates in the molecular electronic field.

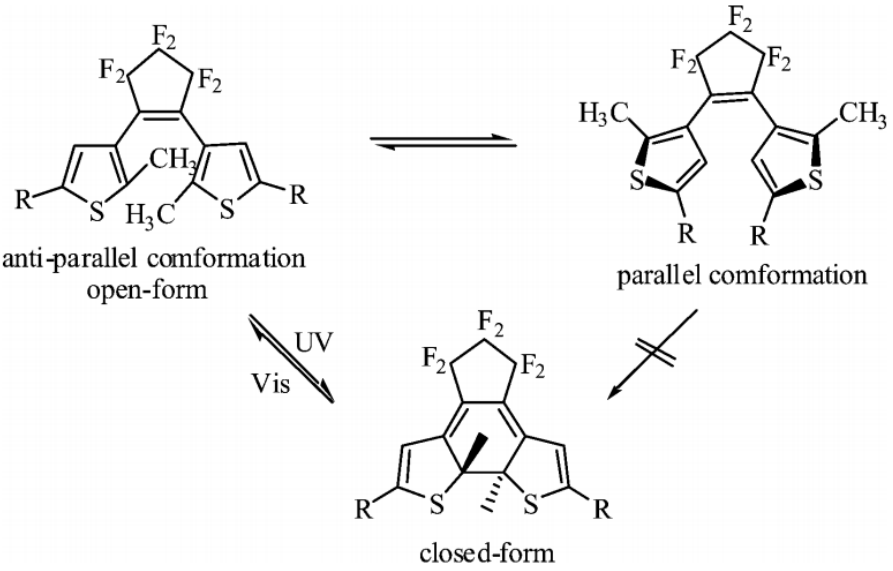

Figure 1.5: Photochromic activity of Diarylethenes. Reprinted with permission from Ref [253] Copyright © 2004 The Royal Society of Chemistry

i) Thermal Stability: The thermal stability of the closed ring isomers is a crucial factor behind the excellent photochromic performance of diarylethene systems. Some of the explicit members even have a half-life period around 400000 years at room temperature. The nature of aryl groups also contributes to this stability factor. The diarylethenes with heterocyclic rings like thiophene, furan etc as the aryl groups are able to stand stable even at 100 °C. The other factors which control the

stability are i) nature of substituents on the aryl groups, ii) aromatic stabilization energy of aryl groups and iii) steric hindrance by the substituent groups (Irie et al. 1988; Irie 2010).

ii) Fatigue Resistance: The undesirable side reactions are a part of photochromic reactions. This is a challenge to the repeatability of photochromic conversions over a number of cycles. Therefore, the fatigue resistance is an important controlling property for the photochromic molecules. The diarylethenes have good fatigue resistance. Some of the members show the cyclisation/cycloreversion processes to a cycle number around 14000 in solution and 30000 in single crystalline phase (Irie et al. 1992; Jean-Ruel et al. 2011).

iii) Quantum Yield: The open ring isomer of diarylethene can exist in two conformations. The first one is the parallel with the two aryl rings in the mirror symmetry and the second one is antiparallel with C_2 symmetry. The anti-parallel conformation leads to conrotatory cyclisation (Irie and Mohri 1988) and this conformer population can increase the cyclisation quantum yield. The cyclisation quantum yield of diarylethenes is measured as 0.5. The introduction of bulkier substituents, long alkyl chains etc on the aromatic rings can improve the cyclisation quantum yield (Uchida et al. 1999; Yamaguchi et al. 2006). The cyclisation quantum yields also depend on the solvent polarity. The quantum yield is less in polar solvents. The photocycloreversion quantum yields on the other hand is independent of solvent polarity (Ohsumi et al. 2008; Kobatake et al. 2009). The substituents on the aromatic rings can influence the quantum yield of cycloreversion (Morimitsu et al. 2002; Morimitsu et al. 2003). The quantum yield of cycloreversion is temperature dependent whereas photocyclization is not (Irie et al. 2000).

iv) Fluorescence property: Majority of the diarylethenes are non-fluorescent in both open and closed forms. But those with benzothiophene as one of the aromatic substituents exhibit weak fluorescence in both isomeric forms (Yagi et al. 2003; Shim et al. 2007). The fluorescent diarylethenes are synthesized by incorporating fluorescent molecules like furan(Pu et al. 2012), indole (Makarova et al. 2011), pyrazole (Pu et al. 2006), coumarin(Traven et al. 2010), oligothiophene (Feng et al. 2006), pyrrole (Pu et al. 2007) etc as the aromatic substituent. Some other fluorescent diarylethenes derivatives are prepared by linking them to various fluorophores like BODIPY (Golovkova et al. 2005) , perylenebisimide (Ma et al. 2009), porphyrin (Liddell et al. 2002), fluorene(Kawai et al. 2005). These derivatives have high fluorescent quantum yield with efficient photochromic reactivity.

v) Gated reactivity: The diarylethenes also exhibit gated photochromic reactivity. This property is imparted by the incorporation of external stimuli like heat, chemicals or photons to control the photochromic activity. This property is useful in constructing memory devices. A lot of diarylethenes with gated reactivity are developed for fabricating memory devices (Poon et al. 2011; Wu et al. 2012).

These above-mentioned properties make diarylethenes an excellent molecule for various applications (Tian et al. 2004). They are very good for optical memory. Various types of optical memory devices like holographic(Boiko 2009), three dimensional(Corredor et al. 2007), near field memory devices (Myeong-Suk et al. 2003) have been developed using them. The diarylethenes can also be coupled materials especially carbon nanomaterials like graphene for fabricating molecular junctions (Figure 1.6) (Jia et al. 2013), conductance switches (Sciascia et al. 2012).

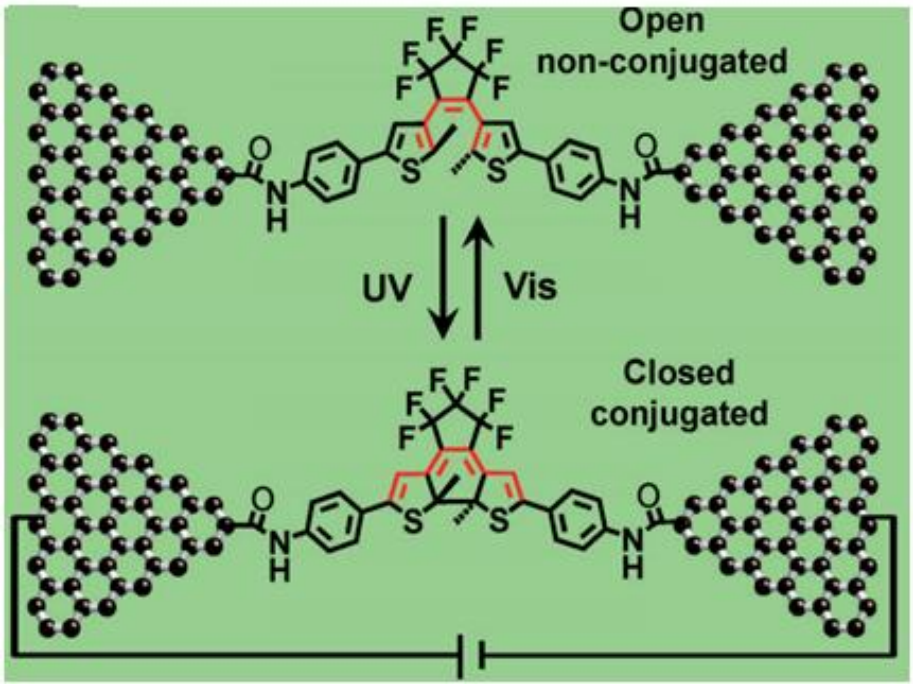

Figure 1.6: Molecular junction formed by graphene-diarylethenes hybrid. Reprinted with permission from Ref [114] Copyright© 2013 Wiley-VCH Verlag GmbH & Co. KGaA, Weinheim.

1.2.1.3. Spiropyrans

Spiropyrans form another interesting class of photochromic molecules. They are widely explored on the material front. There are two isomers. The closed ring isomer is called as spiropyran and the open ring isomer is called merocyanine. Unlike azobenzenes and diarylethenes different names are given to the isomeric forms. It is because of their large distinction in physico-chemical properties. The spiropyran molecule contains an indoline and a chromene group connected through a spiro-junction (Klajn 2014). The groups are oriented in perpendicular direction to each other. The absorption spectra of spiropyran contains two bands at ~272-296 nm and ~ 323-351 nm corresponding to the π-π* electronic transition of indoline

and chromene moieties (Tyer et al. 1970; Moniruzzaman et al. 2007). The ring opening of spiropyran takes place in two ways. The first one is the heterolytic C-O bond cleavage and the second one is through a 6π electrocyclic ring opening. The resulting open ring isomer merocyanine exists as a hybrid of the zwitterionic and quinoidal resonance forms (Swansburg et al. 2000). The absorption spectra of merocyanine is strongly dependent on the environment. The isomer generally shows a single delocalized transition in the visible region in the range 550-600 nm in non-polar solvents (Song et al. 1995; Florea et al. 2012).

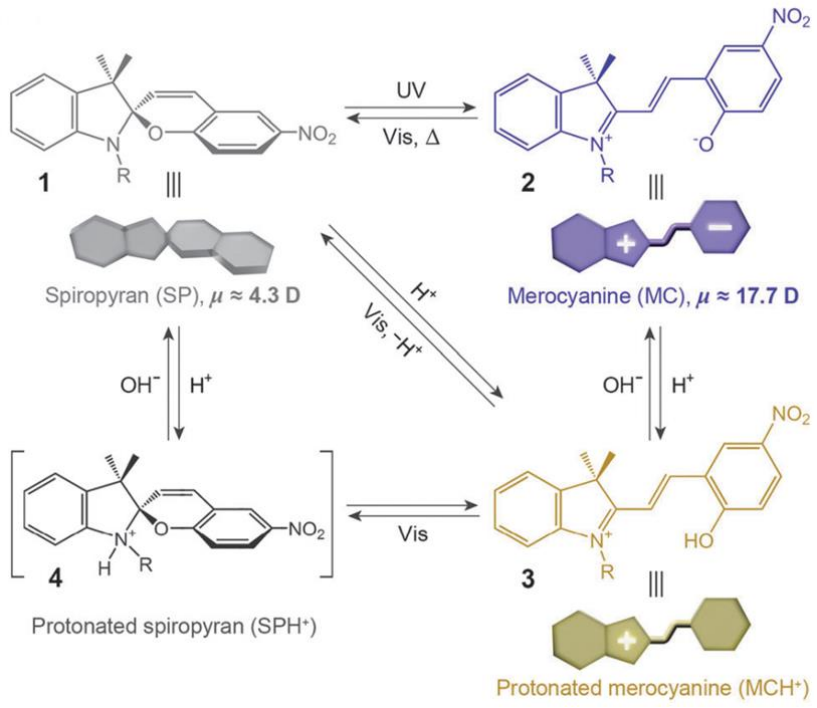

Figure 1.7: Photochromism and acidochromism exhibited by spiropyran. Reprinted with permission from Ref [125] Copyright © 2014 The Royal Society of Chemistry.

The tremendous potential of spiropyran arises from the fact that the two isomeric forms differ in their properties. Figure 1.3 describes the photochromism and acidochromism exhibited by spiropyran (Klajn 2014).

i) Dipole moment: The spiropyran has a weak dipole moment around 4-6 debye. The merocyanine has a larger dipole moment in the range of 14-16 debye since it possesses the charge separation character (Bletz et al. 2002; Shen et al. 2009).

ii) Volume: The Spiropyran system generally occupies smaller volume than merocyanine (Vilanove et al. 1983).

iii) Visible light appearance: The spiropyran is transparent in visible range. Butmerocyanine has a deep blue coloration as it absorbs in the range of 550-600 nm in the visible region.

iv) Emission: The spiropyran is weakly emissive and the merocyanine shows strong emission. The emission band appears around 650 nm. The back isomerization to closed form turns off the emission (Chen et al. 2010).

v) Basic nature: Spiropyran is less basic than merocyanine. The protonated merocyanine produces a band around 420 nm (Hall et al. 1994).

Despite the difference in the behavior of the two isomers, the spiropyran shows ability to respond to multiple stimuli. Apart from photochromism the molecule is capable of responding to other stimuli like temperature (thermochromism) (Minkin 2004), polarity of solvent (solvatochromism), redox potential (electrochromism) (Wagner et al. 2011). This exceptional behaviour makes it possible to construct the stimuli responsive materials by using spiropyran.

The spiropyrans are used for fabricating photoswitches (Buback et al. 2010), chemical sensors (Wan et al. 2014), biomedical devices (De Sousa et al. 2010), optical devices (Frolova et al. 2015), rewritable data storage devices (Petriashvili et

al. 2016) and so on. They are coupled with other materials like polymers (Zhu et al. 2006), carbon nanomaterials (Setaro et al. 2012) for developing multifunctional materials. The figure 1.8 describes such a field effect transistor developed by coupling graphene with spiropyran (Jang et al. 2012).

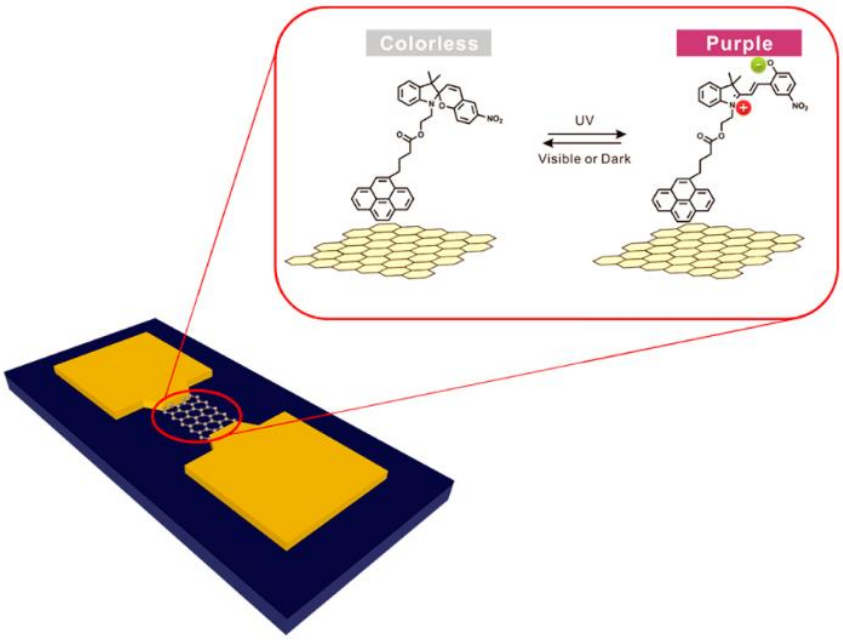

Figure 1.8: A field effect transistor (FET) developed by coupling graphene with spiropyran. Reprinted with permission from Ref [109] Copyright © 2012 American Chemical Society.

1.2.1.4. Stilbenes

1,2-diphenylethene commonly known as stilbene forms another interesting class of photochromic compounds. They also exist in two isomeric forms: E or *trans*-stilbene and Z or *cis*-stilbene. The *trans*-stilbene exist as crystalline solid at room temperature whereas the *cis* stilbene exist as liquid (Abourashed 2017)(Figure 1.9). The two isomers also differ in their properties. Stilbenes are used for various applications like developing dye lasers, non-linear optical materials (Jen et al. 1997), fluorescent materials (Wei et al. 2007) organic scintillators (Esposito et al.

2004). Stilbenes on coupling with polymer materials produce materials with phototunability (Buruiana et al. 2010). Similarly coupling with carbon nanomaterials produce useful optically responsive materials (Zhang et al. 2003).

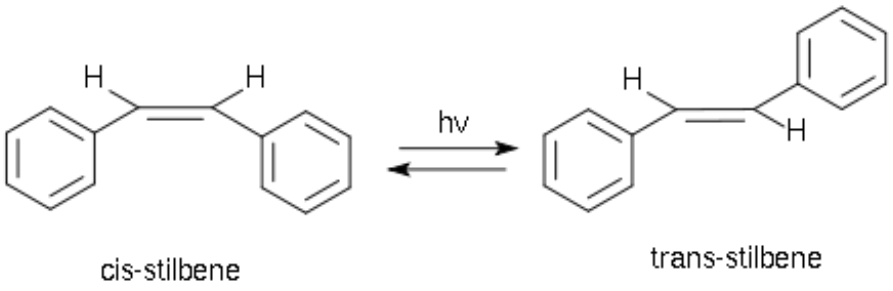

Figure 1.9: Photoisomerization of stilbene. (Courtesy: Wikipedia.com)

1.2.1.5. Bio-based photochromic molecules

The increasing influence of sustainable chemistry urged scientists to develop molecules from bioresource materials. The initial stage involved the modification of the existing ones with other biomaterials. Wang and his group developed photochromic papers by introducing spiropyran onto cellulose fiber surface. In one of their works they made photochromic paper by grafting spiropyran ether methacrylate (SPMA) onto the cellulose fiber through atom transfer radical process (ATRP) (Tian et al. 2016).

In another work, the anionic carboxyl containing spiropyran (SP-COOH) is made into a polyelectrolyte composite layer with cationic chitosan (CS) and this is further coupled with pulp fiber through layer-by-layer assembly method (LBL). The LBL-treated fiber exhibited excellent photochromic reversibility nature. It is compatible even with the untreated fiber due to the presence of hydroxyl groups in

the former. The assemblies are then moulded into hand sheets with photochromic property (Tian et al. 2017).

The next step in this process was the use of bioresource materials like cardanol as such in the process. Cardanol is a widely used biomaterial in the research field. It continues to inspire the researchers across the globe. Cardanol, a phenolic lipid, is a component of cashew nut shell liquid (CNSL), obtained after processing the cashew nut.

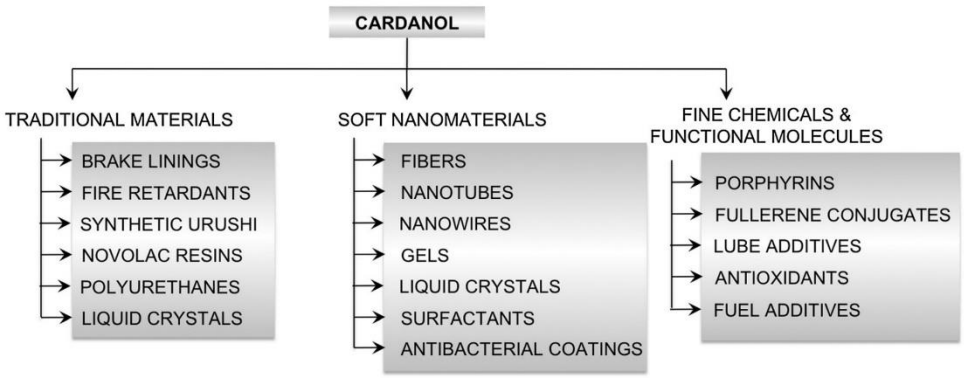

Figure 1.10: The use of cardanol in developing traditional materials, soft nanomaterials and fine chemicals. Reproduced with permission from Ref [15] Copyright © 2013 The Royal Society of Chemistry

The functional flexibility of cardanol arises from its structural features like i) the presence of phenolic group, which helps to achieve a variety of functional modification. ii) the alkyl chain at the meta position with a double bond imparting amphiphilic and lipidic character. iii) the aromatic ring which facilitates π-π stacking. All these functional features make cardanol an ideal candidate for synthesizing materials ranging from small molecules to polymeric species with widespread application in different fields. Balachandran *et al.,* in 2013

(Balachandran et al. 2013) summarized self-assembled soft materials developed from cardanol, ranging from gels, liquid crystals, fibres, tubes etc as follows (Figure 1.10).

The photochromic molecules also have been developed from cardanol. Saminathan (Saminathan et al. 2000) and his group synthesized liquid crystalline polymers containing azobenzene mesogens from cardanol. This molecule is utilized further for developing supramolecular synthon which exhibit light induced size variation at the nanoscale (Figure 1.11)(Mahesh et al. 2014).

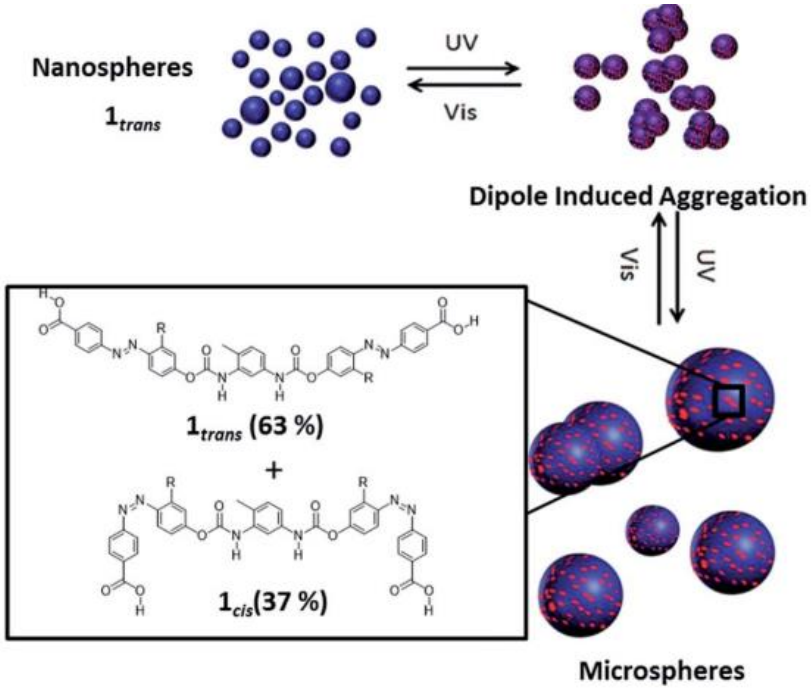

Figure 1.11: The azobenzene system developed from cardanol showing light induced size variation at nanoscale. Reproduced with permission from Ref [163] Copyright © 2014 The Royal Society of Chemistry.

1.2.1.6. Role of photochromic molecules in molecular electronics

The bistability of the organic photochromic molecules made them attractive candidates in the opto-electronic industry (Dulić et al. 2003). The application of photochromic molecules can be mainly categorized into three (Tsivgoulis 1995).

i) Application with single molecules: Here the photochromic units act at the single molecular level and perform useful functions like switching, transport of signals and other molecules, catalytic activity, non-linear optical orientation (Irie et al. 2002; Fukaminato et al. 2004).

ii) Application in polymeric materials. The photochromic molecules are coupled with polymers to improve and modulate various properties of the latter like their solubility, viscosity, conductance, gelation, liquid crystal nature (Jenekhe et al. 2004; Shirota et al. 2004).

iii) Application with biological molecules: The stimuli responsive biomolecules and biomaterials are highly desirable in the material chemistry field. The photochromic molecules can be used to exert a light control over various biomolecules. This artificial light controlled photochromic biosystems are employed in important applications like phototuning of enzymatic activity, improving membrane permeability, imparting bilayer stability (Myles et al. 2001; Kawai et al. 2005; Soh et al. 2007).

Even though the photochromic molecules have excellent properties, sometimes their practical applicability is limited. This arises because of the drawbacks like photo fatigue behavior, average quantum yields, low sensitivity and low storage capacity. This makes the devices based on photochromic systems less reliable and durable. This is overcome by coupling photochromic molecules with other materials. Hybrids with excellent properties are thus developed.

The photochromic molecules are coupled with a range of inorganic materials especially metals, coordination compounds etc (Kume et al. 2008; Feringa

et al. 2011). The hybrids are utilized for multiple applications like switches and sensors (Ipe et al. 2003; van der Molen et al. 2009). But the excessive use of inorganic materials creates environmental hazards and therefore the scientists shifted their focus to the other organic materials and carbon nanomaterials for coupling with the photochromic molecules. In terms of performance and versatility of applications the carbon nanomaterials are superior to the inorganic materials. They are utilized for developing smart materials and devices. The coupling of carbon nanomaterials with photochromic molecules resulted in the production of optically responsive smart materials (Zhang et al. 2016). Such materials/hybrids are then coined into devices. These devices are employed for numerous applications. For example, the sensors for fluoride ions are developed by the self-assembled graphene oxide-spiropyran hybrid (Figure 1.12 a) (Li et al. 2013) and field-effect transistors are fabricated by spiropyran-carbon nanotube hybrids (Figure 1.12 b) (Guo et al. 2005). The other applications include memory storage (Lin et al. 2013) and solar thermal storage (Luo et al. 2015) and etc.

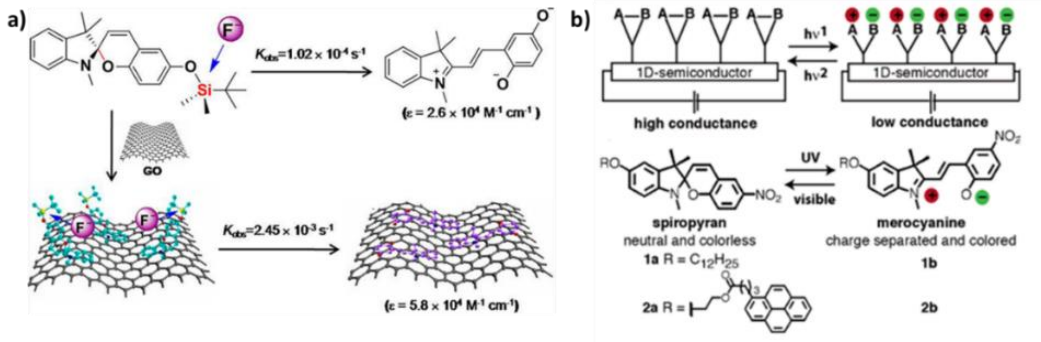

Figure 1.12: Photochromic molecules coupled with carbon nanomaterials for various applications. a) Self-Assembly of Graphene Oxide with a Silyl-Appended Spiropyran Dye for Rapid and Sensitive Colorimetric Detection of Fluoride Ions. Reproduced with permission from Ref [143] Copyright © 2013, American Chemical Society. b) Directing and Sensing Changes in Molecular Conformation on Individual Carbon Nanotube Field Effect Transistors. Reprinted with permission from Ref [80] Copyright © 2005, American Chemical Society.

1.3. Functionalization strategy for coupling of carbon nanomaterials with photochromic molecules

The integration of carbon nanomaterials with various photochromic molecules can be effected through two different functionalization modes (Figure 1.13) (Zhang et al. 2016). One mode is through covalent approach which involves direct bond formation between the components. The direct bond formation is carried out through different chemical reactions like cyclo-addition (Schuster et al. 2003), condensation reaction (Wang et al. 2014; Liao et al. 2015), diazonium coupling (Sadowska et al. 2009; Wang et al. 2009) and Click chemistry (Yan et al. 2012). The main advantage associated with covalent approach is the control over degree of functionalization. The extent of functionalization can be estimated by different techniques like X-ray Photoelectron spectroscopy and thermogravimetric analysis. In majority of works hundreds to thousand carbon cores get associated with one photochromic molecule.

The second method of functionalization involves a non-covalent approach. In this method there is no linkage between the coupling counterparts. There occurs a physical adsorption of photochromic molecules over the surface of carbon nanomaterials. Different supramolecular interactions like hydrogen bonding, π-π stacking and van der Waal's forces are responsible for this adsorption (Imin et al. 2012; Perry et al. 2015). This non-covalent functionalization does not cause any alteration in the structure or functionality of either photochromic molecule or the carbon nanomaterial. This is the added advantage of this functionalization mode.

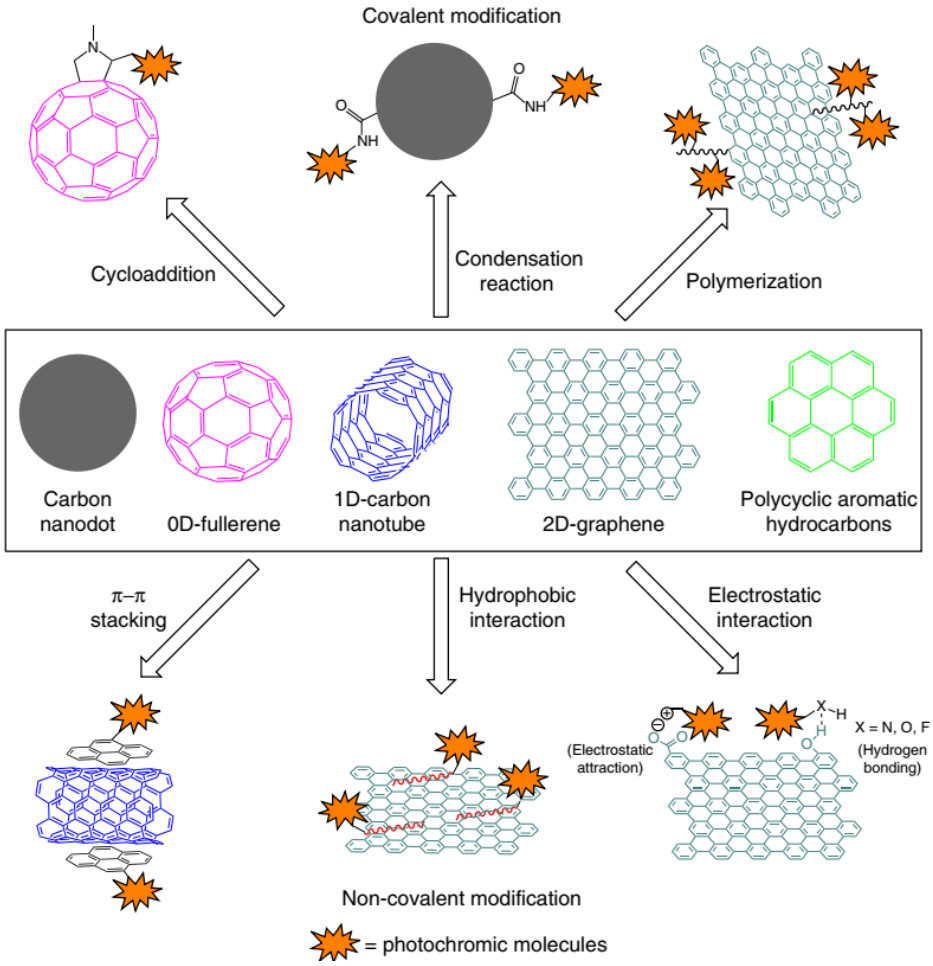

Figure 1.13: Covalent and non-covalent functionalization methods for coupling photochromic molecules with carbon nanomaterials. Reused with permission from Ref [311], copyright, Nature publishing group-2016.

Both functionalization strategies have significantly contributed to the development of hybrid materials with enhanced properties. These are widely used for better device development in the opto-electronics industry.

1.4. Assembling carbon nanomaterials with azobenzene Systems

The hybrids containing azobenzene units have potential application in the field of photonic devices. The inherent property of photo-isomerisation of azobenzene molecule imparts a photoswitching ability to the entire system. Compared to other members of the photochromic family azobenzene possesses the advantage that its photoisomerization has lesser rate of photobleaching and occurs with larger conformational change. The association of azomolecules with carbon nanomaterials has resulted in developing multi-functional materials. This multifunctionality arises due to the tuning of properties of carbon nanomaterials by azobenzene molecules through their *trans-cis* photoisomerization. The properties modulated include magnetism, photoconductivity, fluorescence, dispersibility, morphology and conductance change etc. The azomoieties are linked with carbon nanomaterials through both covalent and non-covalent modes. Both kinds of hybrids led to the development of devices with desirable applications.

1.4.1. Coupling of carbon nanotubes with azobenzene molecules

Carbon nanotubes are one-dimensional conjugated nanostructures of the carbon nanomaterial family with a wide range of applications. The carbon nanotube can be easily manipulated through various functionalization methods, both covalent and non-covalent. This property led to the fabrication of multi-functional devices by coupling carbon nanotubes with organic molecules, especially photochromic ones. The photochromic molecules modulate various properties of carbon nanotubes ranging from conductance, dipole moment, magnetism etc. The covalent

and non-covalent assemblies of carbon nanotubes with azomolecules continue to be a hot subject of scientific investigation. Many of the researchers in the material field have reported interesting opto-electronic applications of these hybrids.

1.4.1.1. Covalent Assemblies

Wei Feng and his group (Feng et al. 2007) have developed different assemblies between nanotubes and azobenzene systems. They investigated the influence of azochromophores on various properties of nanotubes. In one of the initial works, they synthesized a covalently linked hybrid by reaction between diaminobenzene and aminododecane with MWCNT (AZO-MWCNT). The UV-Visible absorption measurements proved that the AZO-MWCNT hybrid exhibits two peaks. The peak at 297 nm corresponds to π-plasmon transition in nanotube and that at 406 nm corresponds to the π-π* transition in azobenzene. The photoluminescence (PL) measurements also supported the electronic interaction between azo molecule and the nanotube.

The time dependent absorption studies under UV illumination showed that the AZO-MWCNT has a continuously decreased absorption due to the *trans-cis* photoisomerization of azobenzene in the hybrid. Therefore, it is possible to exert a photoresponsive control over the behavior of nanotube through the association with photochromic azobenzene systems. Later the same group fabricated a light electronic switch by utilizing a covalent hybrid between few-walled carbon nanotube (FWCNT) and an azomolecule. Two types of hybrids are synthesized. The first one is the simple FWCNT-AZO and the second one is the FWCNT-chain-Azo which contains a flexible alkyl spacer between the nanotube and the

azomolecule. From the time dependent UV irradiation experiments, the FWCNT-chain-Azo solution gave the value for the rate of *trans-cis* photo-isomerisation of azogroup in the hybrid as $k_p = 6.7\times10^{-1}s^{-1}$. This value is four times higher than that for simple FWCNT-Azo hybrid ($k_p = 1.4 \times 10^{-1}s^{-1}$). Similarly, for the back *cis-trans* isomerization, the rate constant for FWCNT-Azo hybrid is $0.7\times10^{-1}min^{-1}$ and that for FWCNT-chain-Azo hybrid is $1.4 \times10^{-1}min^{-1}$. These results proved that the presence of a flexible alkyl spacer can enhance the photo-isomerisation of the azomolecule in the hybrids with nanotubes.

Another reason for the enhanced photoisomerization efficiency is due to the increased free volume. The FWCNT-chain-Azo hybrid is coated over the (ITO) Indium Tin Oxide plate (ITO) and a conductance switch is fabricated. The measurement of current as a function of voltage with UV illumination showed an increase in current with time. This is due to the *trans-cis* isomerization of the azomoiety. Upon removing the source, the current decreases due back isomerisation. This process is reversible over multiple cycles (Figure 1.14b) (Feng et al. 2010).

The basis of the conductance switch was actually established by a theoretical study done by Del Valle and his group. In their work they studied the charge transport characteristics of a system where a single azobenzene molecule is connected to two carbon nanotubes through -NHCO linkage. The carbon nanotubes act as true nanoscale electrodes. The low-energy conduction characteristics of the junction can be adjusted by altering the chirality (armchair and zigzag) and topology of the nanotubes. By measuring the linear conductance, the switching

effect of three different types of CNTs-azobenzene junctions are investigated. It is observed that the armchair and zigzag junctions exhibit a dependence of their linear conductance on the charge injection energy. Also the system exhibits higher conductance in the *trans* configuration of azobenzene than *cis* form. Further analysis confirmed that the structures of both electrodes and molecules are important while designing nanoscale electrodes for measuring the low voltage transport (Del Valle et al. 2007).

At another level, azobenzene polyurethanes (AzoPU) are functionalized with MWCNTs having hydroxyl groups. Two types of polyurethanes are synthesized. This is done by treating an azobenzene system having a bis-hydroxyl unit; with the soft monomer aliphatic hexamethylene diisocyanate (HDI) and rigid monomer aromatic tolylene 2,4-diisocyanate (TDI). The resulting MWCNT-AzoPU system acts as a core-shell system. The MWCNT is the hard core unit and AzoPU is the polymer shell. The grafting of AzoPU over MWCNTs improves the thermal stability and dispersion properties of nanotubes. The rate of photoisomerization of AzoPUs is decreased upon grafting with MWCNT due to the steric effects and heat sink effect. This can be overcome to a certain extent by adjusting the main chain flexibility of grafted polyurethanes on nanotubes (Yang et al. 2007).

In another work, MWCNTs are covalently grafted with an azobenzene liquid crystal polymer poly{6-[4-(4-methoxyphenylazo)phenoxy]hexyl methacrylate (PMMAZO) through atom transfer radical polymerization. Linear PMMAZO is a thermotropic liquid crystal polymer having both smectic phase and nematic phase. The hybrid CNT-PMMAZO also has the same liquid crystallinity

as the homopolymer PMMAZO. Then the orientation behavior of both MWCNTs and CNT-PMMAZO embedded in a PMMAZO matrix in the presence of an electric field is investigated. The orientation of the MWCNTs is affected by the viscosity of the matrix whereas that of CNT-PMMAZO is controlled by both the viscosity and the presence of liquid crystalline phase. The increased compatibility between MWCNT and PMMAZO after covalent modification is responsible for this. The hybrid is a promising candidate for developing electro-responsive materials (Figure 1.14c)(Hu et al. 2011).

Photoinduced anisotropic response of the hybrid between MWCNT and azomolecules is also investigated. In one of such work, the covalent MWCNT-AZO film is subjected to polarized UV light at a range of 265 to 400 nm. The film exhibited photoinduced anisotropic response. A continuous increase of polarized absorption is observed when the polarized light is measured parallel with respect to the incident light. On the other hand, there is a decrease when the measurement is made perpendicular to the incident light. The reason behind this photoinduced anisotropic response is the photoisomerization of azochromophore (Feng et al. 2007).

Recently solar thermal fuels have been developed based on molecular-nanostructure hybrids. For solar thermal fuel application the single-walled carbon nanotubes are directly linked with azobenzene chromophores through amide linkage. The bundled hybrid shows an increased energy storage capacity from 58 to 120 kJ mol^{-1}, along with higher life time and cycling stability. The conformational restriction and photo-induced steric strain controlled by the

azomolecule is responsible for this efficient performance of chromophore-nanotube template as a solar thermal fuel (Figure 1.14a) (Kucharski et al. 2014).

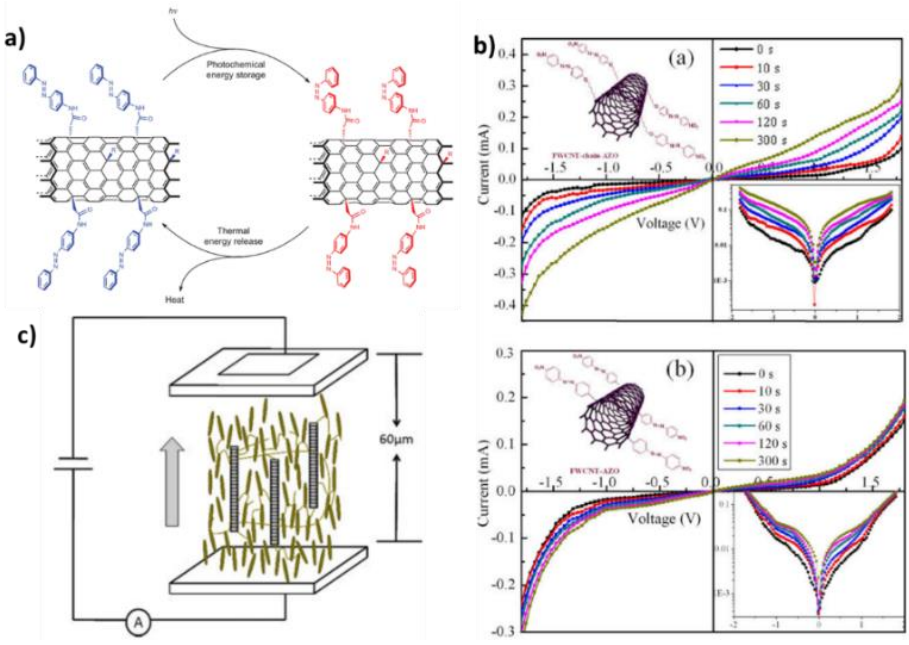

Figure 1.14: a) Schematic representation of photochemical energy storage and thermal energy release by the hybrid solar thermal fuel developed with azobenzene functionalized single-walled carbon nanotube. Reproduced with permission from Ref [130] Copyright © 2014, Springer Nature.b) Linear current-voltage (I-V) characteristics of conductance switches (a) FWCNT-Chain-AZO & (b) FWCNT-AZO with molecular structure and log I-V current traces at the insets. Reproduced with permission from Ref [66] Copyright © 2010 Elsevier Ltd. c) Scheme for the orientation of MWCNTs in the liquid crystal cell under electric field. Reproduced with permission from Ref [90] Copyright © 2010 John Wiley and Sons.

1.4.1.2. Non-covalent assemblies

The isomers of azobenzene exhibit two different dipole moments at *trans* and *cis* states. This ability was used by Simmons *et al.*, in 2007 where they modulated the conductance in single-walled carbon nanotube. They made use of a dye namely Disperse Red 1 (DR1) containing an azochromophore. The molecule exhibits a dipole moment of 9D in *trans* state and 6D in *cis* state. By incorporating an anthracene tether, the molecule is non-covalently functionalized with single-

walled carbon nanotube and the system functions as a transistor. Under UV illumination, the dipole moment change in azogroup induced by *trans-cis* isomerization results in a charge distribution around the nanotube. This leads to a change in local electrostatic potential as well as a shift in threshold voltage of transistor there by modulating its current characteristics. This modulation is repeatable over cycles promising the development of photodetectors (Simmons et al. 2007).

Field effect transistors (FET) also can be developed by combining single-walled carbon nanotubes (SWCNT) with azochromophores. These can function as nanoscale colour detectors. The azobenzene systems are developed by coupling 1-pyrenebutyric acid with three dyes namely disperse red 1 (DR1), disperse orange 3 (DO3) and 4-(4-nitrophenyl)azophenol (NPAP). The hybrids are fabricated through the adsorption of azochromophores over the carbon nanotube surface through non-covalent interactions between nanotube sidewalls and pyrene moieties. The azomolecules are developed in such a way that they function as specific absorption windows. Therefore, the azochromophores function as photo absorbers and the SWCNTs serve as transducers which produce electric signals. This is possible through the photoisomerization of azomolecules which changes the dipole moment and in turn alter the electrostatic environment of the nanotube (Zhou et al. 2009).

The dynamics of orientation and photoisomerization kinetics of azobenzene molecule at the azobenzene/SWCNT interface is also studied. Optical second harmonic generation (SHG) is used for probing the acentric orientation of chromphores in ultrathin films, bulk systems etc (Shen 1989; Simpson et al. 2000). SHG can identify the radial component of chromophore orientation with respect to

the nanotube surface. The azobenzene molecule used here is the pyrene tethered DR1 (DR1-P). The DR1-P is non-covalently functionalized with SWCNT with the surface coverage of three molecules per hundred carbon atoms in it. The average chromophore tilt angle ψ for the net chromophore orientation over the SWCNT surface is 40° ± 3° as measured by the *p*-polarized SHG signal. The photoisomerization dynamics of the DR1-P/SWCNT samples are probed by irradiating the samples using unpolarized light of wavelength 495 nm and 710 nm. It is observed that under 495 nm light the SHG signal subsides. Upon removing the light for a small interval, a slow recovery occurs. The storage under dark for a long time leads to almost full recovery. The *trans-cis* isomerization of DR1-P with illumination is responsible for the fall in SHG signal as there occurs a decrease in the molecular hyperpolarizability. The reverse *cis-trans* isomerization leads to recovery. But there was no detectable change in the SHG signal upon illumination with 710 nm light as it is beyond the absorption range of DR1-P (Figure 1.15b).

Again, a corona poling field is applied to study the impact of electric field over the photo-isomerisation kinetics. Under corona field, the tilt angle ψ is reduced to zero and SHG signal shows enhancement due to the orientation of DR1-P molecules along the field direction. The simultaneous illumination experiments with 495 nm light showed a fall in SHG signal under light and recovery upon removing the light source. But here a different time dynamic is observed. Under the corona field, the *cis-trans* rise time is mono-exponential while the same without field is bi-exponential. Similarly, the *trans-cis* dynamics has a fast switching time of 0.5s with the field applied. Thus, an applied electric field can enhance the chromophore orientation. Simultaneously there is an alteration in the photo-

isomerisation dynamics. This is highly useful for developing FET type devices (McGee et al. 2012).

The same group also reported the spectroscopic properties of SWCNT-azobenzene hybrid systems through both experimental and theoretical methods. Three types of chromophore-nanotube hybrids are developed by choosing three different DRI azobenze molecules. They are i) simple DR1 molecule, without any tether (DR1U), ii) anthracene functionalized DR1 (DR1A) and iii) pyrene functionalized DRI (DR1P). Comparison of the binding strength of these chromophores with SWCNTs is done using various techniques like Raman spectroscopy, UV-Visible absorption measurements and XPS analysis. The DR1P with pyrene tether proved to be more efficient in binding to the nanotube surface. The DR1P forms more stable chromophore-nanotube hybrid due to better π-π stacking ability of former compared to other azomolecules. Theoretical analysis using DFT calculations proved that DR1P with parallel orientation to the nanotube surface has more binding energy.

Further analysis with SHG showed the heterogeneous nature of the adsorption of azomolecules over the nanotube surface. Here also with UV illumination at 365 nm, SHG signal intensity decreases and on removing the source the intensity is recovered. This supported the presence of perpendicular configuration of DR1P in addition to the parallel one. The fluorescence measurements exhibited that upon binding to the nanotube surface, there occurs a quenching of fluorescence in the DR1 systems. The non-linear nature of the stern-volmer plots supported the involvement of both static and dynamic quenching. The

photoluminescence studies excluded the possibility of charge transfer between nanotubes and DR1 azomolecules (Huang et al. 2011).

The pyrene appended azobenzene systems also enhance the solubility properties of nanotubes in common organic solvents. When azobenzene polymers with pyrene pendants are non-covalently functionalized with SWCNTs, composite materials are formed with good solubility in organic solvents. The composites also exhibited higher thermal stability. Here also the good π-π stacking ability of the pyrene groups with nanotubes enhance solubility of the hybrids formed as it facilitates proximity of azopolymers near the nanotube surface. This also helps a better electronic interaction between the components. The wrapping of the azopolymer over the nanotube surface gives more volume for the photoisomerisation of azochromophore in them, resulting in a faster kinetics of the photoisomerization ability of the former in the composite. The kinetics results are superior compared to the other reported works, where the azochromophores suffered a greater restriction in photoisomerization upon composite formation with nanotubes (Yang et al. 2007; Umeyama et al. 2010). The photoinduced birefringence studies proved that composite exhibits better photoalignment property than the azopolymer alone (Vijayakumar et al. 2011).

Generally, carbon nanotubes have poor solubility in water. The surfactants with aromatic core as well as alkyl chains are used to solubilize the nanotubes in water. A molecule pyrene-azobenzene-PG (PAPG) which contains an azomolecule with polyglycerol dendron and a pyrene group is non-covalently functionalized with carbon nanotubes. This molecule acts as a surfactant and facilitates the dispersion of CNTs in water (Bluemmel et al. 2010). Similarly, an amphiphile

molecule which contains an azobenzene chromophore with a long alkyl chain in third generation glycerol dendron namely G3azoC11 is used to solubilize as well as debundle nanotubes in aqueous media. The *trans-cis* isomerization of the amphiphile led to the bundling and precipitation of nanotubes and with back *cis-trans* isomerization the nanotubes got debundled and redissolved. The entire process is found to be reversible over a large number of cycles (Figure 1.15a) (Kördel et al. 2012). In order to achieve a reversible supramolecular control over the dispersion of MWCNTs, photothermally responsive supramolecular polymers are used.

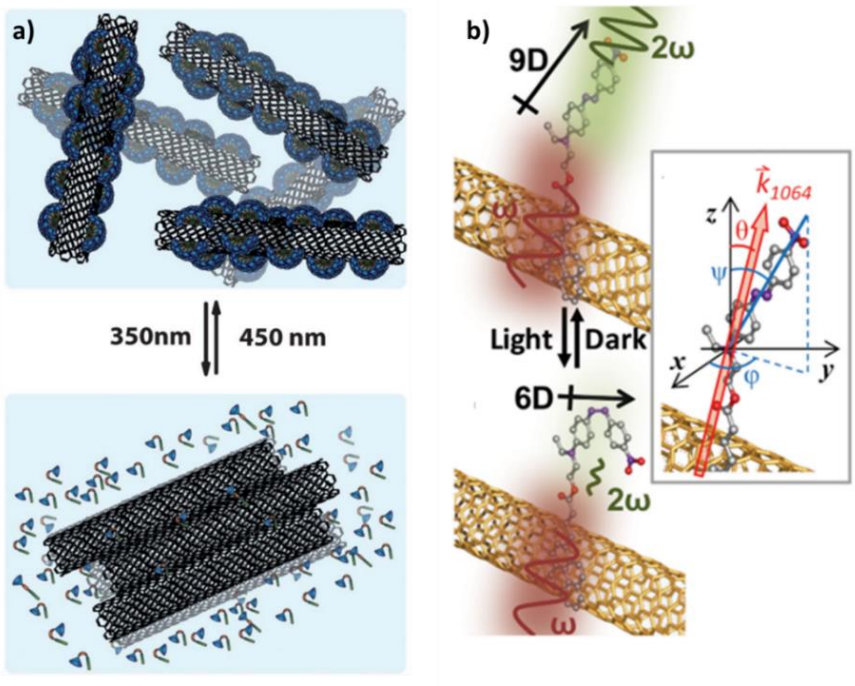

Figure 1.15: a) Mechanism for the optically controlled bundling and debundling of single-walled carbon nanotubes by G3azoC11 amphiphile. Reproduced with permission from Ref [128] Copyright © 2012 The Royal Society of Chemistry. b) Representation of simple harmonic generation (SHG) in trans and cis DR1-P on SWCNT. Reproduced with permission from [170] Copyright © 2012 American Institute of Physics.

The monomer unit consist of three parts i) azobenzene molecule ii) O-alkylated catechol spacer to ensure dispersion of MWCNTs in organic solvents iii)

a uracil unit capable of hydrogen bonding. The polymer formed by the self-assembly of this monomer facilitates the light induced dispersion and precipitation of MWCNTs. The *trans-cis* isomerization of azochromophore induces the precipitation of CNTs and the thermal *cis-trans* isomerization facilitates dispersion (Maggini et al. 2013).

Faupel and his group investigated the light induced conductance switching in carbon nanotube-polymer composites. Here they made composite films between SWCNTs and 4-hexyl-phenyl-[4-(propyl-butoxy)-phenyl]-diazene) with polymethyl methacrylate (PMMA) as support. The samples are produced in six batches with varying SWCNT concentration and they exhibit percolation behavior. The percolation threshold is 0.39 weight percentage. The conductance switching behavior of all the samples near the percolation threshold is observed. Stable switching amplitudes up to 28% were obtained with them. The samples show Pool Frenkel type conduction behavior (Schneider et al. 2015). It is difficult to study the relation between the conductance switching and molecular motion of azobenzene chromophores while using high elastic polymer matrices. Therefore, the group extended their study by choosing polycaprolactone (PCL) as the host matrix as it has low bulk elastic modulus value. For investigating the impact of molecular motion over conduction properties, twelve batches were prepared with 20 weight percentage azochromophore with increasing amounts of SWNTs from 0.16 to 3.12 weight percentage with PCL was used as the host matrix. The percolation threshold is 1.06 ± 0.83 weight percentage. The incorporation of PCL as the matrix helped in achieving intrinsic photomechanic activity.

The photoinduced molecular motion of azobenzene molecules can induce reversible macroscopic thickness changes. The thickness varies around 0.85% for PCL/azobenzene and 0.3–0.35% for SWCNT-containing polymer composites. This photomechanic effect can clearly affect the conductance switching near the percolation threshold. Here a reverse direction is obtained in the case of conductance switching. This is due to the greater influence of photomechanic activity over the electronic effects (Schneider et al. 2017).

1.4.2. Coupling of graphene materials with azobenzene molecules

The graphene is a two-dimensional carbon nanomaterial with sp^2 hybridized carbon atoms. Its superior structural and electronic properties like zero band gap, hall effect, near ballistic transport etc made it an excellent candidate for optoelectronic applications. The assemblies of graphene materials with azobenzenes have resulted in materials with photoswitchable properties. The advantage of graphene over carbon nanotube in current modulation is that, it does not have a variable diameter and chiral nature. This helps in avoiding the modulation of properties by the electrode chirality. The graphene has a low production cost compared to other carbon nanomaterials. This also makes graphene a preferable material in the optoelectronic world (Allen et al. 2009).

1.4.2.1. Covalent assemblies

Wei Feng and his group (Zhang et al. 2010) have developed some covalent graphene oxide-azomolecule (GO-AZO) hybrids with excellent phototunable conductance. One of the GO-AZO hybrid connected through amide linkage

exhibited an enhanced reversible photo-driven conductance switching performance. The GO-AZO hybrid shows increased current upon UV illumination and the current declines after removal of source. The graphene oxide (GO) sheets here are good electron acceptors and the azomolecules function as a good electron donors. A quick charge transfer takes place in this donor-acceptor system, which eventually results in higher photocurrent upon UV irradiation. The photoresponse ratio of the system is 800%. The system exhibited a faster photoresponse time around 500ms.

The same group in 2015 developed a nano-template by covalently linking reduced graphene oxide (RGO) with two different azobenzene molecules,

i) 4-((3,5-dimethoxyaniline)diazinyl)-benzene (AZO-1) and

ii) 4-((3,5-dimethoxyaniline)diazinyl)-4-benzoic acid (AZO-2) which is employed as a solar thermal fuel.

RGO is selected as the nano-platform because of its high dispersibility in water as well as high functionalization density due to the combination of partial restoration of conjugated structures. The presence of two methoxy groups at the ortho position of both azo molecules facilitates the molecular interaction and steric hindrance. The AZO-2 molecule in addition contains a carboxylic acid group at the para position, which induces an intermolecular hydrogen bonding and proximity induced interaction monitored by steric configuration and specific intermolecular distance. These features in turn result in the high functionalization density and packing interaction due to inter-planar bundling in the solid state. Thus, the RGO-AZO nano-templates have improved storage capacities around 112 W h kg^{-1} and storage half-life time of 33 days. The nano-template has greater cycling stability

which promises a good performance for 4.5 years comparable to Li-ion batteries(Luo et al. 2015).

Again, another photothermal fuel (PTF) is developed by making a film by coupling RGO with bisazobenzene (rGO-bisAzo). The increase in number of chromophore units has resulted in more steric hindrance, which leads to a restriction in photoisomerization ability, which in turn increases the half life time of the PTF. The system contains a large number of inter and intra-molecular hydrogen bonding interactions. The hybrid system exhibited a high energy density of 131Whkg^{-1}. The half-life time is 37 days and the system showed stability for more than 50 cycles. The maximum temperature difference of the released and accumulated heat of this closed cycle PTF is 15 °C. This gets reduced to 10 °C after 30 minutes. This is true even when the environment has a temperature of more than 100 °C. This solid state material with controlled heat release is of great interest in device application (Zhao et al. 2017).

The graphene-azobenzene devices developed by Cao *et al.*, (Cao et al. 2013) through dash-line lithographic method (DLL) showed differential conductivity. It is a reversible light-driven single molecule switch. The azobenzene link connecting the carboxylic acid functionalized graphene molecule is responsible for this distinct conductance state. Since the azobenzene bridge contains sulphonyl acid groups, the system also responds to pH as the external stimulus. The system showed higher conductance at low pH and vice versa.

Again Nguyen *et al.*, in 2013 (Nguyen et al. 2013), modulated the current in a trilayer graphene. Here the azobenzene molecule is covalently linked with the

graphene material through hydroxyl, epoxy and carboxylic acid linkages. The dipole moment changes associated with the photoisomerization results in a great quantum capacitance and a large carrier confinement. The azomolecule reversibly modulates the carrier density of trilayer graphene which is around 4.4×10^5 holes / μm^2. The molecular dipole moment changes of azomolecule induces a voltage around 0.097V. This results in additional six quanta of holes per azomolecule. The quantum capacitance value of 72.5 $\mu F/cm^2$ ensures the sensitivity of the system (Figure 1.16a).

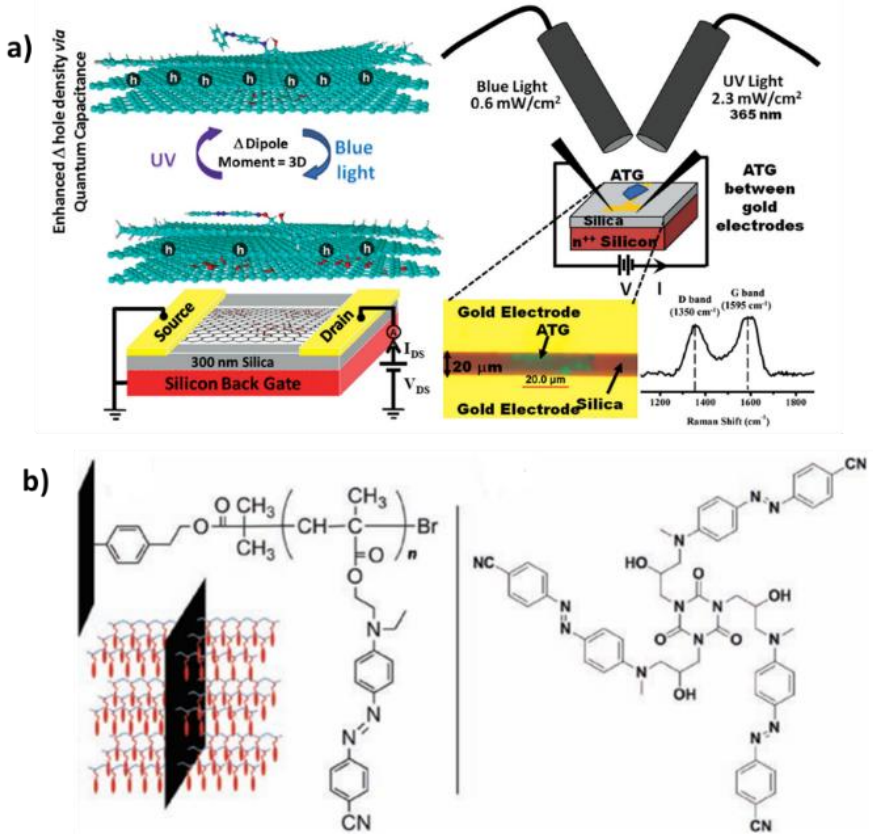

Figure 1.16: a) Schematic representation of azobenzene molecule covalently attached to trilayer graphene for the modulation of current. Reproduced with permission from Ref [188] Copyright © 2013, John Wiley and Sons. b) Graphene grafted with azopolymer brushes (G-PCN) doped with Tr-Az-CN molecular glass. Reproduced with permission from Ref [275] Copyright © 2011, John Wiley and Sons.

Devi *et al.,* in 2014 (Devi et al. 2014) synthesized a hybrid assembly between graphene oxide and two different azo chromophores i) 5-((4-methoxyphenyl) azo)-salicylaldehyde and ii) 5-((4-ethoxyphenyl) azo)-salicylaldehyde. They synthesized the azochromophores in such a way that one end contains an electron donating group and other end contains an electron withdrawing group. The incorporation of azomolecules with GO results in an increased thickness of around 4-5 nm. The hybrids exhibited a quenched fluorescence due to the photoinduced energy/electron transfer from azobenzene to GO sheets.

Some of the Graphene-AZO hybrids can be used to form surface relief grating (SRG) patterns. Wang *et al.,* in 2011 (Wang et al. 2011) reported single layered graphene grafted with azopolymer brushes, which is used as a filler to induce SRG formation. The graphene grafted with azopolymer brushes (G-PCN) (Synthesized by coupling modified graphene initiator with diazonium salt of modified 4-aminobenzonitrile.) are doped with Tr-AZ-CN, a star shaped azocompound (Synthesized by coupling the precursor formed between 1,3,5-Triglycidyl isocyanurate and *N*-methylaniline with 4-aminobenzonitrile through diazonium coupling reaction (Yin et al. 2010).) which is used as a stable molecular glass. The doping is with 0.5% and 1%of G-PCN. The films are then exposed to p-polarized argon laser beam for SRG formation. The diffraction efficiency (DE) of SRG patterns are significantly increased with a very low filler content, where the G-PCN is present in 0.5%. This increase in DE is due to the transport of graphene along with Tr-AZ-CN molecular glass, on a micrometer scale upon exposure to visible light (Figure 1.16b).

1.4.2.2. Non-covalent Assemblies

A lot of non-covalent assemblies are also prepared by incorporating graphene materials and azobenzene systems. Here the components interact through self-assembly by employing various supramolecular interactions like hydrogen bonding, π-stacking etc. Wang and his group (Wang et al. 2011) fabricated a self-assembled graphene-azo polyelectrolyte multilayer film. The azochromophore utilized in the cationic polyelectrolyte (QP4VP-co-PCN) is a push-pull system. This polyelectrolyte then undergoes a layer by layer self-assembly (LBL) with negatively charged graphene sheet. The LBL films showed good capacitance property and can be employed as a electrochemical double layer capacitor (EDLC).

Nurbawono *et al.,* in 2013 (Nurbawono et al. 2013) proved theoretically that azobenzene molecules can induce a reversible photo-tuning of magnetism in transition metal-embedded graphene systems. The scanning transmission electron microscope (STEM) is used to create vacancies over the graphene surface and transition metals (TM) like Fe, Co, Ni and Mo can be deposited in those vacancies. The TM embedded graphene systems can have a magnetic moment ranging from $1\mu_B$ to $3\mu_B$. In their work they selected cobalt embedded in double vacancies of graphene. Th measured magnetic moment of this system is 1.3 μ_B. On adsorbing *trans* azobenzene over the cobalt embedded graphene system the magnetic moment value changes to 0.8 μ_B. The azobenzene on photo-isomerisation to *cis* form results in a drastic decrease in the magnetic moment until the value become 0.0 μ_B. Therefore, it is possible to reversibly switch the magnetic property of graphene

molecule by using azobenzene molecule. This photo-controlled magnetism results give higher hope in future magnetic spintronic devices.

Kim *et al.*, in 2011 (Kim et al. 2011) non-covalently latched a pyrene tethered azobenzene system over graphene. The azobenzene system DR1P, is the pyrene tethered disperse red 1 (DR1) dye. The non-covalent functionalization between DR1P and graphene through π-π stacking has resulted in p-doping of graphene with a hole concentration of $\sim 5 \times 10^{12}$ cm^{-2}. The reversible photoisomerization of azobenzene molecule in DR1P led to modulation of charge carrier concentration by $\sim \pm 1 \times 10^{12}$ cm^{-2} (up to ~18% of carrier concentration in DR1P/graphene) without altering the mobility of pristine graphene. Besides this ability of preserving the high mobility and modulation of doping, the entire system can function as a light gated transistor due to its sensitivity towards minute changes in electrostatic potential. This promises the development of a new class of optical interconnects.

In a similar way the methyl orange (MO), another dye containing azochromophore is non-covalently linked with graphene doping modulation. Among the two benzene rings in methyl orange, one ring is substituted with a dimethyl amine group, which is electron donating and the other ring is substituted with an electron withdrawing sulfonate group. The chemical doping of MO over graphene is then probed by Raman analysis. The Raman studies revealed that the *trans*-MO-modified graphene exhibits stronger doping than the *cis* counterpart. The electrical transport studies also supported this photo-reversible doping modulation in MO-Graphene. The difference in doping behavior induced by the two isomers arises due to the distinction in their geometrical alignment and interaction with

graphene molecule. The *trans*-MO aligns parallel to graphene surface and forms good π-π stacking. The dimethyl amine group over one benzene ring in MO is as hydrophobic as graphene and adheres to graphene through a hydrophobic interaction. On the other hand, the sulfonate group is hydrophilic resulting in a repulsive interaction between it and graphene. Upon UV illumination *trans-cis* photo-isomerisation occurs and this results in the lifting of sulfonate group along with the aromatic ring causing a decreased hole transfer efficiency from the azomolecule to graphene. This decreased charge transfer weakens the chemical enhancement and doping level. These hybrid systems promise a better platform for probing conformation transition at the sub molecular level (Peimyoo et al. 2012).

A monolayer of mechanically exfoliated graphene is placed over a gold surface functionalized with a mixed self-assembled monolayer (mSAM) made with an azobenzene unit (4-(1-mercapto-6-hexyloxy)-azobenzene) and with spacer molecule 6-mercapto-1-hexanol. The hybrid exhibited resonant oscillation of current density. This occurs due to the photo-isomerisation of azochromophore in them. The conductive atomic force microscopic (C-AFM) measurements proved that current resonance strength of hybrids can be gated on and off in a reversible manner through the reversible photo-isomerisation of azobenzene in mSAM. From the solutions of Dirac equation, the gating potential is approximately 7 ± 2 nm having strength greater than or equal to 0.5 eV. This promises more tuning of transport properties in such hybrid systems (Margapoti et al. 2014).

The graphene multilayers are transferred over the polymer film made from azomolecule. The graphene multilayer flakes function as nano-strain gauge over polymer films. Under UV illumination surface relief patterns get inscribed over the

polymer surface. The valleys in the optically inscribed surface relief gratings show more strain (0.45%) compared to other positions like hills, slopes etc. The experimental observations proved that internal pressure in the films due to surface relief grating pattern can exceed 1 GPa. Thus the multilayer graphene can be used as a nano-strain gauge which can quantitatively measure the optically induced mechanical forces developed during the surface relief grating formation in azopolymers (Di Florio et al. 2014).

Chen and his group (Chen et al. 2015) prepared another GO-AZO hybrid, where a cationic azosurfactant ($AzoC_7NO$) is linked with GO sheet through electrostatic interactions. Their self-assembly produces an aggregate which is able to disassemble upon UV irradiation and reassemble upon visible light irradiation.

The reason behind this is the change in polarity associated with the photoisomerization of azobenzene surfactant. The *trans* isomer has lower surface polarity and hence lower surface tension which favors assembly formation. The UV illumination results in *cis* surfactant with larger polarity leading to disassembly of the aggregate. The hybrids also exhibited photo-tuned conductance behavior. The cyclic voltammetry studies proved that the hybrids have distinct specific capacitance. The specific capacitance of GO- $AzoC_7NO$ hybrid increased from 51 $A.g^{-1}$ to 85 $A.g^{-1}$ upon UV illumination. Further exposure to blue light resulted in decrease in specific capacitance from 85 $A.g^{-1}$ to 63 $A.g^{-1}$. This hybrid materials can also be employed as photoresponsive super capacitors (Figure 1.17).

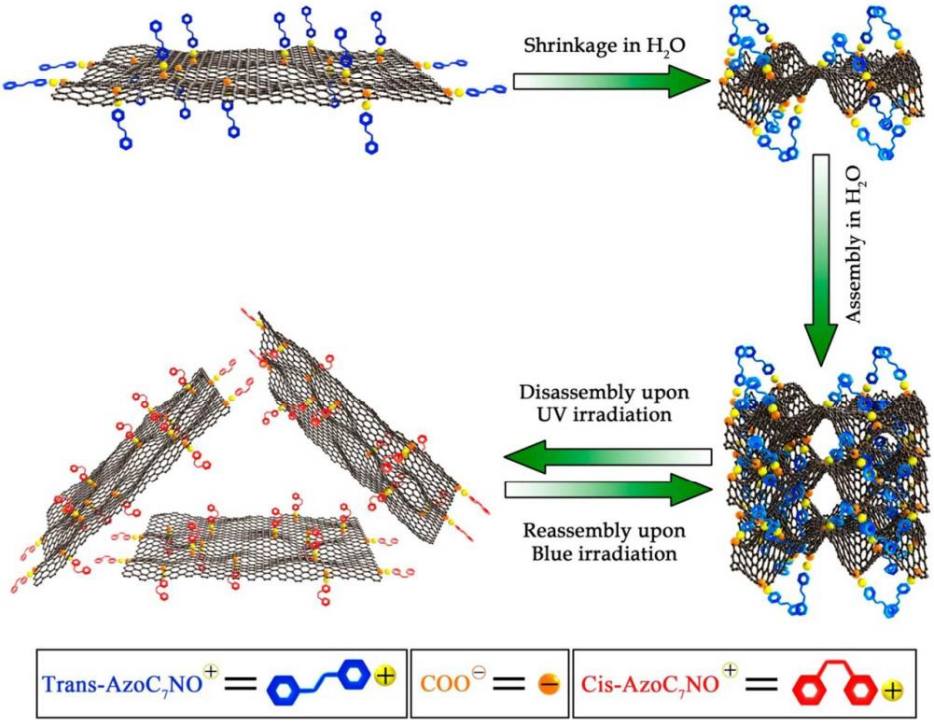

Figure 1.17: a) Schematic representation of photoresponse behaviour of cationic azobenzene-surfactant-modified graphene hybrid in water under light irradiation. Reproduced with permission from Ref [42] Copyright © 2015 The Royal Society of Chemistry.

1.4.3. Coupling of fullerene molecules with azobenzene molecules

Kay *et al.*, synthesized dendritic fullerenes where the fullerene system is the central core and azobenzene groups are attached at the periphery. Three different types of dendritic fullerenes are synthesized with a number of azobenzene peripheral groups as two, four and eight. The systems exhibited good thermal stabilitity and excellent photo-responsiveness. The studies with polarized optical microscopy proved that films derived from these dendritic fullerenes are uniform and non-birefrigent. Therefore they can be fabricated as highly stable non-scattering glasses (Kay et al. 2002).

In another work, azobenzene linked porphyrin-fullerene dyads are synthesized. Here the synthesis of dyad is made through two steps. Initially a free base tris-aryl-p-aminophenyl porphyrin is made to undergo oxidative heterocoupling reaction with p-aminophenylacetal followed by deprotection to yield an aldehyde. Then the free base porphyrin aldehydes are treated with fullerene and sarcosine to yield the final azolinked dyad. The The photophysical studies proved that for these kind of systems, charge recombination occurs with a magnitude 3 or 4 times slower than charge separation. This clearly establishes that in these systems back electron tranfer occurs within the Marcus inverted region (Schuster et al. 2007).

Sasaki and his group (Sasaki et al. 2008) constructed a photoactive nanovehicle, a nanoworm, by incorporating both fullerene molecule and the azobenzene system. The fullerene unit acts as the wheels of the nano vehicle upon which the azomolecule executes a worm like movement. The chassis and axles of the vehicle are made through ethynylic linkages. This completes the nanoworm structure. The photoisomerization capability of the nanoworm is then investigated. It is observed that the yield of photoisomerization is low due to the steric hindrance offered by the alkoxy groups and periconjugation effect exerted by fullerene moiety. This result imparts more insight into the photoactivated motion over the surface.

A tetraacidic azobenzene system NN4A synthesized by Li *et al.,* is capable of forming Kagome open network through hydrogen bonding interactions. The network consists of two different types of cavities differing in size as well as symmetry at the solid-liquid interface. The first cavity A-type is larger with size

around 12 A° and has a six-fold symmetry, where six benzene rings are attached through the hydrogen bonds. The B-type cavity arises from the triangular arrangement of three NN4A molecules with a cavity size around 8.6 A°. The network is capable of accommodating fullerene molecules in the cavities. The normal C_{60} does not have any selectivity towards the cavities but the bulkier C_{80} and $Sc_3N@C_{80}$ shows size specific selectivity towards A-type cavity. This result is promises the development of more supramolecular templates for fabricating functional molecular arrays (Li et al. 2008).A covalent assembly is synthesized by coupling N-methylfulleropyrrolidine (NMFP) and (E)-N,N-dimethyl-4-(*p*-tolyldiazenyl)aniline (AZNME) as constituents. The Assembly (E)-N,N-dimethyl-1,4-(*p*-pyrrolidinofullerenediazenyl)aniline (DPNME) shows self-organization in THF/water binary solvent.

The donor-acceptor dyad exhibited a solvent dependent dynamic equilibrium among the monomers, J-aggregate and H-aggregate. This aggregation behaviour is monitored by the supramolecular interactions like van der Waal's forces and π-π stacking between the components and through the intermolecular donor-acceptor interaction between electron-deficient fullerene ring and the electron-rich azo aromatic ring. An analysis with single crystal XRD proved that the system has a monoclinic unit cell with a C2/c space group. The supramolecular dyad is highly directional, π-extended and crystallizes in a layered manner. This is the first example of such a system realized between an azo molecule of linear geometry and conformationally rigid fullerene system (Figure 1.18 a & b) (Kumar et al. 2011).

The same group further explored the self-assembly behaviour of DPNME. Here they synthesized different hierarchical self-assembled structures through simple techniques Langmuir-Blodgett (LB), solution cast, immersion liquid-air and immersion in solid-air interfaces as a function of DPNME concentration, media pH, time, and supporting substrate characteristics. The resulting self-assembled structures are investigated through various spectroscopic and microscopic techniques and also by molecular modelling.

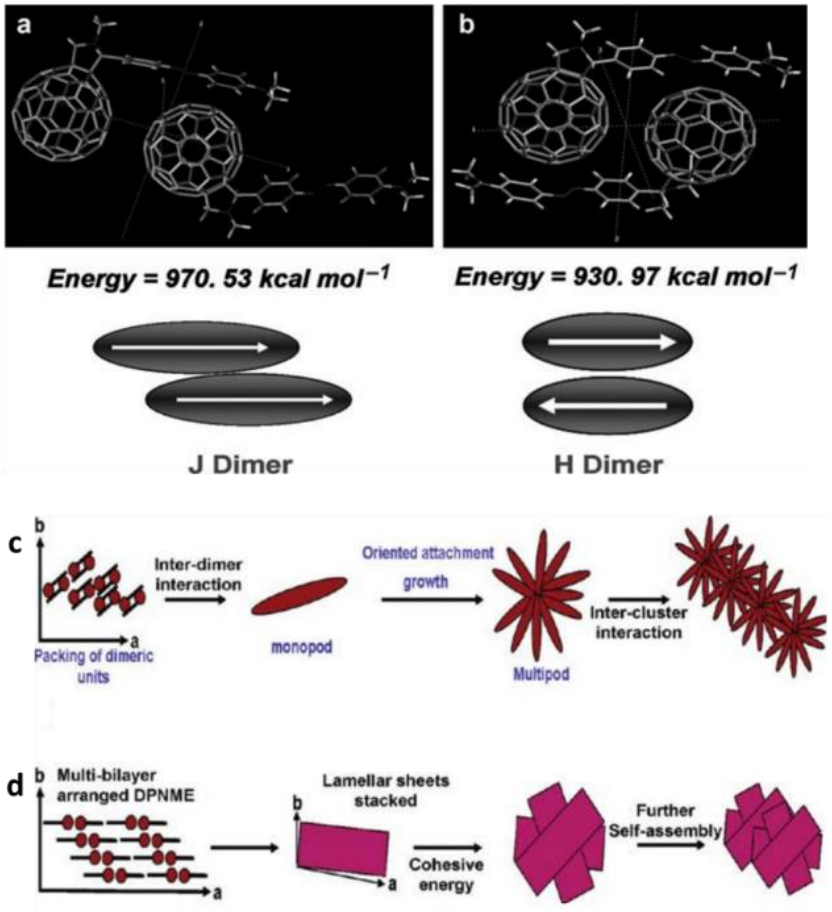

Figure 1.18: a) Molecular Mechanics (MM) geometry optimized structural patterns of a) J dimer & b) H dimer. Reproduced with permission from Ref [132] Copyright © 2011, John Wiley & Sons. Proposed mechanism for the self-assembly of DPNME under c) neutral and d) 1 mM acidified chloroform solutions through immersion growth method. Reprinted with permission from Ref [133] Copyright © 2011, American Chemical Society.

Different interactions like van der Waal's forces, π-π stacking and inter molecular donor-acceptor sharing play an important role in the self-assembly processes. Under neutral and acidic conditions, one-dimensional and two-dimensional structures are formed and further solvent evaporation results in multipods and stacked squares. The bilayer structures also evolve into flower shaped fractal objects. This controlled structure evolution from the fullerene-azobenzene dyads opens up a new pathway in the self-assembled systems (Figure 1.18 c & d) (Kumar et al. 2011).

Ortiz *et al.,* reported the synthesis of novel dendronized azo-dyes containing a fullerene C_{60} unit and a well-defined oligo(ethylene glycol) spacer. They synthesized six different types of such systems with different groups substituted at the para position of the azo molecule. Their optical characteristics were studied using UV-Visible spectroscopy as a function of dipole moment. Three of the systems exhibited higher dipole moment and the other three lower dipole moment. The presence of H-aggregates in all the derivatives are confirmed. The photo-protonation effects are studied in systems having highest and lowest dipole moments and their behaviour is found to be unaffected by the presence of fullerene-C_{60}. The photoisomerization ability of the systems is decreased compared to the free azo molecules since the fullerene system is a potential quencher. The investigation of photo-isomerisation in the cast films of fullerene-C_{60}-azobenzene indicated the presence of J-aggregates. But here also the photoisomerization yield is significantly reduced due to the quenching ability of fullerene system (Ortíz-Palacios et al. 2017).

1.4.4. Coupling of other carbon materials with azobenzene molecules

By grafting fluorescent carbon nanoparticles (CNPs) with azobenzene dendrons Wang *et al.*, prepared dendronized carbon nanoparticles. The azobenzene dendrons enhance the fluorescence ability of CNPs as they act as light antenna to harvest light energy. The particles show increased quantum yield with dilution and at low concentration (2.2×10^{12}/mL) the quantum yield of dendronized CNPs increased to 74 %. The enhanced fluorescence of CNPs upon grafting with non-fluorescent dendronized azomolecules is due to exposure to light. This generates additional excitons within azomolecules transverse to the energy bands within CNPs through inter-system crossing. This is a new direction in the field of functionalization of CNPs with photochromic molecules for opto-electronic applications (Figure 1.19a) (Wang et al. 2014).

Chiral carbon nanodots are synthesized from D-methionine, L-methionine, D-glucose, D-glucosamine, L-aspartic acid and L-alanine. The prepared D- and L-carbon dots interact differently with photochromic azobenzene molecules. The azomolecule in its *trans* form does not interact with the chiral carbon dots. On the otherhand the *cis* azomolecule interacts very well with the carbon dot and this is supported by UV irradiation experiments as there is a reduction in the intensity of prominent peaks in the UV-Visible spectra. The D- and L- carbon dots have different functional groups and hence different orientations. This also leads to a distinction in their behaviour upon coupling with *cis*-azomolecule. For the same irradiation time 20 minutes, the UV peaks of D- and L- carbon dots exhibited

different shifts and intensities for the UV peaks. Therefore, it is possible to deduce the exact chiral nature of carbon dots from their interaction with azomolecule under UV light (Figure 1.19b)(Deka et al. 2017).

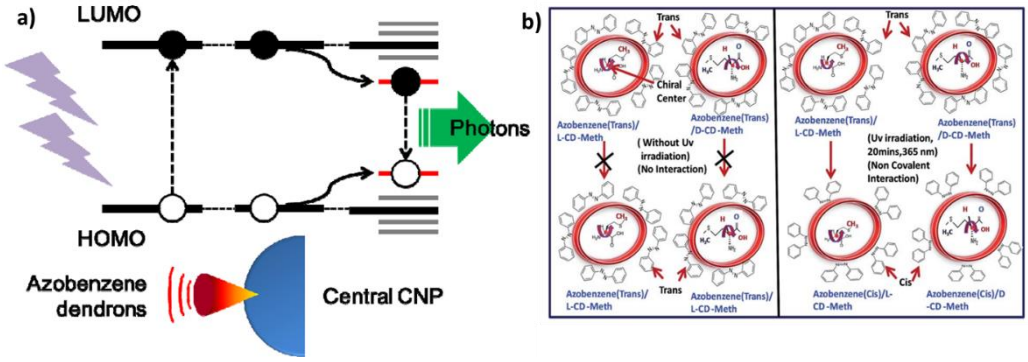

Figure 1.19: a) Mechanism for the enhanced emission of dendronized carbon nanoparticles. Reproduced with permission from Ref [279] Copyright © 2012 The Royal Society of Chemistry. b) Interaction of chiral carbon dots with azobenzene molecules. Reproduced with permission from Ref [48] Copyright © 2017 The Royal Society of Chemistry.

1.5. Scope and objectives of the present thesis

The coupling of carbon nanomaterials with photochromic molecules led to a large number of hybrid materials with applications in numerous fields. Among the photochromic molecules, azobenzene systems stand out as they exhibit low photobleaching rate, relatively medium change in dipole moment etc. The recent research scenario mainly focuses on greener materials and greener technology. This made the scientists working in molecular electronics to go for 'sustainable materials'. Thus, synthesis of organic molecules from bioresources became an active area of research. Only a few photochromic systems were developed from bioresources till date. The synthesis of bioresource based photochromic molecules is highly desirable as it will make the synthetic routes easier and economically

viable. The coupling of bioderived photochromic molecules with carbon nanomaterials is a step ahead. This leads to the development of sustainable molecular electronic materials within economically and environmentally viable reach.

Cardanol is a well-known bioresource material obtained from cashew nut shell liquid. Over the years cardanol is utilized for developing small molecules, polymers, dendrimers etc for various applications. The high reactivity and easy availability of cardanol makes it an interesting molecule to be explored further. Therefore, the synthesis of photochromic molecules from cardanol is very promising because of easy and cheap availability. The process of synthesis is also less complicated and rewarding because of the high yield.

The coupling between carbon nanomaterials and photochromic molecules is done through two different types of functionalization. The first one is the covalent functionalization. This method involves direct bond formation between the components through typical reactions like condensation, addition etc. The second type is non-covalent functionalization. Here the components interact with each other through hydrogen bonding and π-π stacking. Even though scientists have utilized both functionalization methods to fabricate hybrids between carbon nanomaterials and photochromic molecules, there are no reports till date which make a comparison of the two types of functionalization with the same components.

The present thesis therefore focuses on developing photochromic azobenzene systems from cardanol and coupling them with different carbon nanomaterials of varying dimensions. The specific objectives of this thesis are listed below.

i) Synthesis of azobenzene molecules from cardanol and coupling those molecules with carbon nanomaterials to produce photo-tunable hybrids.

ii) Developing fluorescence switch between cardanol derived azomolecule and zero-dimensional graphene quantum dot, which facilitates the construction of a sustainable molecular keypad lock and logic gate.

iii) Fabrication of sustainable conductance switches between cardanol derived azomolecules and carbon nanomaterials in three different dimensions: multi-walled carbon nanotube (one-dimensional), graphene oxide (two-dimensional) and single-walled carbon nanohorn (three-dimensional).

iv) Comparison of the mode of functionalization, covalent or non-covalent to find out which process is better for fabricating a perfect conductance switch.

******

Chapter 2

Construction of Fluorescence Switch from Graphene Quantum Dots and Photochromic Azobenzene Molecule derived from Bioresources

This chapter describes the synthesis of Graphene Quantum Dots (GQDs), a zero-dimensional carbon nanomaterial from a bioresource product honey. The GQDs emits a strong green fluorescence. A photochromic azobenzene system DOAZOC1 is derived from cardanol which is a biomaterial obtained as a fraction of cashew nut shell liquid. Both GQDs and DOAZOC1 are coupled and the binary system is utilized for selective screening of harmful carbamate pesticide, carbofuran. This process leads to the formation of a fluorescence switch, GQDs-DOAZOC1-Carbofuran.This switch has three distinct applications: a molecular logic gate, a molecular keypad lock and a molecular fluorescent probe.

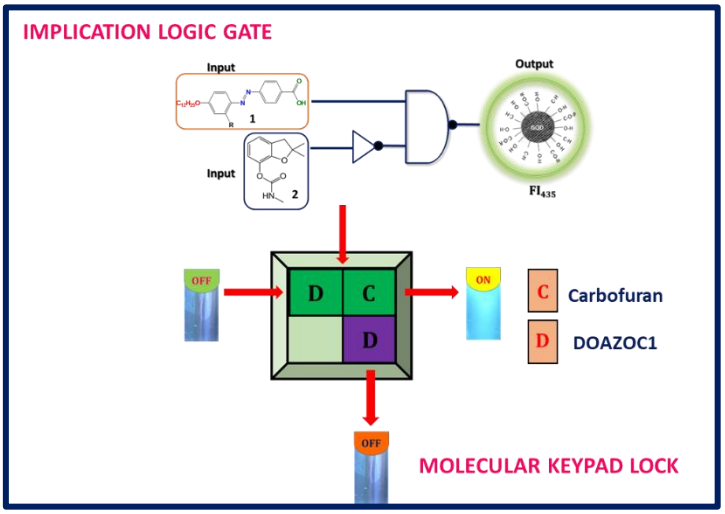

*Contents of this chapter was published in the following journals:

i) *Chemistry Select*., **2017**, *2* , 11615-11619.

ii) *Particle & Particle Systems Characterization.*, **2016**, *33* (2), 70-74.

2.1. Introduction

Graphene Quantum Dots (GQDs) is one of the fascinating members of the carbon nanomaterial family. It is one of the highly explored materials in the contemporary research scenario. The GQDs are basically nanosized fragments of graphene and possess a finite band gap. This band gap leads to a photoluminescence character in the GQDs and under the impact of strong quantum confinement and edge effect, they show strong luminescent nature (Tetsuka et al. 2016). The GQDs are characterized by other excellent properties like higher quantum yield, high photostability against photobleaching and blinking, tunable and narrow spectral emission, low toxicity, biocompatibility, dispensability in water etc. The fabrication of GQDs fall under two main categories namely, top-down and bottom-up approach. The top-down method deals with the breakage of carbonaceous materials into nano-dimensional structures through physical or chemical processes such as oxidation (Peng et al. 2012), electrochemical methods (Liu et al. 2011) etc. The bottom-up method deals with the synthesis of GQDs from components largely of organic origin through processes like carbonization etc (Dong et al. 2012).

Due to the switchover of preference to sustainable/green chemistry in the recent times, the synthesis of GQDs from bioresource materials has become a highly explored area in the carbon nanomaterial research (Mahesh et al. 2017). Recently one research group synthesized GQDs from dead neem leaves. Then they are modified as amine terminated GQDs (Am-GQDs) which exhibit enhanced

emission. The Am-GQDs selectively detect Ag^{+} ions in solutions (Suryawanshi et al. 2014). Chang *et al.* synthesized two types of GQDs: one from leaf extracts of neem (N-GQDs) and the other from fenugreek (F-GQDs) (Roy et al. 2014). Both exhibit strong green fluorescence, good photostability and also higher quantum yields. They find applicability as white light emitting diodes. Later the same group modified the N-GQDs with Annexin V antibody (AbA5). The (Ab_{A5})-modified GQDs (Ab_{A5}-GQDs) are then used for labelling apoptotic cells through *in vivo* process in zebrafish (Roy et al. 2015).

Another important source of GQDs is rice husk biomass. These GQDs marked with strong green fluorescence are good candidates in biomedical applications like cell imaging (Wang et al. 2015). Kalita *et al.*, in 2016 successfully synthesized GQDs from rice grain (Kalita et al. 2016). This is used in the imaging of HeLa cells. The GQDs are also derived from coffee grounds of coffee beans. They are then functionalized with poly (ethylene imine) (PEI) and the resulting highly emissive PEI-GQDs are then used for Fe^{3+} and Cu^{2+} detection, HeLa cell imaging and also for environmental analysis (Wang et al. 2016).

In this work, we synthesized GQDs from honey. Honey is extracted by bees from the nectars of flowers and this is an easily available bioresource. The method adopted for the synthesis of GQDs is emulsion template assisted carbonization. High quality, monodispersed GQDs are thus obtained and they show a strong green fluorescence. The GQDs are then coupled with a photochromic azobenzene system (DOAZOC1) derived from cardanol, another popular bioresource material obtained from cashewnut shell liquid. The binary system is then employed for the selective screening of the harmful pesticide Carbofuran. Further coupling of the binary

system with carbofuran yields GQD-DOAZOC1-Carbofuran which again is a fluorescence switch. This switch can be put to use in three devices, all molecular. They are a molecular logic gate, a molecular keypad lock and a molecular fluorescent probe.

2.2. Experimental Section

2.2.1. Reagents and Materials

All commercially available reagents and solvents were used without further purification. The honey is purchased from Dabur India and from local market. Solvents 1-Butanol and Methanol were purchased from Aldrich India and used without further purification. TEM grids (400 Mesh) purchased from Ted Pella Inc, USA were used. Silica gel plates were 250 µm thick, 60 F_{254} grade from Merck. Silica gel was grade 60N (Spherical, Neutral, 100-200 mesh) from Merck, India.

2.2.2. Preparation of GQDs

The GQDs were synthesized via emulsion-templated carbonization of carbohydrates. This method of synthesis proved to be a facile one with a good yield of nearly monodispersed GQDs. In this method, aqueous solutions of honey is emulsified in 1-Butanol. The hydroxyl functional group stabilizes the emulsion against coalescence. Since each emulsion contains a limited amount of honey molecule, the formation of undesirable bulk structures get prevented. This emulsion act as micro reactors. The nearly monodispersed GQDs were synthesized via carbonization of honey molecules allocated in water-in-oil emulsions (Scheme 1). To form the emulsions, a 10 wt % honey solution (aq.) was mixed with 1-Butanol and the mixture was aged at 80 °C under vigorous stirring for 1 hour. To the mixture

a catalytic amount of hexadecylamine was then added and the temperature was raised to 160 °C under argon to initiate the carbonization. The GQDs thus prepared were purified by centrifuging. This purified GQDs is then dissolved in Methanol (Kwon et al. 2012) (Mahesh et al. 2016)(Scheme 2.1).

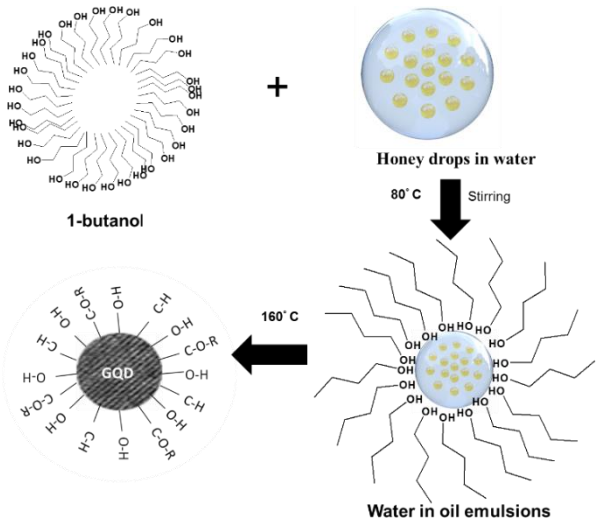

Scheme 2.1: Synthesis of GQDs from honey

2.2.3. Synthesis of 4-[(4-cardanyl) azo] benzoic acid (AZOC1) (3)

4-Aminobenzoic acid (1.371 g, 0.01 mol) (Sigma Aldrich, Mumbai) was dissolved in dilute HCl and diazotized with sodium nitrite (0.690 g, 0.01 mol in 2 ml of water) solution at 0 °C with stirring. The solution was diluted with chilled methanol (40 mL). Cardanol (3.005 g, 0.1 mol)(obtained by distillation of cashew nut shell liquid under vacuum) dissolved in a chilled solution of potassium hydroxide (1.077 g, 0.019 mol) in methanol (10 mL) was added drop-wise to the above solution. The diazonium coupling reaction forms a red dye. This was stirred for further 2 hours and poured into dilute HCl solution. The red solid separated was

filtered, washed thoroughly with water, and dried. The dye was then purified by column chromatography on silica gel (100–200 mesh) using a mixture of petroleum ether and ethyl acetate as eluent. The solvent was removed by evaporation and the product was recrystallized from petroleum ether (Saminathan and Pillai 2000).

Yield: 3.02 g (67 %), red flakes; m.p.134-135 °C

IR (KBr; cm^{-1}): 3298 (Ar-OH), 2860(-CH_2-), 1686 (Ar-COOH), 3020,790 (-CH=CH), 1575(-N=N-)

^{1}H NMR (500 MHz, Acetone d_6) δ : 8.06-7.82(d,2H), 7.62-7.80 (d,2H), 7.53-7.47 (m,2H), 6.67-6.77 (s,1H), 6.66-6.59 (d, 1H), 5.18-5.183 (m, -CH=CH-), 3.04-3.0 (s,2H),1.90-1.92(m,2H),1.85-1.92(m,6H),1.23-1.57(m,2H), 1.12-1.23(m,14H),0.7-0.75(m,2H) ppm

^{13}C NMR (Acetone d_6) δ: 13.3; 22.4, 28.5, 29.0, 29.3, 30.8, 31.5, 31.9, 113.9, 114.8, 116.4, 116.8, 121.9, 129.4, 130.5, 131.4, 143.5, 146.6, 155.5, 161.5, 166.4 ppm.

HRMS-FAB: $[M]^+$ Calculated for $C_{28}H_{38}N_2O_3$: 450.29, found: 450.81.

2.2.4. Synthesis of 4-[4-dodecyloxycarbonyloxy-2-pentadecyl phenylazo] benzoic acid (DOAZOC1)(1)

AZOC1 (2 gm, .0030 mol) was dissolved in 50 ml methanol and 2 ml Conc.H_2SO_4 is added to it. The mixture is refluxed for 24 hours. Then the methanol is evaporated in a rotary vapour. To the residue, 50ml *N*,*N*-DMF and 7.5 g of KOH are added. The mixture is kept refluxing at 80°C. After 10 minutes, 20ml of 1-bromododecane is added and the refluxing is continued for further 96 hours. The compound is extracted using dichloromethane after acidifying with dilute HCl. It is then purified by column chromatography on neutral alumina using petroleum ether

as eluent. The solvent is removed by evaporation and the purified product is recrystallized from Tetrahydrofuran (Devi et al. 2016) (Scheme 2.2).

Yield: 1.5gm (55%), red coloured viscous liquid

IR (KBr; cm^{-1}): 3461(Ar-COOH), 2920, 2847(-CH_2-), 1726(Ar-COOH), 3012, 777(-CH=CH-), 1594 (-N=N-), 1212(Ar-C-O-), 1113 (R-C-O-Ar).

^{1}H NMR (500 MHz, toluene d_8) δ: 8.25-8.23(d, 2H), 7.96-7.94(d, 2H), 7.09(s, 1H), 6.79- 6.78(d, 1H), 6.62-6.60(d,1H), 5.43-5.39(m, CH=CH-), 4.21-4.19(t, 2H), 3.20-3.17(t, 3H), 2.09-1.99(m, 5H), 1.74-1.57(m, 4H), 1.39-1.25(m, 32H), 0.94-0.88(m,6H) ppm.

^{13}C NMR (toluene d_8) δ: 13.7, 14.1, 22.6, 22.8, 26.0, 27.2, 28.7, 28.9, 29.2, 29.3, 29.5, 29.8, 31.7, 31.9, 32.2, 112.5, 114.6, 117.0, 122.4, 129.7, 129.9, 130.5, 131.3, 144.6, 146.5, 155.6, 162.7, 166.2 ppm.

ESI-MS: [M+1] Calculated for $C_{40}H_{62}N_2O_3$: 619.48, Found: 619.48

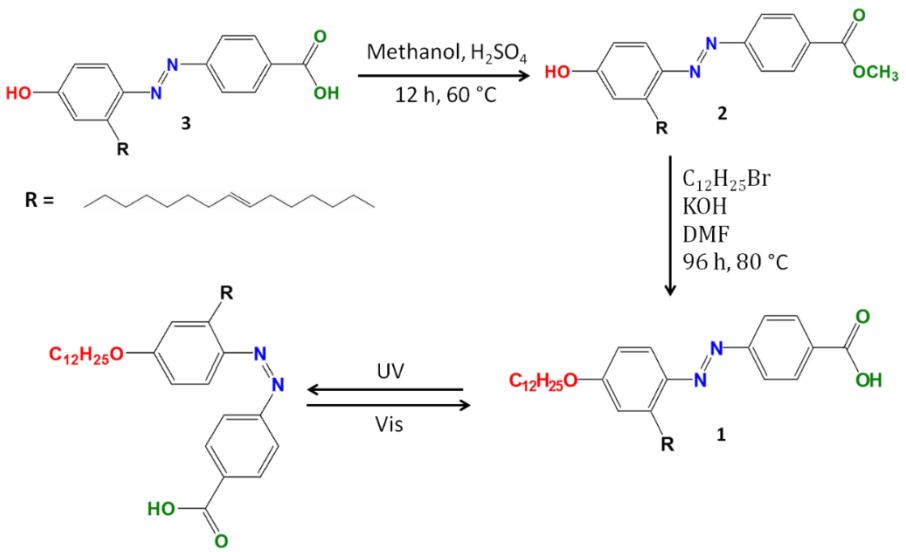

Scheme 2.2: Synthesis of DOAZOC1 (**1**)

2.2.5. Instrumentation

UV-Vis absorption spectra of GQDs and DOAZOC1 dissolved in methanol was taken using Varian Cary Bio 100 UV Spectrophotometer with wavelength ranging from 210 nm to 600 nm at room temperature. For Photoluminescence (PL) characterization, the excitation and emission spectra of the GQDs solution and mixtures with DOAZOC1 and carbofuran were recorded using a Fluoromax-4 spectrofluorometer (Horiba Scientific). The lifetime measurement was done using 340 nm LED source. A diffused reflectance Fourier Transform Infrared (FTIR) spectrum of the samples was taken on Perkin-Elmer Spectrum 100 FTIR spectrophotometer at room temperature. ^{1}H NMR and ^{13}C NMR spectra of azobenzene molecules were recorded using Bruker AV III 500 MHz FTNMR spectrometer. toluene-d_8 and acetone-d_6 formed the solvents with TMS as internal standard. Mass spectra of azobenzene systems were recorded under ESI/HRMS using Thermo scientific Exactive mass spectrometer and also by HRMS-FAB.

X-ray photoelectron spectroscopic studies (XPS) was carried out with Kratos Analytical Axis Ultra X-ray photoelectron spectrophotometer equipped with a monochromatic Al Kα X-ray source. X-ray diffraction (XRD) analysis of the obtained powder was performed with a Bruker AXS D8 Advanced X-ray diffractometer of Cu Kα radiation (λ=1.54 Å). Raman spectrum of the samples was recorded using a WiTech alpha 300 Raman System with Laser excitation source at 488 nm. TEM imaging was performed on a JEOL-JEM0310 microscope with an

accelerating voltage of 300 kV. Samples were prepared by drop casting the GQDs solution in methanol over carbon coated copper grids (400 meshes).

2.3. Results and Discussion

2.3.1. Characterization of GQDs

The morphology of the GQDs prepared from bioresource is analyzed by transmission electron microscopy (TEM) (Figure 2.1). The monodispersed GQDs possess an average diameter around 2.4 nm. The full-width at-half-maximum (FWHM) of the fitted Gaussian curve is 0.48 nm, which corresponds to the narrow

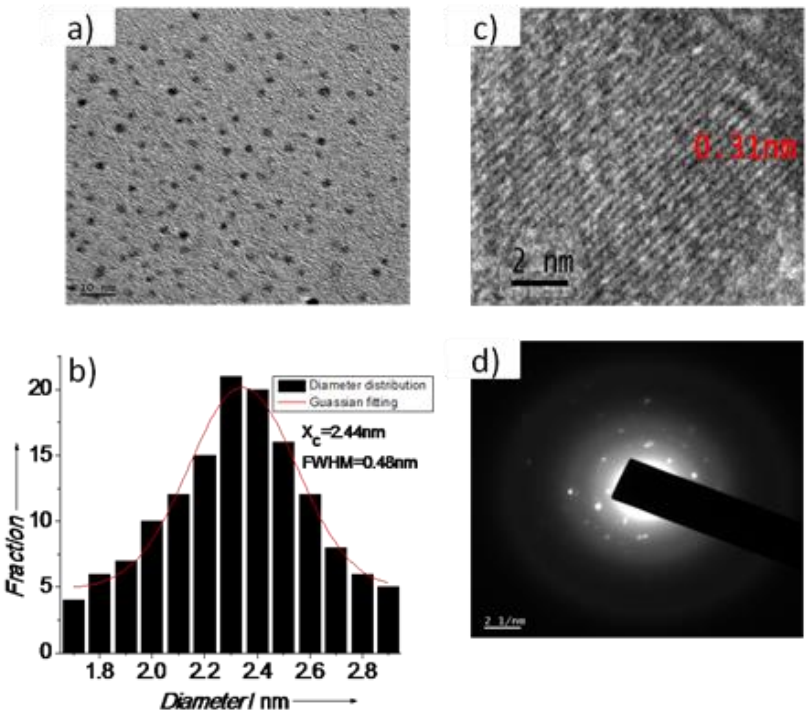

Figure 2.1: a) TEM image of the GQDs assembled on Cu grid coated with ultrathin amorphous carbon film b) Diameter distribution of the GQDs, the red line is the Gaussian fitting curve c) HRTEM image of GQD d) SAED pattern of the GQD

distribution nature of the GQDs. The high-resolution TEM (HRTEM) studies reveal the high crystallinity and uniform size of the synthesized GQDs. The d spacing between the graphene layers is 0.31 nm which corresponds well with that of basal plane distance of bulk graphite, which is 0.335 nm.

The selected-area electron-diffraction (SAED) pattern exhibited the presence of detectable rings confirming the crystalline nature of GQDs. Well-resolved lattice fringes with an interplanar spacing 0.31 nm was observed. This is close to that of (100) facet of graphite.

Further characterization with Fourier transform infrared (FTIR) spectroscopy revealed the type of functional groups present in the GQDs. The FTIR spectrum exhibits characteristic absorption bands of O–H stretching vibrations at 3319 cm^{-1}, C=O stretching vibrations at 1659 cm^{-1} and a peak centered at 1551 cm^{-1} caused by C=C stretching. The absorptions at 1027 and 1076 cm^{-1} are attributed to C–O and absorptions at 1360 and 2927 cm^{-1} are due to the existence of C–H group (Figure 2.2 a).

The X-ray photoelectron spectroscopy (XPS) supported the existence of carbon (C_{1s}, 284 eV) and oxygen (O_{1s}, 532 eV). The measured spectrum of C1s can be deconvoluted into five surface components, corresponding to sp^2 (C=C) at a binding energy of 284.5 eV, C–OH at 286.7 eV, C–O–C at 287.4 eV and C=O at 289 eV. The deconvoluted spectrum of O_{1s} shows two peaks at 531.2 and 532.3 eV corresponding to C=O and C–O groups respectively. The high carbon to oxygen ratio (C:O = 87.72:12.28) shows that the quantum dots are graphitic in nature

(Figure 2.2 b). The Raman spectroscopy gave corroborating evidence to the formation of GQDs. The GQDs shows a G band at 1593 cm^{-1} which is attributed to sp^2 carbons, and a D band at 1364 cm^{-1} attributed to sp^3 carbons. The intensity ratio between the disorder D band and the crystalline G band (I_D/I_G) is found to be 0.93 (Figure 2.2 c). The GQDs exhibit a broad peak at 20° in the X-ray diffraction analysis with a d-spacing around .401 nm (Figure 2.2 d).

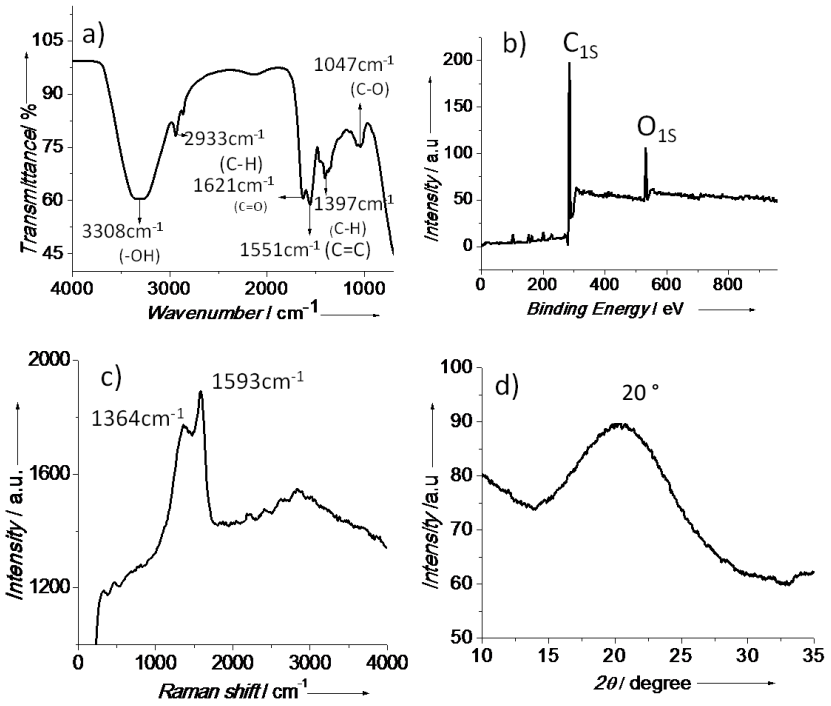

Figure 2.2: a) FTIR spectrum of GQDs b) XPS survey spectrum of GQDs. c) Raman spectra of GQDs d) XRD pattern of GQDs

The UV-Visible absorption studies showed the presence of two peaks in GQDs. The absorption peak at 267 nm is due to π–π* transition of C=C bond and the absorption at 340 nm corresponds to π–π* transition of C=O bond (Figure 2.3 a). It is observed that under UV light, the GQDs have a strong green emission. The photoluminescence studies are conducted with a fluorometer. Upon excitation at

340 nm, the GQDs exhibited a broad peak around 435 nm along with a strong green fluorescence under UV light (Figure 2.3 b). GQDs are derived from honey which is non-fluorescent. But the derivative GQD is fluorescent.

The GQDs also have an excitation dependent fluorescence behavior. Upon changing excitation wavelength from 340 to 500 nm, the emission spectra shifts from 435 to 520 nm (Figure 2.3 c). It is observed that the emission peaks are red

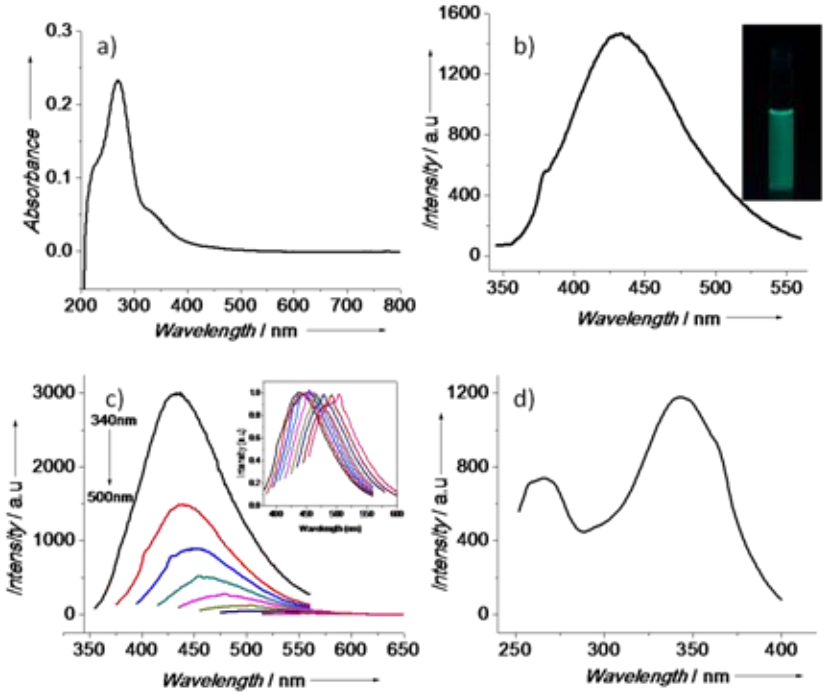

Figure 2.3: Optical properties of the GQDs. a) UV-visible spectra of GQD. Inset is the photograph of the corresponding GQD under UV light) PL (at 340nm excitation) spectrum of GQD c) The excitation-dependant PL behaviour of GQDs, GQDs were excited at wavelengths ranging from 340nm to 500nm (10nm interval) Inset; the normalized PL emission spectra d) PLE spectra of GQD.

shifted and intensity is decreased. The formation of electronic conjugated structures, which acts as emissive traps are responsible for this phenomenon. The fluorescent emission is due to the presence of functional groups on the surface of

the GQDs. The photoluminescence excitation spectrum (PLE) of the GQDs is recorded by monitoring the emission at 420 nm. Two peaks are obtained at 265 nm (4.679 eV) and 340 nm (3.647 eV) (Figure 2.3 d).

The quantum yield of the GQDs is 3.6%. This low value indicates the aggregation behavior. Further evidence for the aggregation behavior is obtained from variable temperature fluorescence studies (Figure 2.4). When the temperature increases, the intensity of fluorescence emission increases. This is due to the breakage of hydrogen bonding as well as the π-π stacking between the aggregates.

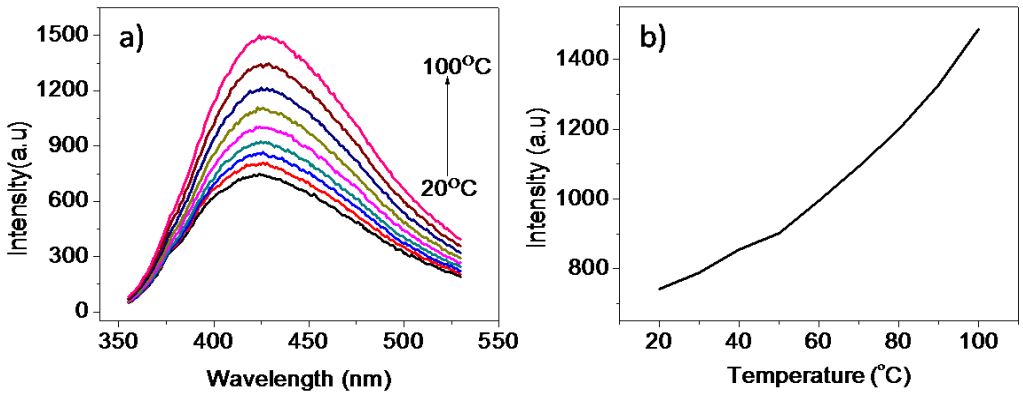

Figure 2.4: Temperature dependent emission spectrum of GQD

The fluorescence lifetime (τ) measurements of GQDs are done using a 340 nm LED source. The decay curves are fitted with three exponential functions, a fast component (τ_1 = 0.129 ns) and two slow components (τ_2 = 2.36 ns and τ_3 = 8.165 ns). The slow components correspond to the oxygen present in GQDs (Figure 2.5).

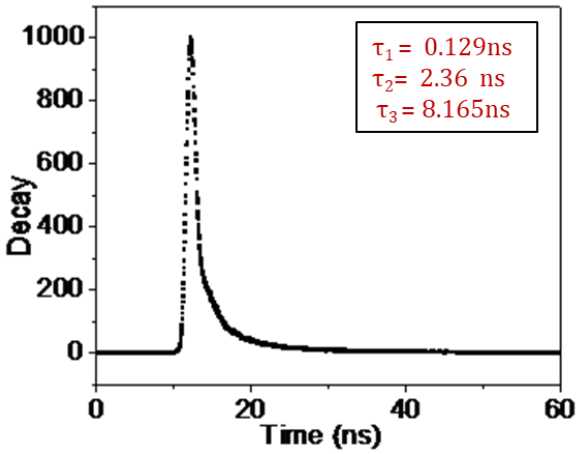

Figure 2.5: Decay profile of GQD.

2.3.2. Construction of IMPLICATION Logic Gate and Molecular Keypad Lock

The increasing speed of daily life demands the regular upgradation in the field of technology, especially in electronics. The miniaturisation of the electronic devices to the molecular level have contributed to the tremendous revolution in the smart material scenario (Xiang et al. 2016). Scientists have been exploring various molecular machines over the time ranging from molecular motors,(Browne et al. 2006; Kassem et al. 2017) molecular switches,(Feringa et al. 2001) shuttles,(Zhu et al. 2012) sensors(Valeur et al. 2000) and logic gates(Sreejith et al. 2012),(de Silva et al. 1993),(Nie et al. 2017),(Andréasson et al. 2015). The main advantage of these molecular systems is that their response can be controlled and monitored with external stimuli such as heat, light,(Yagai et al. 2008) pH,(Ahn et al. 2015) electric field(Schindler et al. 2006) etc. Among the various molecular devices in use the keypad locks are least exploited. These keypad locks are capable of protecting information at a molecular level (Misra et al. 2012). The unlocking of these

information is possible only upon the correct sequential combination of the chemical inputs (Guo et al. 2007). Due to this important feature, it is possible to set a particular password for each keypad lock. Unless this password is used the system cannot be unlocked (Margulies et al. 2007). The advantage of a molecular keypad over the conventional electronic pad is that the former is more susceptible to external stimuli than the latter.

There are some available reports on molecular keypad locks based on organic systems (Suresh et al. 2008; Wang et al. 2010; Ritchie et al. 2017) ,(Andréasson et al. 2009; Carvalho et al. 2015),(Kumar et al. 2009). The fluorescent carbon dots (carbon quantum dot and graphene quantum dot) are a new class of materials with potential application as molecular electronic devices (Bak et al. 2016). But to the best of our knowledge this avenue has not been explored so far in the development of keypad locks from the graphene quantum dots (GQDs). Here a molecular keypad lock was constructed by utilizing the sustainable bioresource derived components. The components of the keypad lock include GQDs derived from honey (Mahesh et al. 2016) and a photochromic azobenzene system derived from cardanol (Devi, et al. 2016). This is the first example of such a molecular keypad lock that can be developed using components of sustainable origin.

As mentioned earlier, an IMPLICATION Logic Gate can also be constructed using the same inputs and output. Here the chemical inputs are the photochromic azobenzene system DOAZOC1 and harmful carbamate pesticide carbofuran. The fluorescence of GQDs are ON only when the inputs are added in the correct sequence in the exact combination. Thus, it is evident

that the molecular system derived from sustainable bioresource components can be utilized for three distinct applications like a molecular keypad lock, a molecular logic gate and a molecular fluorescent probe.

The UV-Visible spectrum of DOAZOC1 (Figure 2.6) shows an absorption maximum corresponding to π-π* band at 372 nm and n-π* band at 258 nm. The π-π* band of DOAZOC1 shows a blue shift from 372 nm to 365 nm upon complex formation with GQDs. Similarly, the peak of GQDs at 266 nm shows a red shift to 280 nm and n-π* of DOAZOC1 at 258 nm is shifted to 232 nm.

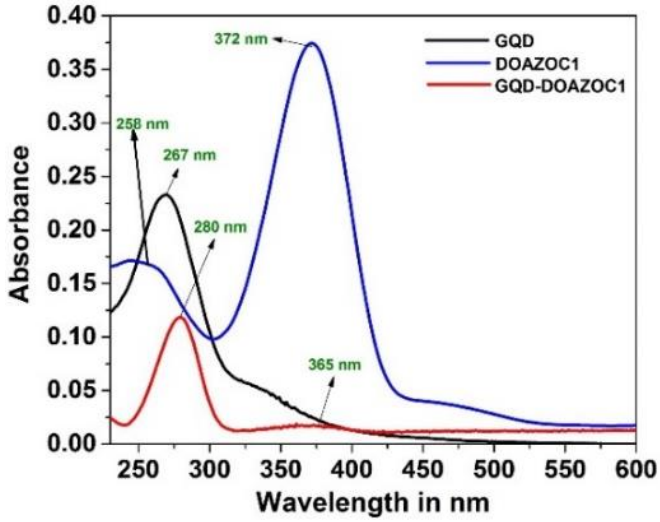

Figure 2.6: UV-Visible absorption spectra of GQDs, DOAZOC1 and complex GQDs-DOAZOC1

These observations clearly depict formation of the adduct between GQDs and DOAZOC1. The absence of new absorption peaks in the mixture of GQDs and DOAZOC1 indicates that no non-emissive substance is formed during the complexing between GQDs and DOAZOC1 (Liang et al. 2016) and also there is no ground state interaction between them (Ghosh et al. 2015).

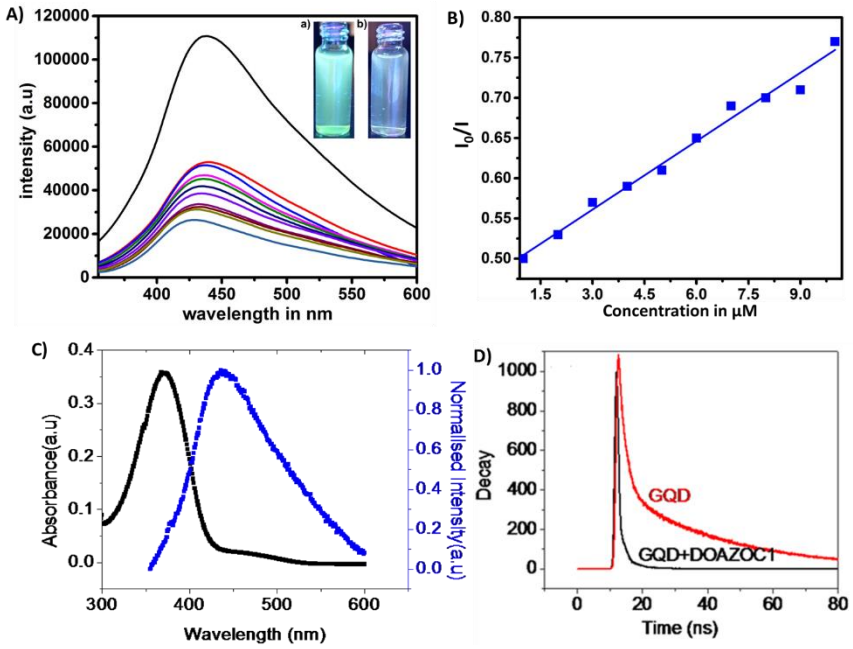

Figure 2.7: A) Fluorescence spectra of GQDs and complex GQDs-DOAZOC1.Inset is the visual fluorescence of A) GQDs b) GQDs-DOAZOC1 complex. B) Stern Volmer plot for quenching of GQD by DOAZOC1. C) Absorption spectra of DOAZOC1 (black) and the Emission spectra (blue) of the GQDs. D) Comparison of decay profile of GQD and GQD-DOAZOC1 complex.

When a solution of DOAZOC1 in methanol at a concentration of 10^{-4} M is added to GQDs solution, a fluorescence quenching of GQDs occur (Figure 2.7 A). It is observed that there is no significant overlap between the absorption spectra of DOAZOC1 and the emission peak of the GQDs (Figure 2.7 C). The possible reason for the fluorescence quenching of the GQDs by DOAZOC1 may be the photo-induced electron transfer (PET) and the hydrogen bonding between GQDs and DOAZOC1.

Generally, the GQDs are good electron acceptors,(Li et al. 2011) whereas DOAZOC1 with two nitrogen atoms are good electron donor (Ghosh, Chatterjee et al. 2015).Fluorescence lifetime (τ) measurement is used to understand the excited

state quenching mechanism of GQDs. The fluorescence lifetime of GQDs and GQDs- DOAZOC1 are assessed by time resolved photoluminescence measurements using 340 nm LED source. (Figure 2.7D). The typical decay curve is the best one fitted with multi exponential function which suggests that multiple radiative species are present in the samples. Hence, it is necessary to consider the average lifetimes of the decaying species (Bhunia et al. 2013). The average lifetime of the GQDs and GQDs - DOAZOC1 are found to be 6.2 and 4.3 ns respectively. The reduction in the average lifetime of GQDs - DOAZOC1 confirms the occurrence of PET in the system. Hydrogen bonding also plays a crucial role in the quenching of fluorescence of GQDs.(Sun et al. 2013; Hwang et al. 2016). The GQDs are derived from honey which is rich in sucrose. As such there are a large number of hydroxyl functional group on the surface of GQDs. This makes a strong hydrogen bonding with DOAZOC1 and thereby decreases the fluorescence intensity (Figure 2.8).

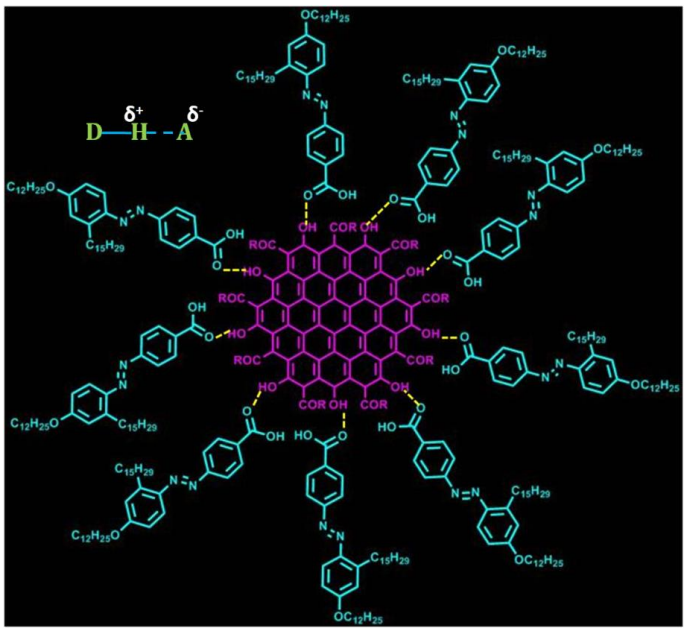

Figure 2.8: Pattern of hydrogen bonding between GQDs and DOAZOC1

The fluorescence quenching process is further analyzed by Stern-Volmer (S-V) relation $F_0/F=1+K_{SV}[Q]$ (Dhenadhayalan et al. 2012). From Figure 2.7 B, it is clear that DOAZOC1 possess a good linear relationship in the concentration range 2-6µM. A linear dependence with the correlation coefficient value of 0.99257 would suggest dynamic quenching process. The value of K_{SV} as obtained from the Stern-Volmer plot for DOAZOC1 is 2×10^3 M^{-1}.

The fluorescence property of GQDs - DOAZOC1 system is used for the detection of poisonous carbofuran pesticide. Different concentrations of carbofuran solution are added to the GQDs–DOAZOC1.The enhancement in fluorescent intensity with increasing concentration of carbofuran is observed (Figure 2.9 A).

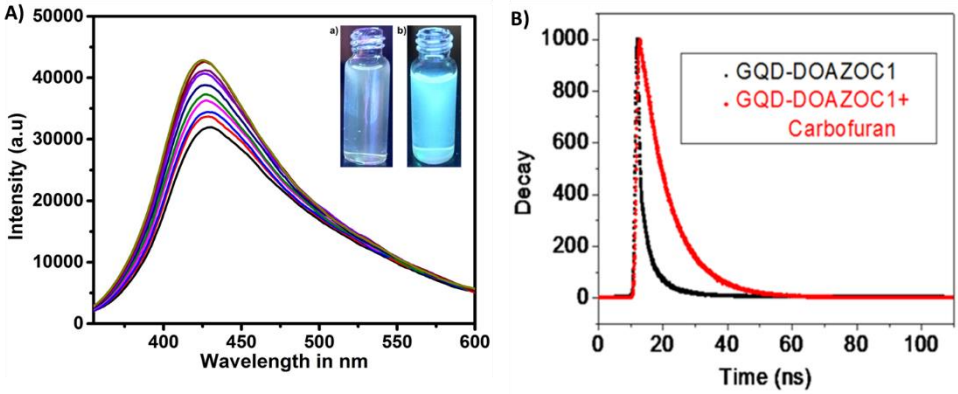

Figure 2.9: A) Fluorescence spectra of GQDs-DOAZOC1-CARBOFURAN complex. Inset is the visual fluorescence of a) GQDs-DOAZOC1 b) GQDs- DOAZOC1-CARBOFURAN complex. B) Comparison of decay profile of GO-DOAZOC1 complex and that in presence of Carbofuran.

The time resolved fluorescence analysis also confirms the enhancement in the fluorescence intensity. After the addition of carbofuran, the average lifetime of GQDs – DOAZOC1 system is increased from 4.3 to 5.2 ns. This confirms the dissociation of DOAZOC1 from the complex (Figure 2.9 B). This fluorescent enhancement is due to the dissociation of GQDs from DOAZOC1 after the

introduction of carbofuran. This is because of the fact that DOAZOC1 shows higher affinity to carbofuran than the GQD.

When carbofuran approaches the GQDs- DOAZOC1 complex there occurs a competition in hydrogen bonding between GQDs and DOAZOC1 with carbofuran. Since the hydrogen bonding between the amide group (carbofuran) and carboxylic acid group (DOAZOC1) is strong compared with that of hydroxyl group (GQD), (Figure 2.10) addition of carbofuran enhances the fluorescent intensity by dissociating the GQDs-DOAZOC1 complex. The typical enthalpy of the hydrogen bond between the hydroxyl donor and oxygen acceptor is 21 kJ/mol whereas that between amide donor and oxygen acceptor is 8kJ/mol.

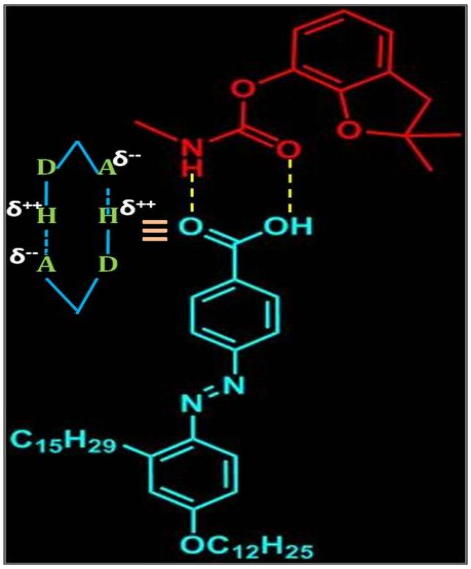

Figure 2.10: Pattern of hydrogen bonding between Carbofuran and DOAZOC1

So, the complex between carbofuran and DOAZOC1 possess a total enthalpy of 29 kJ/mol compared to 21 kJ/mol between GQDs-DOAZOC1.

This additional enthalpy factor favours the dissociation of GQDs-DOAZOC1 upon addition of carbofuran (Emsley 1980; Larson et al. 1984).

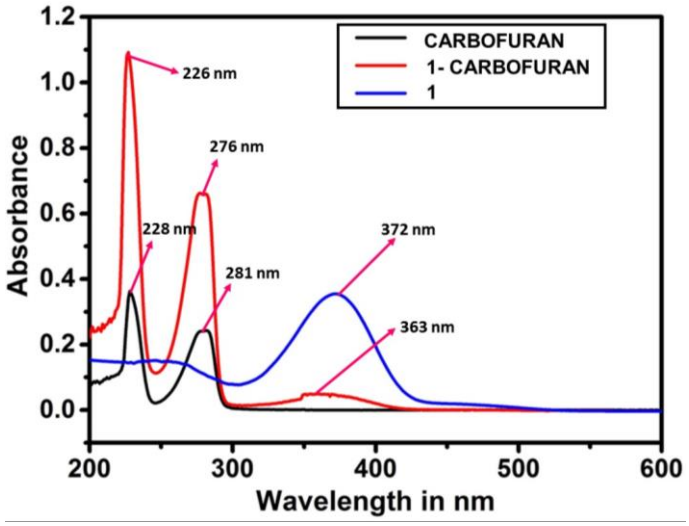

Figure 2.11: The UV-Visible absorption spectra of Carbofuran, DOAZOC1 (**1**) and DOAZOC1-Carbofuran complex.

The formation of complex between DOAZOC1 and carbofuran interferes and diminishes the PET effect in GQDs-DOAZOC1 complex. This is clearly evident from the UV-Visible absorption spectra (Figure 2.11). Upon complex formation the π- π* band of DOAZOC1 shows a blue shift around 9 nm ; the carbofuran peak at 281 nm shifts to 276 nm and 228 nm goes to 226 nm.

The stoichiometry for the interaction of GQDs-DOAZOC1 with the carbofuran is analysed by Benesi-Hildebrand plot (Figure 2.12 A). The association constant (K_a) is calculated by dividing the intercept with the slope of the straight line which gave the value of 1.074×10^{-3} mol^{-1}. The detection limit is found to be 0.68μM (Figure 2.12 B).

The selectivity for carbofuran was established by further experiment. The influence of fluorescent intensity of four different pesticides other than carbofuran on the GQDs-DOAZOC1 system was studied. These pesticides were diazinon,

phorate, malathion and carbaryl. It was proved that the GQDs-DOAZOC1 system has high degree of selectivity for carbofuran (Figure 2.12 C).

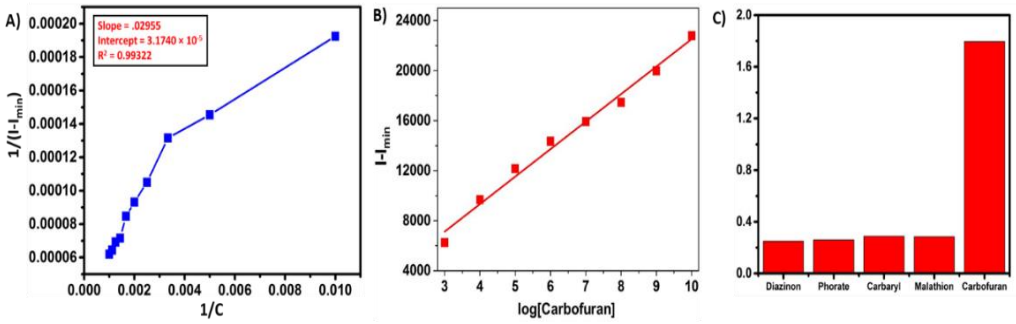

Figure 2.12: Benesi–Hildebrand plot of GQD-DOAZOC1 complex with Carbofuran. The excitation wavelength is 340 nm and the observed wavelength is 428 nm. B) The detection limit of GQD-DOAZOC1complex for Carbofuran is estimated from plot of normalized fluorescence changes of complex verses Log [Carbofuran] using equation $10^{-(\text{Slope/Intercept})}$ C) Selectivity studies of Carbofuran with other pesticides.

A molecular logic gate is developed by observing the change in the fluorescence intensity of the GQDs – DOAZOC1 by the addition of carbofuran. The excitation wavelength for all the logic functions was set at 340 nm and the emission wavelength is taken as 435 nm. DOAZOC1-Carbofuran induced fluorescence of the GQDs enabled the design of "IMPLICATION" logic system based on Boolean operations (Figure 2.13 A).

For input, the presence of DOAZOC1 or Carbofuran is defined as "1" and the absence as "0". The fluorescence intensity at a wavelength of 435 nm (FI_{435}) is defined as the output (0 or 1) for the logic gate. Only with the input of DOAZOC1 and without carbofuran (1/0), the fluorescent intensity is low and the output is "0" which implies off state (Curve pink in Figure 2.13 B). With all other possible input combinations [(0/0), (0/1), (1/1)], the output signal is "1" which corresponds the on state. With no input or with the input carbofuran alone, there is no change in the

fluorescent intensity. The output signal remains at “1”. When the system is subjected to the two inputs together, there is more interaction between DOAZOC1 and carbofuran. This results in the release of DOAZOC1 from the GQDs.

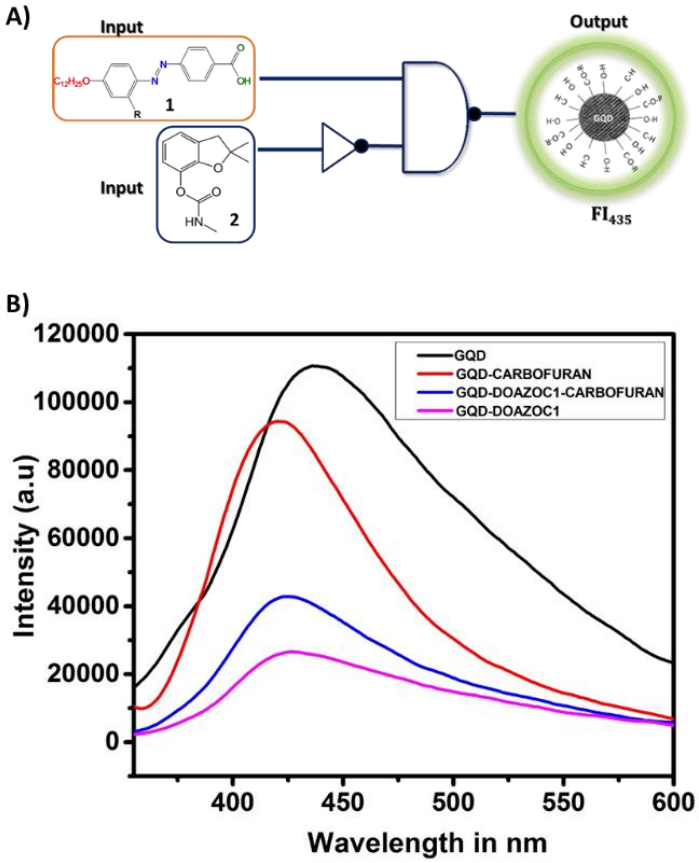

Figure 2.13: A) IMPLICATION Logic Gate designed with DOAZOC1 and Carbofuran as inputs. The output is the measurement of fluorescence intensity of GQD. B) Comparison of Emission Spectra of GQDs, GQDs-DOAZOC1, GQDs-carbofuran and complex GQDs-DOAZOC1-carbofuran

The output signal is 1. The truth table (Table 2.1) contains the details of all combinations. The symbol of the IMPLICATION logic gate is represented in Figure 2.13 A.

Input		Output
DOAZOC1 (1)	**Carbofuran (2)**	**FI_{435}**
0	0	1
1	0	0
0	1	1
1	1	1

Table 2.1: Truth Table

The system is then employed as a security device to store the information at the molecular level. The important criteria that must be satisfied for the system to act as a molecular keypad lock is that, it should get unlocked only by a particular sequence of chemical inputs.(Liu et al. 2012).The system is then examined to find out whether the emission of GQDs-DOAZOC1 complex is sequence dependent or not.

The emission intensity at 340 nm is monitored for the system. If the fluorescence intensity I>30 the output is '1' and if I<30 it is '0'. The emission intensity of GQDs at 340 nm is dependent on the sequence of addition of inputs DOAZOC1 and carbofuran. From the Figure 2.14 it is clear that in the sequence where DOAZOC1 is first added to GQDs followed by carbofuran the output is '1'. On the other hand, a reversal in the sequence produces an output of '0'. The probable reason for the change in output in the sequence GCD is that the initial bonding between GQDs and carbofuran may cause a reduction in number of the carbofuran units available for the coordination with DOAZOC1, thereby decreasing the fluorescence recovery of GQDs.

A molecular keypad lock is constructed to visualize this sequence dependent addition. It appears as a crossword puzzle which can be solved by the correct password only. As given in Figure 2.17, the chemical inputs DOAZOC1 and carbofuran are represented by the letters 'D' and 'C'. When the sequential input 'D' is executed first followed by 'C' the emission at 340 nm becomes switched ON. Therefore, the password 'DC' can unlock the system. In contrast when the input 'C' is executed first, by 'D', the system is OFF due to low emission at 340 nm.

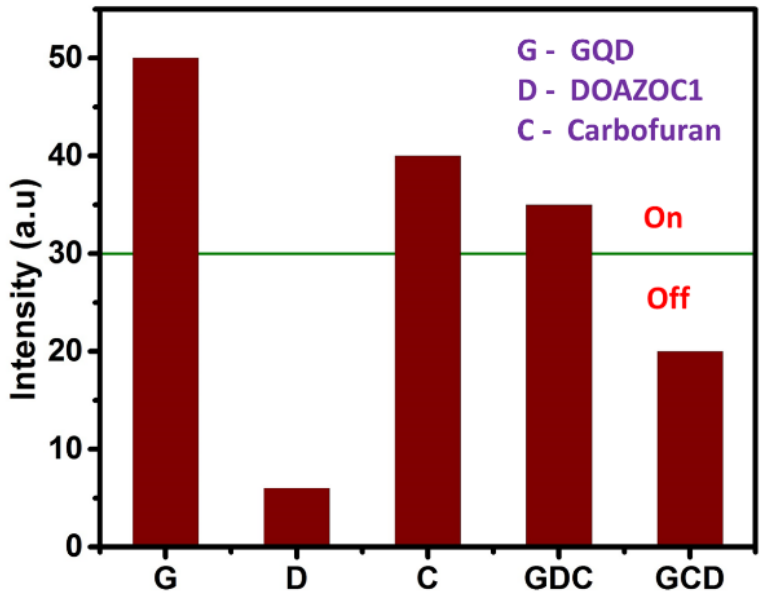

Figure 2.14: The impact of DOAZOC1 and carbofuran on the Fluorescence emission of GQDs at 435 nm upon distinct input sequences. The letters G, D and C stand for GQDs, DOAZOC1 (1×10^{-4} M) and carbofuran (1×10^{-4} M) respectively. GDC and GCD are the two sequences of addition. The output is designated as '0' or'1' depending on whether the intensity of fluorescence emission is higher or lower than 30.

So, the system remains locked. The keypad lock can be unlocked only by the input of the correct password 'DC'. The wrong password 'CD' fails to unlock the system. More importantly the fluorescence outputs at 435 nm created by the sequential inputs of DC and CD are found to be stable even after one week.In the experiments conducted so far, the *trans* form of the DOAZOC1 is used. So, it is an

interesting task to find what will be the effect if the *cis* isomer replaces the *trans*. The quenching of fluorescence intensity of GQDs are more for *trans*-DOAZOC1 (76.4%) compared to the *cis*-DOAZOC1 (63.5%) (Figure 2.15)(Van Amersfoort et al. 1994). But the fluorescence recovery is more for *cis* when the carbofuran is added. It is observed that the turn on sequence 'DC' is unaffected by the isomeric change of DOAZOC1 from *trans* to *cis* (Figure 2.16 A). This is true for the turn off state also (Figure 2.16 B). Thus, it is established that the system cannot be unlocked creating a new password which involves only a change in the isomeric form.

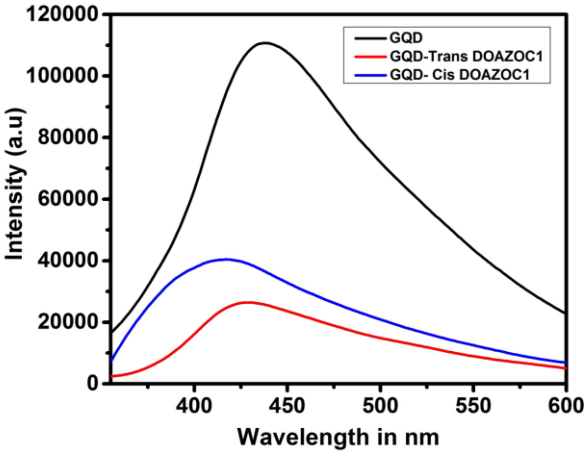

Figure 2.15: The quenching of Fluorescence intensity of GQD by *trans*-DOAZOC1 and *cis*-DOAZOC1.

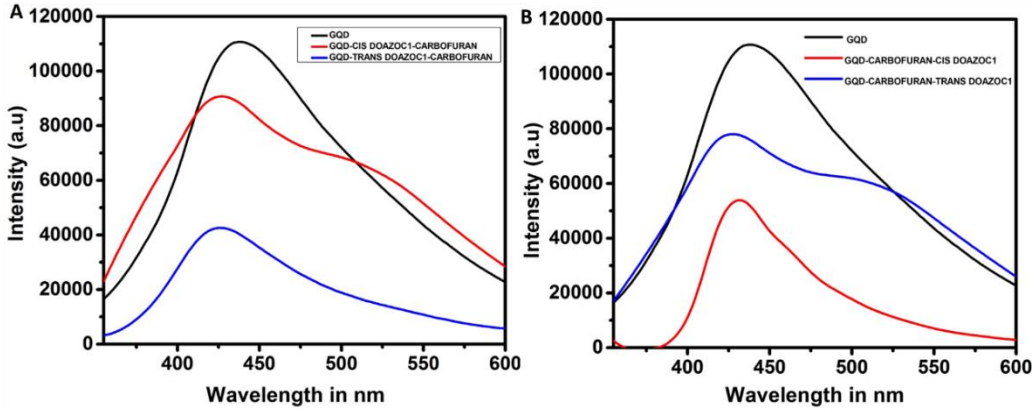

Figure 2.16: A) The sequential addition 'DC' with both *trans* and *cis* isomers of DOAZOC1 B) The sequential addition 'CD' with both *trans* and *cis* isomers of DOAZOC1.

In the light of the above observations the molecular keypad lock with password ‘DC’ is a security lock. The lock consist of a photoswitchable unit which is capable of existing in two different isomeric forms. The system can be unlocked with only one password ‘DC’ irrespective of the type of isomer is present. This is an added advantage in the sense that even if the lock is exposed to different conditions like light or dark, the access is possible with only one password. This can be utilized as a lock for storing a series of information that can be opened only by applying the keyword ‘DC’ (Figure 2.17). This is the first example of a molecular keypad lock developed from a system containing a photo-isomerisable unit derived from a bioresource material.

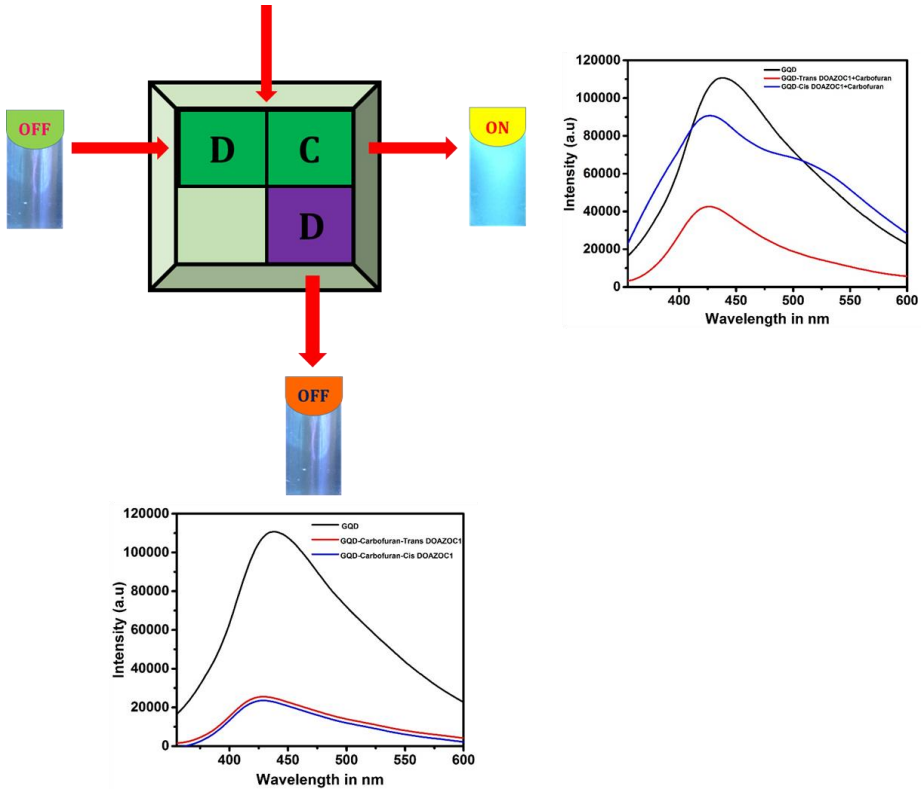

Figure 2.17: Schematic representation of Molecular Keypad Lock with corresponding fluorescence curves. The letters ‘D’ and ‘C’ represent the chemical inputs DOAZOC1 and Carbofuran respectively. The keys ‘I’ and ‘O’ depict the Fluorescence On (Unlock) and Fluorescence Off (Lock) states respectively.

2.4. Conclusion

We have developed a simple, cost effective method for the synthesis of GQD from easily available bioresource honey. The GQDs are then characterized by various methods TEM, XPS, Raman, XRD, PL etc. These GQDs are stable, and shows excitation-wavelength-dependent Photoluminescence properties (PL).

Further we have developed a system GQDs-DOAZOC1-Carbofuran with three distinct applications: molecular logic gate, molecular fluorescent probe and a molecular keypad lock. The inputs and output of both the logic gate and the molecular keypad lock are the same. The logic gate here constructed is an IMPLICATION logic gate. The fluorescent probe is also highly sensitive and selective for the detection of pesticide carbofuran. The design of molecular keypad lock is a shift from the conventional electronic keypad lock as its components are of sustainable origin. The system has only one authenticated password 'DC' irrespective of the isomeric form of the photo-switchable azobenzene unit DOAZOC1. The system can be unlocked only upon the sequential addition of chemical inputs DOAZOC1 and carbofuran. Any reversal in sequence of addition causes a failure in unlocking the system. This is the first example of such a security keypad mimicked at the molecular level. The added advantage is that the lock a cost-effective one. This potential application of securing information at the molecular level can pave way to the tremendous development in the field of molecular security information storage devices.

******

Chapter 3

Molecular Conductance Switch from Cardanol Derived Photoresponsive Molecule (DOAZOC1)-Multi-Walled Carbon Nanotube Hybrid

Developing assembles of organic molecules with carbon nanotubes has always been a hot topic in the research scenario. But most of these hybrid materials are constructed through covalent approach. Recently the assembly development through non-covalent interaction gained better prominence. This was because of the advantage that in the non-covalent assembly the electronic structure of the components will be preserved better. In this work we have demonstrated the development of such a non-covalent assembly between functionalized MWCNT and an photoresponsive molecule synthesized from cardanol, a bioresource material. Further we illustrated how the trans-cis photo-isomerisation of the azosystem allows the reversible tuning of the conductance property of MWCNT under light illumination. We then compared the phototuned conductance performance of the non-covalent hybrid with that of the covalent hybrid. The hybrids as well as the individual components are characterized by different techniques. This is the first attempt to develop hybrids based on a bioresource material exhibiting tunable conductivity. We expect that this novel photo-switchable hybrid with reversible conductance will have potential applications in nanoscale molecular electronics, solar cells, OLEDs etc.

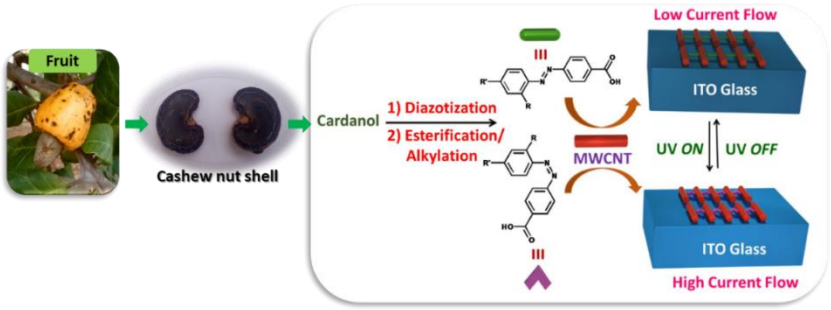

* Content of this chapter was published in the following journal

ACS applied materials & interfaces., **2017**, *9* , 1167- 1172.

3.1. Introduction

Carbon nanotubes are a popular class among the carbon nanostructures with unique and exceptional mechanical, electronic and optical properties (Iijima 1991),(Ajayan et al. 2001). They find wider applicability in various fields of nanoscience and technology (Endo et al. 2007; Schnorr et al. 2010; De Volder et al. 2013). The structure of nanotubes is best described as a single sheet of graphite rolled to form a seamless cylinder. There are two different types of carbon nanotubes i) single-walled carbon nanotubes (SWCNTs) and ii) multi-walled carbon nanotubes (MWCNTs). The MWCNTs are larger as they contain a large number of SWCNTs stacked over one another. The nanotubes are synthesized mainly through three different processes: arc discharge, chemical vapor deposition, laser ablation(Awasthi et al. 2005).

The manipulation of carbon nanotubes is done through various functionalization strategies including both covalent (Hauke et al. 2010; Lovley 2017) and non-covalent methods (Herranz et al. 2010). This results in the fabrication of hybrid materials between nanotubes and a large range of other molecules like polymers (Breuer et al. 2004), organic molecules (Tournus et al. 2005), metal nanoparticles (Wildgoose et al. 2006) etc. The hybrid assemblies thus synthesized are employed for developing devices like detectors (Liu et al. 2009), memristors (Radoi et al. 2011) etc. The combination of photochromic molecules with carbon nanotubes produced bi- or multi-functional molecular materials (Zhang et al. 2016). These hybrid systems will not only possess the unique properties of each component, but also lead to new properties that can potentially be used for

specific applications in various fields like opto-electronic devices (Malic et al. 2011), field effect transistors (FETs) (Zhao et al. 2013), sensing applications (Guo, Huang et al. 2005) etc. The coupling of nanotubes with azobenzene molecules, one of the important members of photochromic molecules is an interesting field of research (Feng et al. 2012). This is because of the ability of azobenzene molecule to undergo photo-induced isomerization which is used for photo-tuning the various properties of nanotubes like dispersion (Kördel et al. 2012), conductance (Basuki et al. 2015) etc.

Conductance switching is the foundation of many sensitive molecular electronic devices, and has been at the focus of numerous research efforts in recent years. In this work, we have analyzed the reproducible conductance switching triggered by external light on an innovative platform of Carbon Nanotube–Azomolecule junctions. We have focused our attention mainly on developing a non-covalent hybrid of Multi-walled Carbon Nanotube (MWCNT) with photo-responsive DOAZOC1 molecule derived from cardanol. This is the first attempt to fabricate such conductance switch without the addition of a polymer solution as the template. We compared the conductance switching performance of the non-covalent hybrid with that of the covalent hybrid. This was to explore the advantage of non-covalent functionalization in the fabrication of the conductance switch over that of the covalent one.

3.2. Experimental Section

3.2.1. Reagents and Materials

All commercially available reagents and solvents were used without further purification. Silica gel plates were 250 µm thick, 60 F_{254} grade from Merck. Silica gel was grade 60N (Spherical, Neutral, 100-200 mesh) from Merck, India.

3.2.2. Synthesis of Acid functionalized MWCNT

About 1 gram of MWCNT purchased from Sigma Aldrich is then taken in a two-necked 500 ml RB flask. To this about 80 ml of concentrated nitric acid is added and the mixture is kept for refluxing at 110 °C for about 6 hours. The sample is then filtered using a Milli pour filter unit. It is then washed with distilled water till the pH becomes 7. The sample is then dried at 120 °C for 12 hours (Rosca et al. 2005).

3.2.3. Synthesis of 4-[4-dodecyloxycarbonyloxy-2-pentadecylphenylazo] benzoic acid (DOAZOC1) (1)

The synthesis of DOAZOC1 (**1**) is already described in section 2.2.4 of chapter 2.

3.2.4. Preparation of Non-covalent hybrid with 1 and Acid functionalized MWCNT (1.MWCNT)

To a 5 ml (1×10^{-3} M) solution of **1** in toluene, 5 mg of the acid functionalized MWCNT is added. The solution is then made up to 10 ml in a glass vial. It is then

probe sonicated for 2 hours. A dispersion is formed as illustrated below (scheme 3.1).

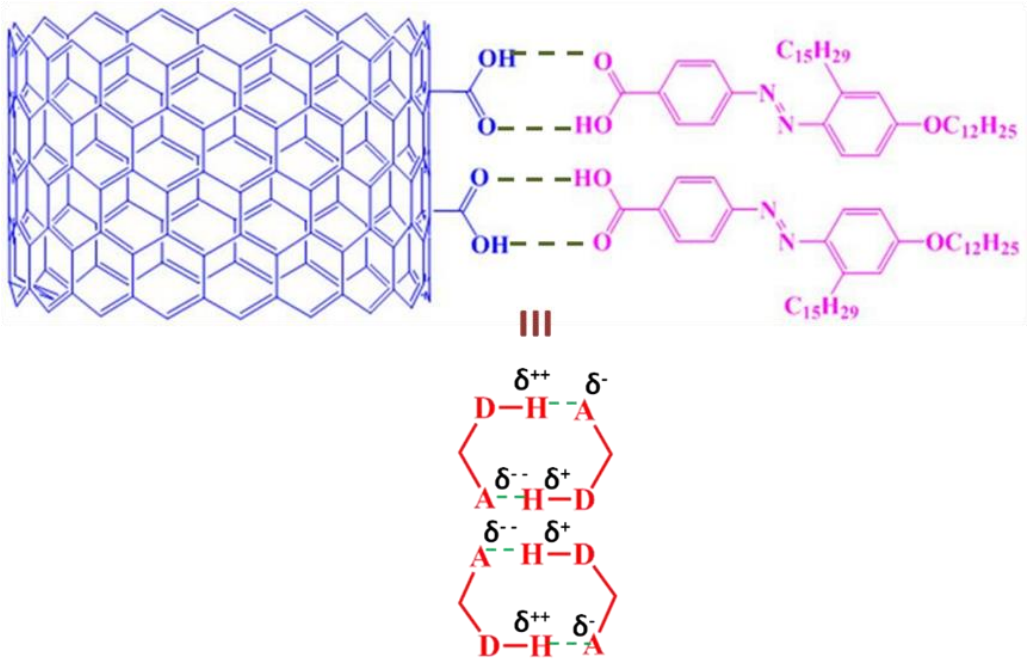

Scheme 3.1: Pattern of hydrogen bonding in heterodimer formed between Acid Functionalized MWCNT and **1**

3.2.5. Preparation of Covalent hybrid with 1 and Acid functionalized MWCNT

10 mg of DOAZOC1(**1**) was refluxed in thionyl chloride for 24 h. The excess of thionyl chloride was removed by vacuum distillation. The acid chloride of **1** is immediately treated with acid functionalized MWCNT in the ratio 1:3. The mixture was stirred at 120˚C for 96 h in dimethyl formamide (DMF) under nitrogen atmosphere. The product MWCNT-**1** hybrid was filtered and repeatedly washed with ethanol until the filtrate became colourless. The product formed is illustrated below (Scheme 3.2).

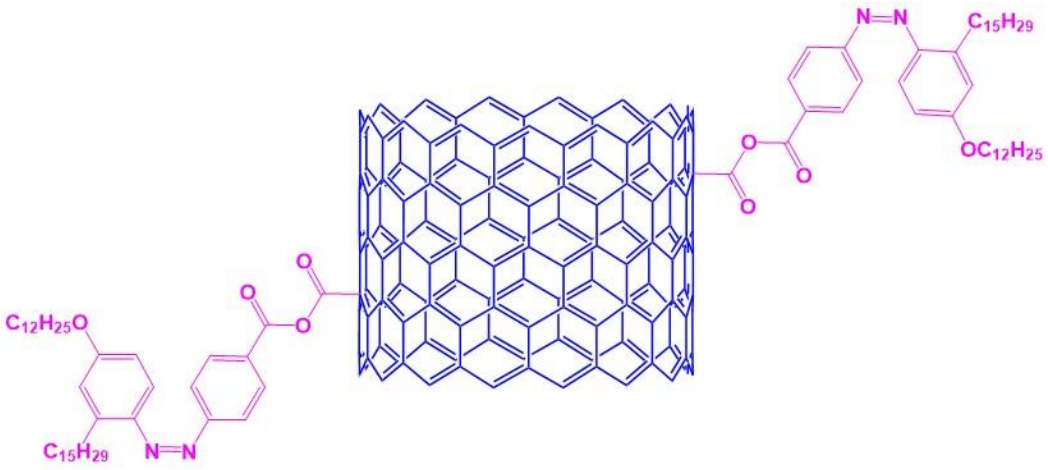

Scheme 3.2: Pattern of anhydride bonding in between the hybrid formed between acid Functionalized MWCNT and **1**.

3.2.6. Instrumentation

UV-Vis absorption measurements were recorded on a Cary 100 Bio. The photoisomerization studies were carried out using Oriel optical bench with a 200 W high pressure mercury lamp. The *trans to cis* photo-isomerisation of **1** and hybrids were observed by irradiating the samples by 354 nm (λ band pass= 354± 20 nm) light. The isomerization was monitored through the change in UV-Vis absorption spectra. In a similar way *cis-trans* isomerization was monitored by irradiating the sample by 600 nm long pass. Temperature dependent studies were carried out on a Shimadzu UV 3101 PC NIR with a thermostat directly attached to the wall of the cuvette holder. The temperature was controlled manually. For the temperature dependent measurements, the initial temperature was set at 15 °C and the data points were collected at intervals of every 5 °C increase up to 70 °C. A diffused reflectance Fourier Transform Infrared (FTIR) spectrum of the samples

was taken on Perkin-Elmer Spectrum 100 FTIR spectrophotometer at room temperature.

Transmission electron microscopic imaging was performed on a JEOL-JEM2100 microscope with an accelerating voltage of 200 kV. Samples were prepared by drop casting the **1** solution in toluene on carbon coated copper grids (400 mesh) and the images were obtained without staining. A required concentration of other samples was prepared by dispersing in toluene by sonication. The solution was subsequently allowed to cool for a few hours followed by drop casting this solution on a carbon coated grid (400 mesh). For the morphology transition experiments, about 250 μL of the solution was placed in a 1 mm cuvette and irradiated with the required wavelength (i.e. 354 nm). Scanning electron microscopy imaging was done using a Zeiss EVO 18 cryo SEM Special Edn with a variable pressure detector working at 20-30 kV. Atomic force microscopic measurements were carried out under ambient conditions by using an Agilent 5500 Scanning Probe Microscope operating in non-contact mode. Silicon cantilevers (Agilent Technologies) with a resonance frequency of ~ 300 kHz were used. The 512 × 512-pixel images were collected at a rate of 2 scan lines per second. A required concentration of all samples (1×10^{-3} M) was prepared in toluene by drop casting on mica sheets.

^{1}H NMR and ^{13}C NMR spectra were recorded using Bruker AV III 500 MHz FTNMR spectrometer with toluene-d_8 and acetone-d_6 as solvents and TMS as internal standard. Mass spectra were recorded under ESI/HRMS using Thermoscientific Exactive mass spectrometer and also by HRMS-FAB. Small

angle X-ray scattering measurements were performed by using XEUSS SAXS system by Xenocs, operated at 50kV and 0.60 mA. The X-ray radiation was collimated with FOX2D mirror and two pairs of scatterless slits from Xenocs. The data were collected in the transmission mode geometry using Cu Kα radiation (wavelength λ =1.54 A°). The fiber diagrams were recorded using an image plate system (Mar 345 detector) and processed using Fit2D software. DLS were measured on particle size analyzer (Zetasizer Nano ZS series, Malvern instruments) by using glass cuvette. TGA was carried out in TAQ50 instrument under nitrogen atmosphere at a heating rate of 5 °C per minute. The photo-current switching performance of the sample was studied by an advanced electrochemical system with three electrode cell, PGSTAT302N electrochemical work station (Autolab, Metrohm, Switzerland). Among the three electrodes the first is the Indium Tin Oxide (ITO) working electrode, the second one is a platinum wire counter electrode and the third one an Ag/AgCl reference electrode. The electrolyte used is 0.1M KCl solution.

The ITO plates are washed by ultrasonicating with water, extran, acetone and isopropyl alcohol. The plates are then covered by an insulation tape leaving 0.4×0.4 cm^2 as active area. Then about 50μL of all the samples are spin coated on to these plates. Before measurements the plates are kept in vaccum oven for 24 hours at 25 °C. For the two-probe measurement, about 5 ml of the hybrid solution is spin-coated onto an ITO plate and the conductance measurements are done without UV irradiation and with UV irradiation at different time intervals using EVERBEING INT'l CORP 2-probe station interfaced with an Agilent B2912A SMU. The whole arrangement monitored by Quick IV computer GUI interface

(Keysight). Four probe conductance measurements on a Keithly 6221A 4-Probestation are done after spin coating ITO plates with sample solutions. The thickness of the films confirmed to be 1 μm using a DEXTAK Profilometer. The UV irradiation is carried out by using a Spectroline E Series UV lamp with AC input 230V and output 8W at 365 nm.

3.3. Results and Discussion

3.3.1. Self-assembly of DOAZOC1 (1) in Toluene

The UV spectrum of **1** (1×10^{-4} M) recorded in toluene shows an absorption maxima corresponding to π-π* band at 368 nm and n-π* band at 458 nm (Figure 3.1). **1** is completely soluble in toluene. This clearly indicates that the introduction of dodecyl chain induces the solubilization in the non-polar solvent. In $CHCl_3$ solvent, **1** showed an absorption maxima at 365 nm corresponding to π-π* band. It is observed that the molar extinction coefficient of **1** in Chloroform (ε= 48170 M^{-1} cm^{-1}) (red line) is greater than that in toluene.

This clearly indicates that **1** more self-assembles in non-polar solvent toluene than in polar chloroform. The self-assembly behavior of **1** in toluene is further investigated by temperature dependent absorption studies. On increasing temperature from 20 °C to 60 °C the absorbance (ε) increases from 0.34 to 0.40, because of the breaking of hydrogen bonded aggregates (Figure 3.1). The melting transition temperature of the aggregates is 52 °C (Mahesh et al. 2012).

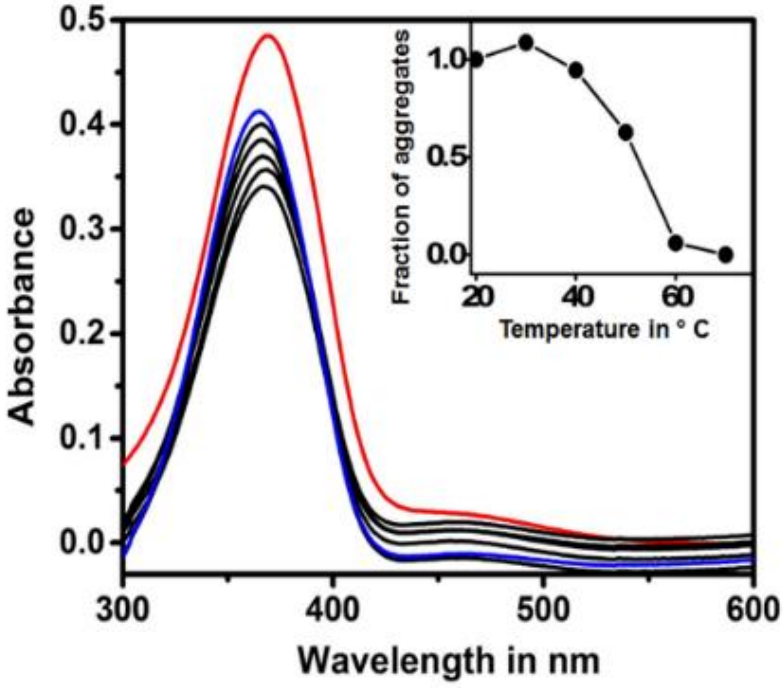

Figure 3.1: Temperature dependent UV-Vis absorption spectra changes of **1** (1×10^{-4}M) in toluene from 20 °C to 60 °C (black), in toluene at 70 °C (blue), in Chloroform (red). Inset shows the plot of fraction of aggregates vs temperature. The melting transition temperature of aggregates is 52 °C.

In order to study the photo-response, we carried out UV irradiation experiments (Figure 3.2) to monitor the isomerization behavior of the systems in toluene. **1** is subjected to UV irradiation using a 354 nm band-pass filter (λ band-pass = 354 ± 20 nm, LOT Oriel 200 W high pressure mercury lamp). The irradiation continued for 25 minutes with the simultaneous recording of the UV spectra at different time intervals. Upon UV irradiation, there is a decrease in intensity at 368 nm (π-π*band) (ε=0.31) with time. The appearance of the band at 458nm (n- π*) (ε=0.02) whose intensity increases with time confirms the *trans* to *cis* isomerization. The Photo-stationery state (PSS) is reached at 10 minutes and the yield of *cis* isomer at PSS is 70 %. The back *cis-trans* photoisomerization of **1** is

recorded by irradiating the UV treated sample using 600 nm light (Figure 3.3) (Airinei et al. 2011).

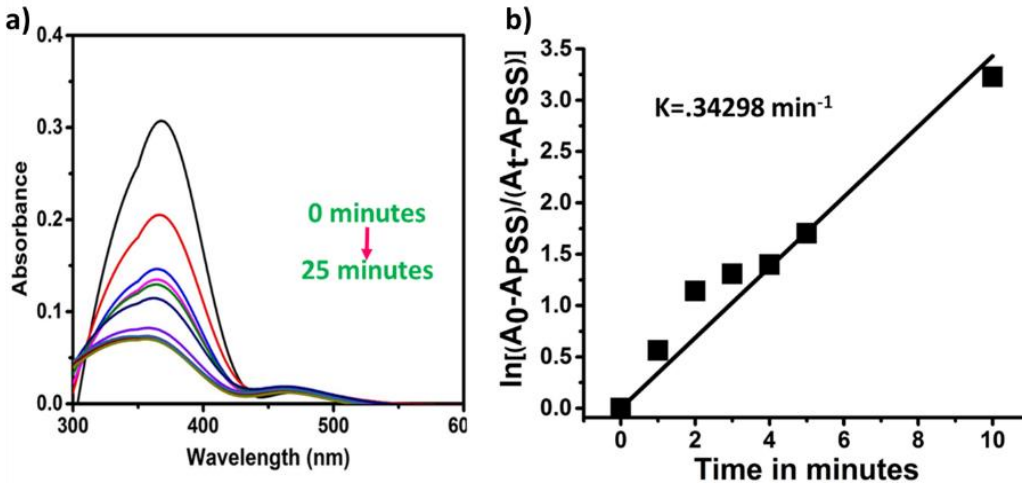

Figure 3.2: a) Spectral changes upon photo-irradiation in toluene (1×10^{-4}M) using 354 nm band pass light at 25 °C of **1**. b) Plot corresponding to the rate constant calculation for the *trans-cis* photoisomerization of **1**.

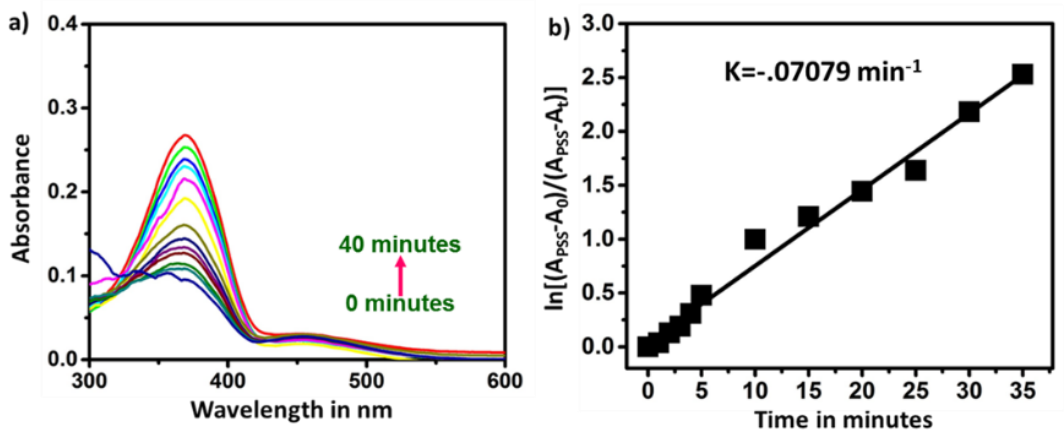

Figure 3.3: a) Back *cis-trans* isomerization of **1** in toluene under visible light of wavelength 600 nm. b) Plot corresponding to the rate constant calculation for the *cis-trans* photoisomerization of **1** under visible light.

Further UV-Visible switching cycle of **1** is carried out by subjecting **1** to UV and visible light alternatively at regular intervals (Figure 3.4).

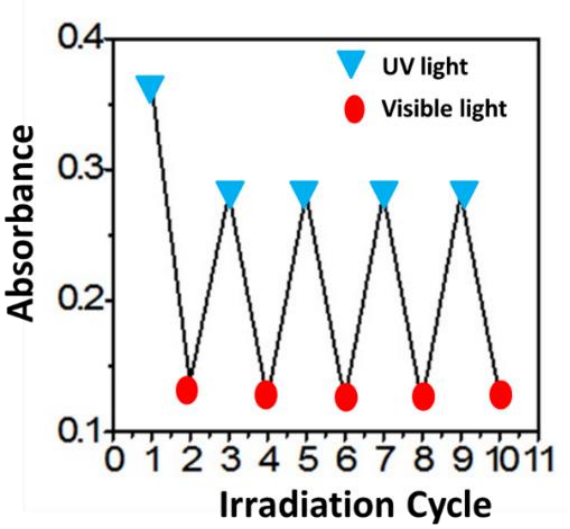

Figure 3.4: UV-Visible Switching cycle of **1** at 354 nm and 600 nm.

The self-assembly of **1** in toluene is observed through Dynamic Light Scattering (DLS) studies, where **1** showed a size increase from 140 ± 5 nm to 207 ± 3 nm upon UV irradiation at 365 nm (Figure 3.5).

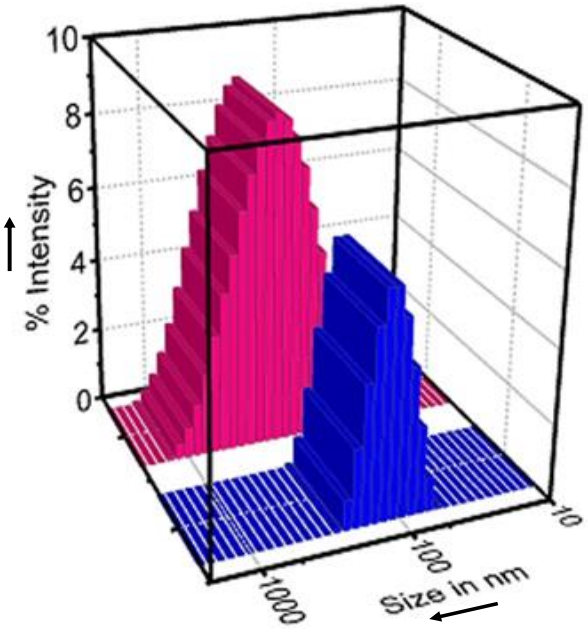

Figure 3.5: Profiles showing the intensity- averaged hydrodynamic radius (R_h) of the self-assemblies of **1** before (blue) and after (pink) photo-irradiation with 365 nm.

Atomic Force Microscopic (AFM) investigations also correlates the above result. Here the size varies from 151 ± 3 nm to 211 ± 4 nm. The morphology of **1** in toluene is also given by AFM. **1** assumes a disc like morphology initially and with UV illumination at 365 nm changes to spherical aggregates (Figure 3.6).

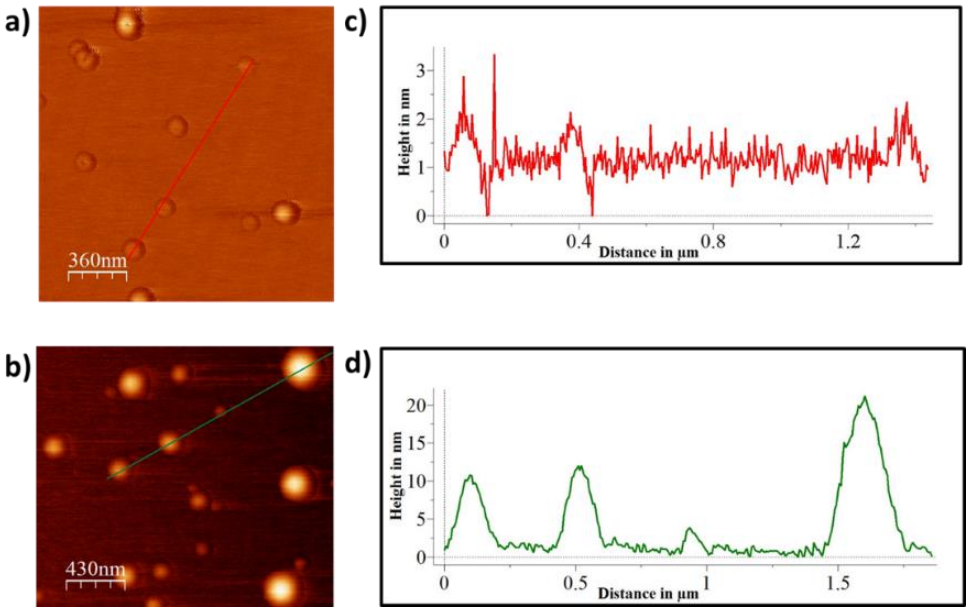

Figure 3.6: AFM images of **1** with height profiles before irradiation a) &c) and after irradiation b) &d).

The UV irradiation experiments are also done at the time of recording the ^{1}H NMR spectra of **1**. The yield of *cis* isomer at PSS is 64.5%) which correlates very well with the value obtained while recording the absorption spectra (Figure 3.7 & 3.8).

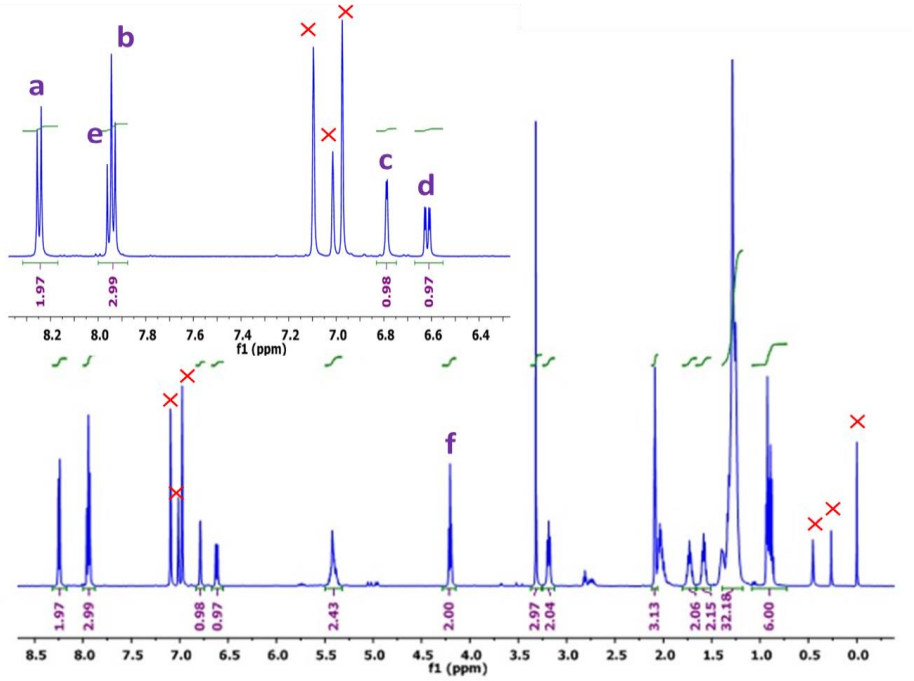

Figure 3.7. ^{1}H NMR spectra of **1** in toluene before irradiation. The inset shows the zoomed region between 6.3-8.4 ppm.

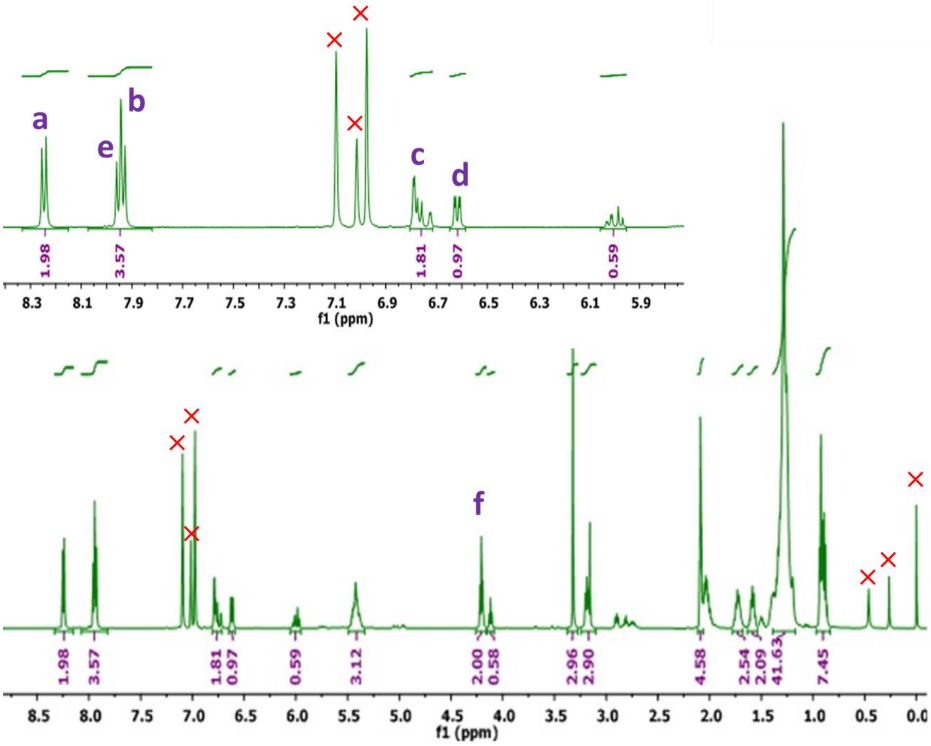

Figure 3.8. ^{1}H NMR spectral changes of **1** at PSS in toluene. The percentage conversion is calculated by the integration of appropriate peaks. The inset shows the zoomed region between 5.9-8.4 ppm.

3.3.2. Non-covalent Hybrid

We prepared the non-covalent assembly of **1** with functionalized MWCNT (**1**.MWCNT) and characterized it through various techniques. UV-Visible absorption spectra of acid functionalized MWCNT shows the absorption maxima around 279 nm. Formation of the non-covalent hybrid **1**.MWCNT is supported by the appearance of an additional peak at 295nm. The π-π* band at 368 nm retained its position but exhibited greater intensity (ε=0.62) compared to **1** (Figure 3.9).

Photo-responsive behavior of the non-covalent hybrid material **1**.MWCNT is studied using UV-Visible absorption spectra. The hybrid exhibits a different photo-responsive behavior compared to that of **1**, with a decrease in the yield of the cis isomer at PSS to 53.1% (**1**$_{trans}$ =70% at PSS) (Figure 3.10).

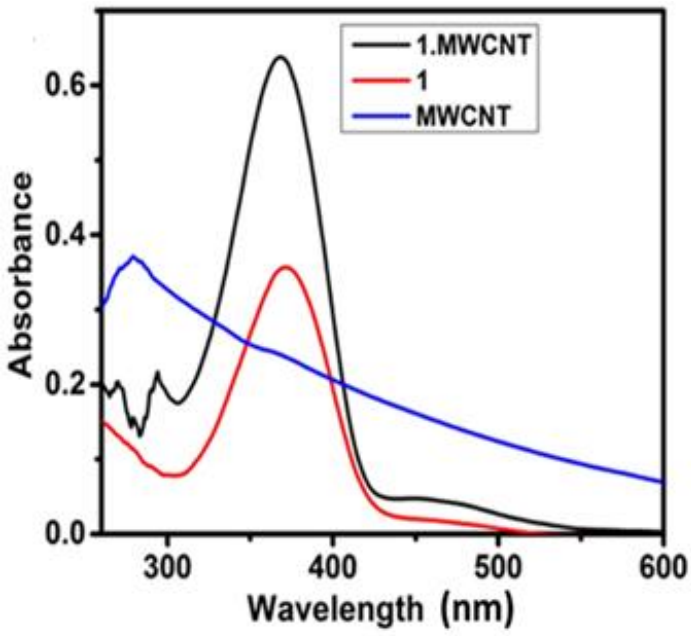

Figure 3.9: UV-Visible absorption spectra of functionalized MWCNT, **1** and Non-covalent hybrid **1**.MWCNT at 30 °C

This decrease in the percentage conversion is due to the strong interaction of **1**$_{trans}$

with MWCNT by means of non-covalent linkages such as hydrogen bonding and π-π stacking. The time required to achieve the photo-stationery state (T_{PSS}) is increased from10 minutes to 15 minutes in the case of hybrid as a result of the strong interaction between the two counterparts.

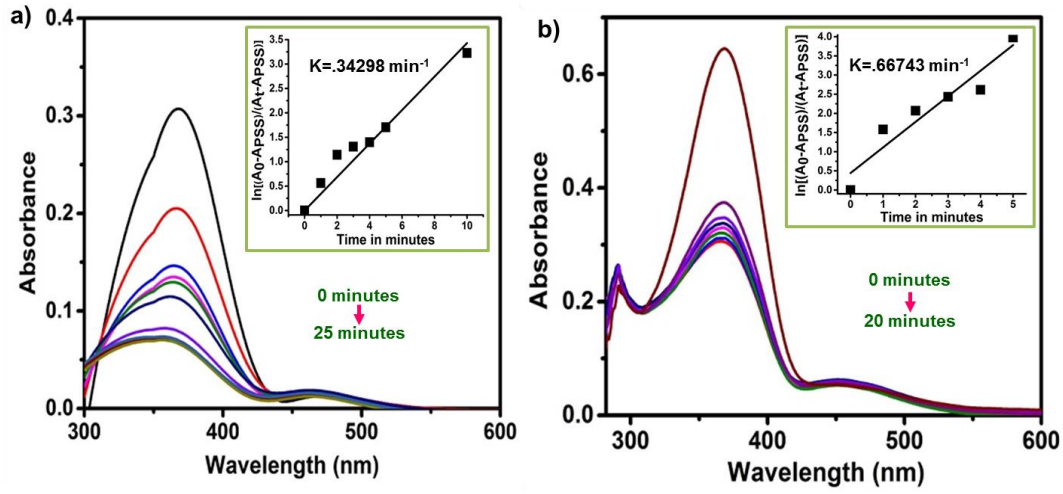

Figure 3.10: Spectral changes upon photo-irradiation in plots, toluene (1×10^{-4}M) using 354 nm band pass light at 25 °C of (a)**1** & (b) Non-covalent hybrid **1**.MWCNT. The inset plots give the rate constant for the trans-cis isomerization.

The back *cis-trans* isomerization of **1**.MWCNT is also monitored at 600 nm. It is observed that the time taken by **1**.MWCNT for back isomerization is longer compared to that of **1** alone (Figure 3.11).

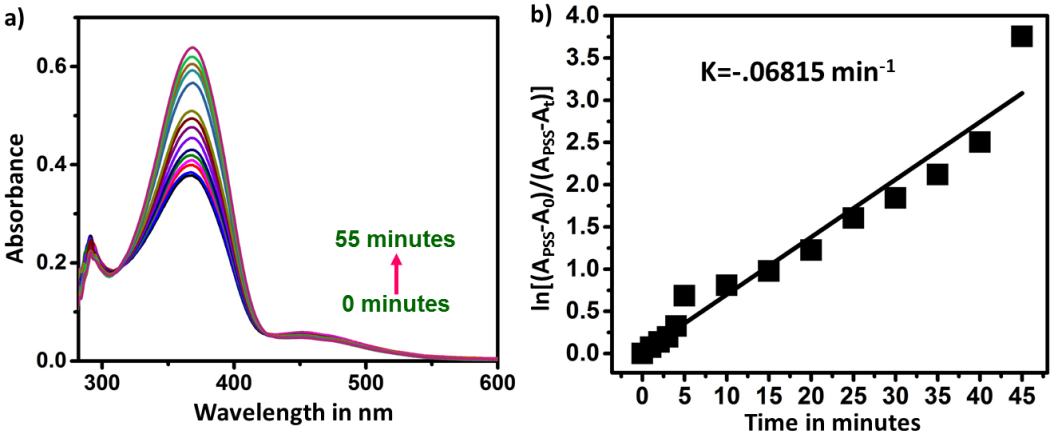

Figure 3.11: UV-Visible spectra for irradiation of **1**.MWCNT at 600 nm b) Plot for calculating the rate constant for *cis-trans* isomerization.

The formation of **1**.MWCNT is again confirmed by Transmission Electron Microscopy (TEM) (Figure 3.12). The non-covalent attachment of **1** to MWCNT with width 23 ± 4 nm results in an increase in width to 30 ± 6 nm approximately. This increase in width around 7 nm shows that when **1** is added to MWCNT it forms a dense layer over the latter due to the non-covalent interactions like hydrogen bonding and π-π stacking (Figure 3.12).

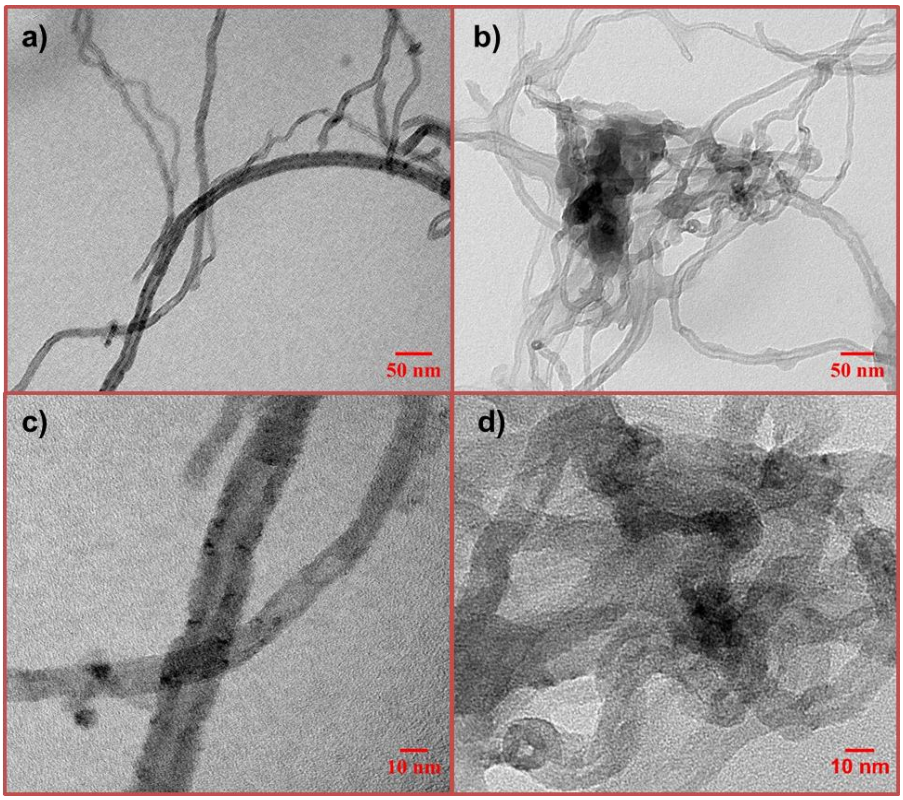

Figure 3.12: Transmission Electron Microscopic images (TEM) of (a) & (c) Functionalized MWCNT and (b) & (d) Non-covalent hybrid **1**.MWCNT in toluene.

The Scanning Electron Microscopy (SEM) images further supports the hybrid formation (Figure 3.13)

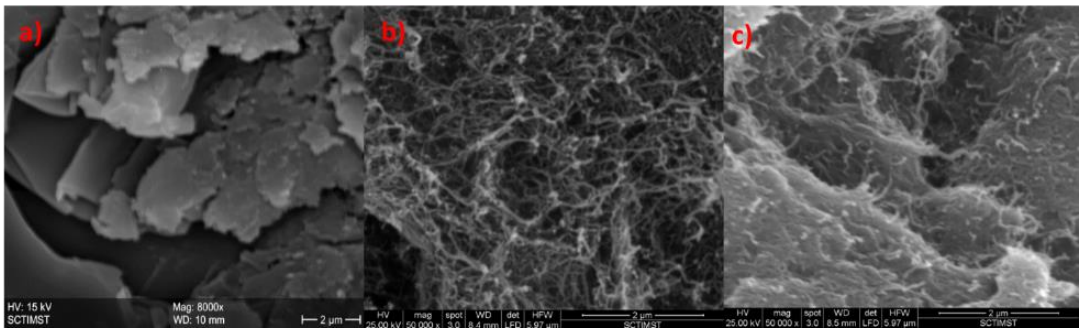

Figure 3.13: SEM images of a) **1** b) MWCNT and c) **1**.MWCNT hybrid in toluene.

The thermogravimetric (TGA) and derivative thermogravimetric (DTG) curves also support the formation of non-covalent hybrid. These curves clearly illustrates the difference in pyrolytic temperatures of **1**, MWCNT and **1**.MWCNT hybrid (Figure 3.14 a) & b)).

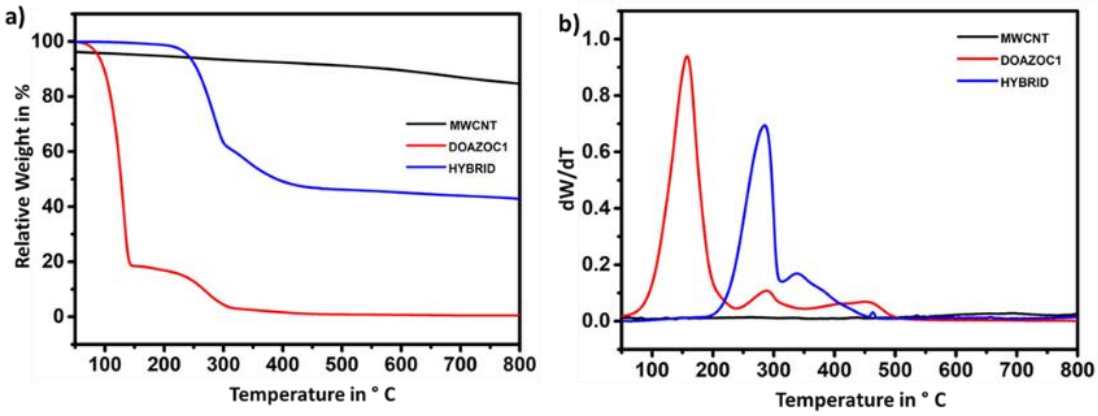

Figure 3.14: a) TGA b) DTA curves at a rate of 5 °C per minute.

Then we investigated the light controlled reversible conductance of **1**.MWCNT through various techniques. First we fabricated a conductance switch using this hybrid. The hybrid was coated on Indium Tin Oxide (ITO) glass substrate by wet etching process as illustrated in scheme 3.3. The ITO plate with hybrid film is utilized for the conductance measurements with a 2-probe system.

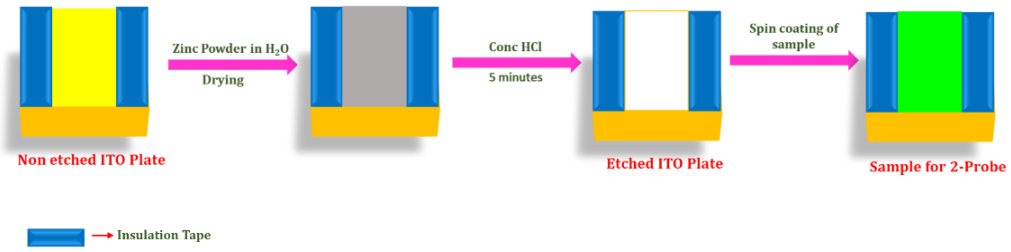

Scheme 3.3: Sample preparation for 2-probe measurement

The Figure 3.15 shows the linear current-voltage (I-V) curves of the hybrid at a voltage range of -2 to +2 volts (V) with UV irradiation at intervals 0, 5, 10 and 15 minutes. It is observed that the hybrid shows a remarkable increase of current on UV irradiation. The log scale at the inset clearly shows increase in conductance with irradiation time. This result is in accordance with that obtained for Feng *et al.*, where they fabricated a conductance switch with a covalently linked few-walled carbon nanotube and azobenzene through a flexible spacer (Feng et al. 2010).

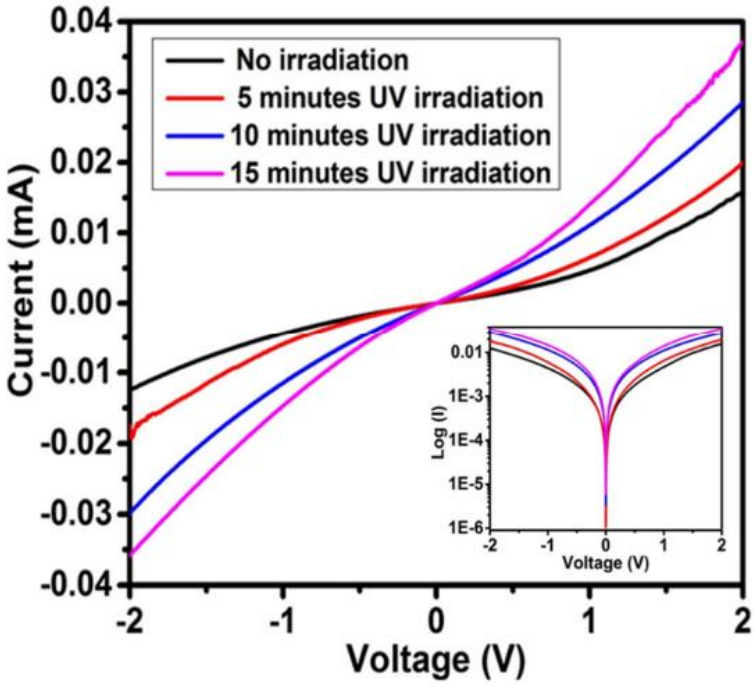

Figure 3.15: Linear current-voltage (I-V) curves of the Non-covalent hybrid **1**.MWCNT without and with UV irradiation. The inset shows the log scale of I-V curve.

This result was further confirmed by using Keithly 4-probe station. Here also the *cis*-hybrid showed more conductivity than *trans* hybrid (Table 3.1).

Sample	Conductivity
***Trans*-1.MWCNT**	**3.5905 S/cm**
***Cis*-1.MWCNT**	**19.4673 S/cm**

Table 3.1: Conductivity studies in a 4-probe station

The reversibility of conductance switching in hybrid is also examined by using an electrochemical workstation in which there is a three-electrode configuration. The photocurrent measurement is done through a chronoamperometric experiment in which current is determined as a function of time. From the Figure 3.16, it is clear that the non-covalent hybrid **1**.MWCNT shows a much better tuning of photocurrent when compared to **1** alone. When the UV light is switched on there is an increase in photo-current. Upon cutting off the UV source there is a drop in it. **1** gives a small photo-response compared to the hybrid. This non-covalent hybrid from cardanol shows potential current switching with larger stability for multiple cycles, clearly indicating its efficiency for phototuning (Zhang et al. 2010). The percentage ratio for the calculated photocurrent response of the hybrid is 466. This is a quite large percentage ratio which clearly indicates that the hybrid exhibits good photoresponse.

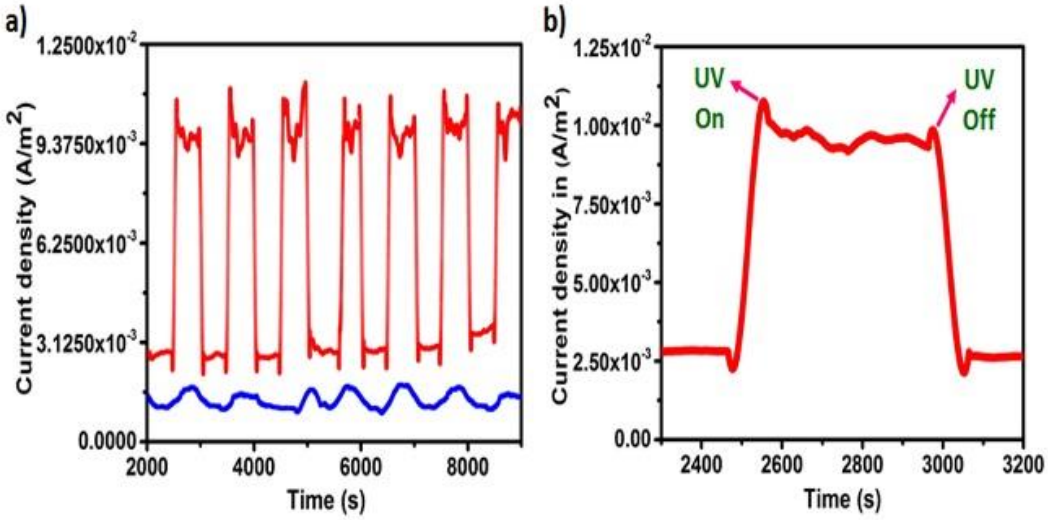

Figure 3.16: (a) Photocurrent response of **1** (blue line) and the non-covalent hybrid **1**.MWCNT (red line) with time upon alternate On/Off cycles of UV irradiation at a +0.5 bias in 0.1M KCl solution. (b) Photo-current response of the hybrid in one on-off cycle.

The plausible mechanism for this conductance modulation with UV light is the variation in tunneling distance with the photoisomerization of azobenzene. Upon UV irradiation the planar *trans* molecule isomerizes to sterically constrained *cis* conformation. This in turn leads to a decrease in overall length of the azo molecule resulting in a reduction in tunneling barrier length of the nanotube. There are reports which support that photo-induced geometrical transformations at the nanotube-azo junction result in a change in conductance (Del Valle et al. 2007).

The mechanism is illustrated in Scheme 3.4. The flexibility of the nanotube-azo junction is another factor influencing the conductance modulation in such systems. Here in our work compound **1** contains two long alkyl chains one of which is an ether linkage and other one containing a double bond. So the system is very much flexible as is evident from the photo-isomerisation studies of the hybrid **1**.MWCNT. Since the yield of cis isomer at PSS is 53% which is not much low

compared to that of **1** alone (70%). The reversibility of conductance switching as illustrated in Figure 3.16 supports the fact that with UV irradiation there is an increase in current due to *trans-cis* isomerization of azo molecule in the hybrid. The fall in current when the UV source is removed is due to the thermal *cis-trans* back isomerisation.

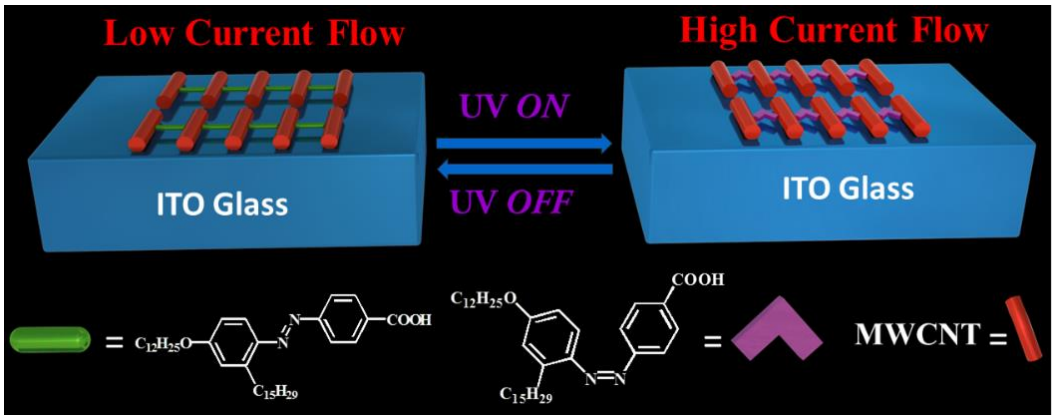

Scheme 3.4: The electronic switch fabricated using ITO glass plate over which the Non-covalent hybrid **1**.MWCNT is coated.

3.3.3. Covalent Hybrid

The covalent hybrid (MWCNT-**1**) formation is clearly evident from the infrared spectra. Hydroxyl peak at the range 3300-3500 cm^{-1} is not present in the case of covalent hybrid because of the formation of the anhydride bond between the components. There is a peak at 1740 cm^{-1} corresponding to the carbonyl stretching of the anhydride bond. The covalent hybrid retains the peak of alkyl chains (2920 & 2837 cm^{-1}) from **1** (Figure 3.17).

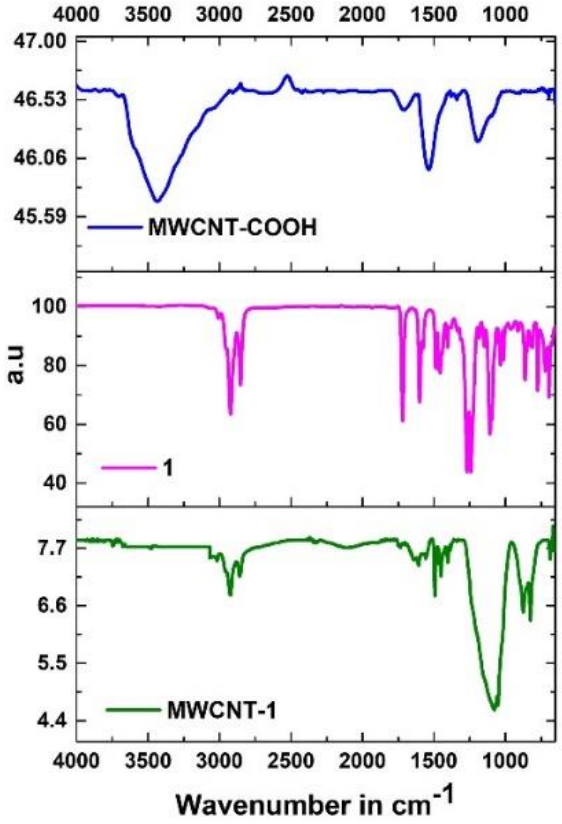

3.17: IR spectra of functionalized MWCNT, **1** and MWCNT-**1** covalent hybrid

The morphological analysis of covalent hybrid is obtained from transmission electron microscopy imaging. Upon hybrid formation the thickness of the nanotube becomes around 27 nm (Figure 3.18).

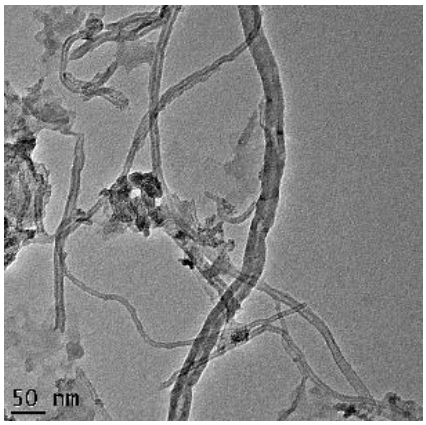

3.18: Transmission Electron Microscopic (TEM) image of Covalent hybrid MWCNT-**1**.

The reversible conductance switching of covalent hybrid is observed by chronoamperometric experiment. Just like the non-covalent hybrid, the covalent hybrid also exhibits an upswing in current with UV illumination and fall in the same upon switching off the UV source. But in the case of covalent hybrid, it is observed that there is a decay in current with each cycle (Figure 3.19). This decay is due to the restriction offered to the photoisomerization of **1** molecule in the covalent hybrid. Since the connection of **1** molecule to the MWCNT is through the strong anhydride bonding, the covalent hybrid MWCNT-**1** remains a rigid system. As a result of this more steric hindrance is offered to the photo-isomerisation of molecule **1** in the system. Therefore with the passage of time, there occurs a decay in the photoresponse of the covalent hybrid. This is in contrast with the steady response of the non-covalent hybrid (Figure 3.16).

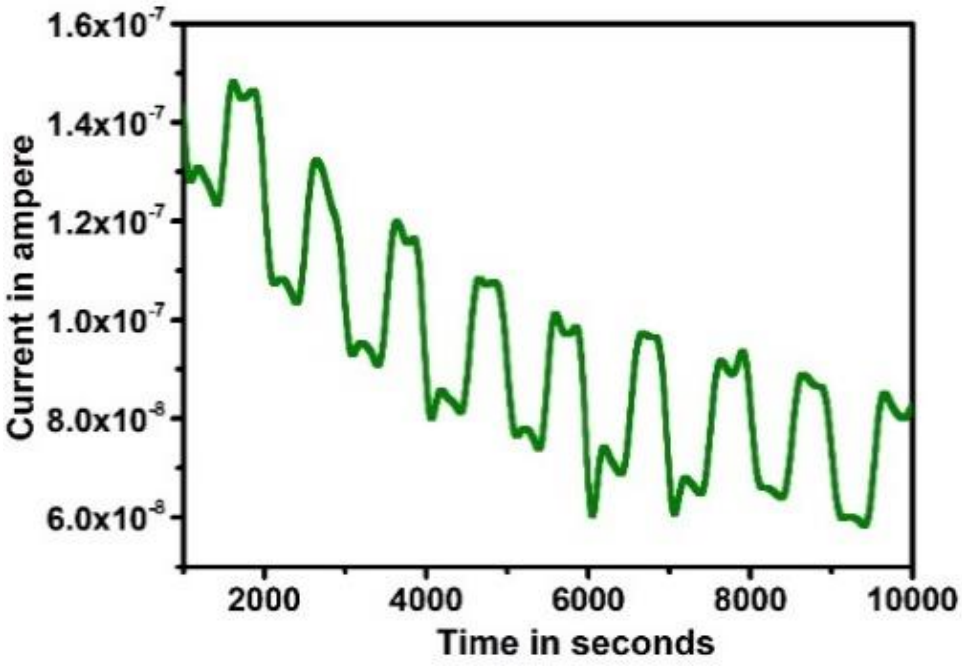

Figure 3.19: Photocurrent response of the covalent hybrid

3.4. Conclusion

In this work, we developed a non-covalent hybrid assembly between an azobenzene derivative developed from a bioresource material cardanol and an acid-functionalized MWCNT. The azo system efficiently controlled the conduction properties of MWCNT through its ability for photoisomerization. This is the first example of such a conductance switch developed from a bioresource material. It is observed that with UV illumination, conductance increases and when the illumination is stopped, conductance drops down. There is a reduction in tunneling distance with *trans-cis* isomerization of azomolecule. This is responsible for the increased current flow upon UV illumination. The hybrid showed a good photo-response ratio also. Another interesting aspect for the fabrication of non-covalent hybrid no polymer is used as the substrate or support. The non-covalent hybrid itself has a stability to stand as a stable dispersion and can form a film.

Further analysis was done after fabricating a covalent hybrid also. The conductance/current switching performance of both hybrids were compared. The non-covalent hybrid shows a steady response in photo-tuning of conductance over multiple cycles. On the other hand the covalent hybrid exhibits a decay in current with each advancing cycle. The reason behind the difference in behavior between the two hybrid systems is the distinction in the linkages present in the non-covalent and covalent systems. In the case the non-covalent hybrid, DOAZOC1(**1**) and MWCNT are connected hydrogen bonding and π-π stacking. There is no change in the functionality and also there is no direct linkage between the components. Therefore, the non-covalent hybrid is a flexible system and the reversible photo-

isomerisation process of the DOAZOC1(**1**) molecule takes place smoothly. This in turn causes a steady conductance switching performance. But in the case of covalent hybrid, the DOAZOC1(**1**) and MWCNT are connected through a strong anhydride bond. There is a steric hindrance caused to the former upon the covalent bond formation. This causes a restriction in the photoisomerization of DOAZOC1(**1**). Therefore the photoswitching of current decays with time.

******

Chapter 4

Molecular Conductance Switch from Cardanol derived Photoresponsive Molecule (AZOC2)-RGO Hybrid

The process of utilizing organic molecules for tuning the properties of carbon nanomaterials has paved way to a tremendous revolution in organic electronics, especially in developing field effect transistors, memory devices etc. Herein this chapter we, have investigated the influence of insulating photochromic molecule on the conductance behavior of carbon nanomaterial. Azobenzene derived from cardanol was functionalized with reduced graphene oxide and this combination showed phototunable conductance behavior with the light induced trans-cis isomerization of azo moiety. The difference in the mode of interaction between the two moieties, i.e. the covalent and non-covalent functionalization also influences the photoconductance behavior of reduced graphene oxide. The rate constant of photoisomerisation for covalent hybrid is 0.04259 min^{-1} and for non-covalent hybrid is 0.04687 min^{-1}. Similarly, the photoresponse ratio calculated for the covalent hybrid system is 0.178 and the same for the non-covalent hybrid is 0.571. This clearly implies that non-covalent mode offers better tuning of photoconductance than the covalent mode as the latter can cause a larger restriction in the photoisomerization activity of azo system. The finding leads to more development in the area of sustainable molecular electronics.

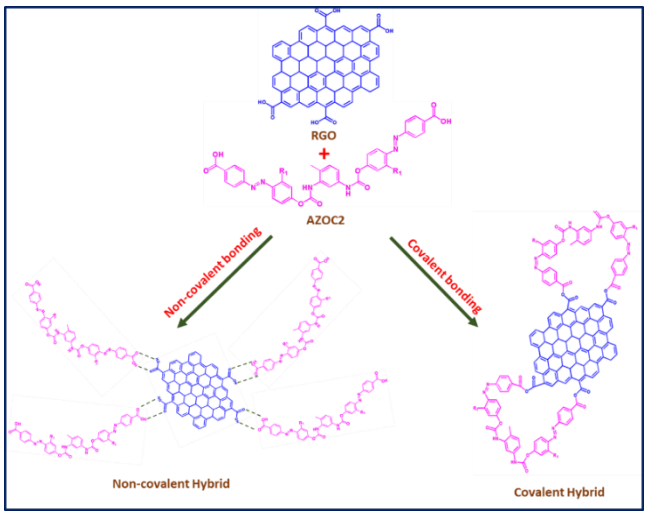

* Content of this chapter was published in the following journal

New Journal of Chemistry.,**2018**, *42* , 18182-18188.

4.1. Introduction

The development of smart materials by coupling more than one component is an interesting aspect of molecular electronics (Xu et al. 2018). Each of the coupling components imparts their unique properties to the multifunctional hybrid product. The new ensemble formed can also exhibit a different behavior other than those acquired from its individual components. In the field of organic electronics, the organic molecules are coupled with a wide range of materials especially with carbon nanomaterials for tremendous applications in solar cells,(Rowell et al. 2006; Luo et al. 2015) field effect transistors (Frolova et al. 2015; Fu et al. 2016), photodetectors (Zhou et al. 2009) and other varieties of photovoltaics (Notarianni et al. 2016).

The organic compounds are generally considered as insulating materials. But their coupling with inorganic and carbon nanomaterials make them capable of influencing the electrical properties of the latter. This is an innovation in the field of organic electronics (Agranovich et al. 2011; Ponnamma et al. 2013). For the modulation of properties in such hybrid materials, at least one component should have a response to some external stimulus. Such systems are more advantageous as they can be made to work in a reversible manner also. The commonly employed stimuli in such material systems include light (Xu et al. 2017; Jaekel et al. 2018), heat (Jochum et al. 2013; Kim et al. 2018), pH (Hariharan et al. 2017; Wei et al. 2017), redox potential (Doistau et al. 2017) etc. Light has a wider impact as a stimulus because of its ease of harvesting, energy efficiency and environmentally

friendly nature. Light sensitive molecules particularly photochromic molecules occupies a prominent place in making hybrid smart materials (Yao et al. 2016).

The azobenzene systems are widely employed class of photochromic systems which possess the ability to stay in two different isomeric forms namely *trans* and *cis* depending upon the wavelength of the light irradiated (Lennartson et al. 2015). Their typical isomerization properties such as large conformational change, low photo bleaching rate and medium change in dipole moment make them a perfect candidate as the coupling counterpart in micro and nanodevices (Nakano et al. 2013). The device fabrication of two-dimensional graphene oxide by incorporating azobenzene systems as the stimuli component has resulted in opto-electronic materials (Feng et al. 2012) with wider applications like sensing (Lee et al. 2013) memory storage (Lin et al. 2013; Min et al. 2013).

The nature of interaction among the coupling components is also important in developing the hybrids with good performance. There are reports dealing with azobenzene system which are covalently linked with different carbon nanomaterials like carbon nanotube, graphene oxide etc (Schneider et al. 2015) (Luo, et al. 2015). Feng *et al.* reports the reversible phototuning of conductance in graphene oxide by azobenzene (Feng et al. 2010). In a recent work our group reported effective phototuning of the conductance of multi-walled carbon nanotube by non-covalent functionalization with azobenzene moiety (Devi et al. 2016). In the light of the studies conducted so far it is clear that both covalent and noncovalent functionalization of azobenzene on carbon nanostructure modulate the photocurrent of the carbon structures. However, it is not clear so far which type of interaction is more suited to influence the photocurrent of the carbon nanostructures.

This chapter deals with the optical modulation of the conductance of two-dimensional reduced graphene oxide (RGO) with photoresponsive azobenzene and effect of covalent and non-covalent functionalization of the azobenzene molecule to the carbon nanomaterial on the conductance modulation. Cardanol is a well-known bioresource material obtained from cashewnut shell liquid. This molecule is widely explored in material research field (Balachandran et al. 2013) due to the ease of modification, availability and low cost. . In this context, we have selected cardanol as the base material for the azobenzene system we developed. The graphene oxide (GO), which is actually the functionalized graphene with oxygen containing functional groups have interesting properties like higher mechanical strength, surface area, tunable electronic characteristics (Li et al. 2015)

In the present work, reduced graphene oxide (RGO) which contain lesser oxygen functionalities than its parent graphene oxide (GO) is employed. The two-dimensional morphology and controlled functionality of RGO over other carbon nanostructures made it a better model system as the carbon counterpart for the study of phototuning of conductance in presence of azomolecules.

4.2 Experimental Section

4.2.1. Materials and Methods

All commercially available reagents and solvents were used without further purification. Silica gel plates were 250 µm thick, 60 F_{254} grade from Merck. Silica gel was grade 60N (Spherical, Neutral, 100-200 mesh) from Merck, India.

4.2.2 Preparation of graphite oxide (GO)

GO was prepared by the well-known modified Hummers and Offeman's method (Hummers et al. 1958; Becerril et al. 2008).In this method first a mixture of graphite (0.5 g), sodium nitrate (0.5 g) and 25 mL of sulphuric acid are stirred for 20 minutes in an ice bath. The solution is then poured in to a bath containing water at temperature of 35 ˚± 5˚ C. It is then stirred for 2 h till the mixture formed a thick green paste. After some time about 50 mL water is added slowly and the temperature is increased to 90˚± 5 ˚C. The stirring again continued for 1 h. Again 90 mL water and 5 mL of H_2O_2 (30%) are added slowly and the solution changes colour from dark brown to pale yellowish brown. The solution is then filtered and washed with water and the product recovered is kept under vacuum for drying.

4.2.3 Preparation of reduced GO (RGO)

The GO is then subjected to reduction following the procedure reported by Lee *et al.* (Lee et al. 2013). Here 300 mg of GO in 250 mL water is sonicated for 1 h. The pH of the solution is then altered to 10 by the addition of 5% sodium carbonate (25 mL) solution. The solution is then refluxed for 9 h keeping at a temperature of 90˚± 5 ˚C. By keeping the pH at 10, sodium borohydride solution (1.6 g in 40 mL water) is added to the dispersion of GO formed. Again, the solution is kept stirring at 80 ˚C for 3h. The completion of reduction is indicated by a colour change from brown to black along with gas evolution. The final product is then

filtered using polyamide membrane filter (0.2 mm) and repeatedly washed with water then vacuum dried.

4.2.4 Synthesis of AZOC1

The synthesis of molecule AZOC1 is already described in chapter 2.

4.2.5 Synthesis of AZOC2

The molecule AZOC2 is prepared from a previously reported procedure. To a solution of AZOC1 (0.5 grams, 0.001 M) in 6 ml of DMF taken in an RB flask, toluene diisocyanate (0.2 grams, 0.001M) was added drop wise. A few drops of the catalyst dibutyl tin dilaurate (DBTDL) were also added and the reaction mixture was kept overnight. The temperature is then increased to 60 °C and the stirring was continued for 6 hours. The precipitate was collected and purified by column chromatography (silica gel 60-120 mesh using ethyl acetate as solvent). Pure compound was dissolved in THF and precipitated by cyclohexane (Mahesh et al. 2014).

Yield 72 % m.p 133-134 °C

IR (KBr; cm^{-1}): 3323 (Ar-OH, -NH), 1698 (Ar-COOH), 1595 (-N=N-).

^{1}H NMR (500 MHz, DMSO- d_6) δ: 10.31(2H, COOH) 8.62(s, 2H, Ar), 8.31(2H,NH),8.11-8.09(d,4H, Ar), 7.85-7.86 (d, 4H, Ar) 7.63-7.65(d, 2H), 6.79(s,1, H, Ar), 6.75-6.72 (m,2H, Ar), 5.26-5.31(m,CH_2=CH_2),3.04-07.1(m,4H,CH_2),2.6-2.7(m,CH_3).

^{13}C NMR (DMSO- d_6) δ: 14.36, 14.43, 22.56, 28.68, 28.94, 29.0, 29.07, 29.16,29.38, 29.45, 31.16, 31.5,31.42, 31.54,31.75, 32.10, 39.44, 39.61, 39.78, 39.94,40.11,40.28,40.37,40.44,99.99,109.61,114.71,115.28,116.10,116.78,117.36, 119.79,121.9,122.49,125.48,126.93,128.19,128.78,129.36,130.01,130.13,131.07,1 50.18,207.05 ppm.

HRMS-FAB: $[M]^+$ calcd for $C_{65}H_{82}N_6O_8$: 1074.62, found: 1075.4

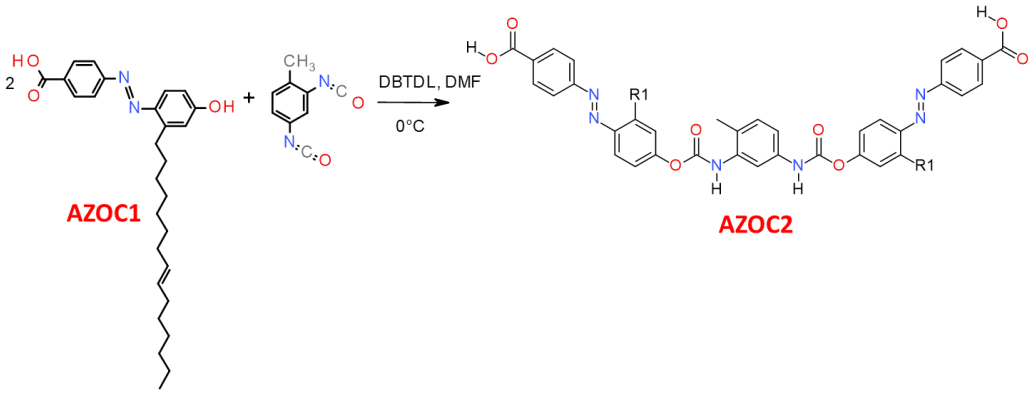

Scheme 4.1: Synthesis of AZOC2

4.2.6 Preparation of covalent RGO-AZOC2 hybrid (RGO-AZOC2-C)

10 mg of AZOC2 was refluxed in thionyl chloride for 24 h. The excess of thionyl chloride was removed by vacuum distillation. The RGO and three times that of acyl chloride functionalised AZOC2 were mixed in 10ml of dimethylformamide (DMF). The mixture was stirred for 120 ˚C for 96 h in

nitrogen atmosphere. The resultant RGO-AZOC2 hybrid was filtered and repeatedly washed with ethanol until the filtrate become colourless.

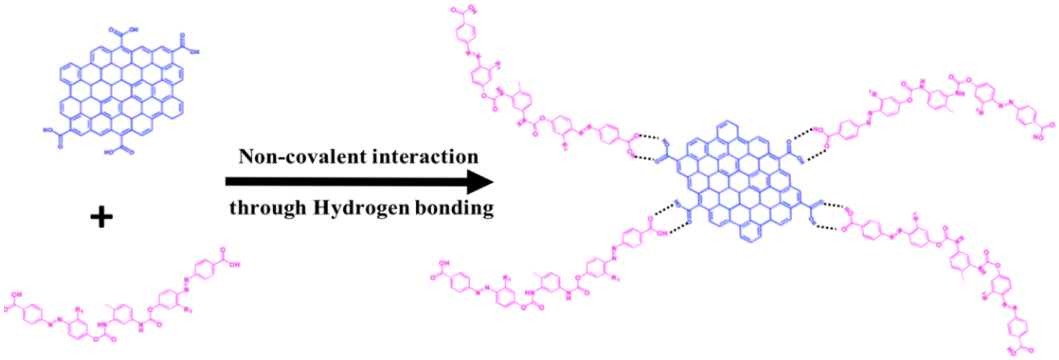

Scheme 4.2: a) Preparation of RGO, (b) Conversion of AZOC2 to acid chloride, and (c) synthesis of covalent RGO-AZOC2 hybrid (RGO-AZOC2-C)

4.2.7 Preparation of non-covalent RGO-AZOC2 hybrid (RGO-AZOC2-NC)

To 10 mL of 1 × 10^{-4}M solution of AZOC2 in toluene, 10 mg of RGO is added and the solution is subjected to probe sonication for one hour. The dispersion formed is then coated over Indium Tin Oxide (ITO) plates through spin coating method.

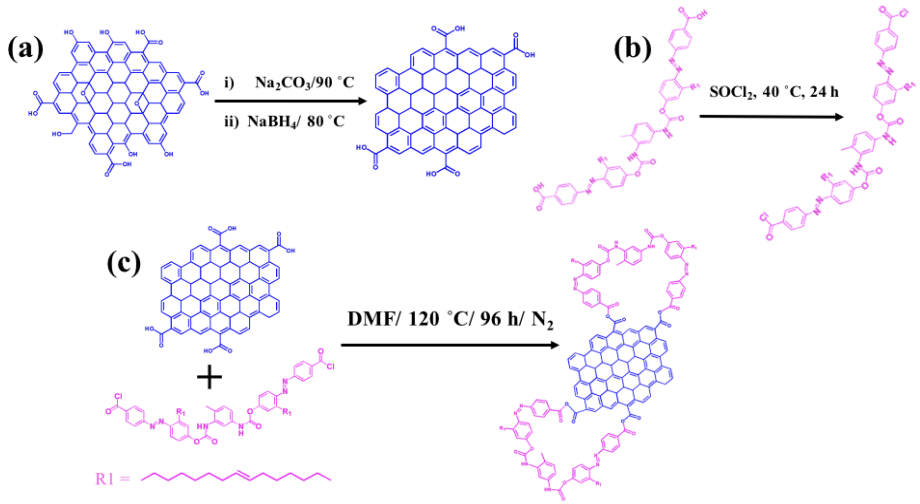

Scheme 4.3: Schematic representation of the synthesis of non-covalent RGO-AZOC2 hybrid (RGO-AZOC2-NC)

4.2.8. Instrumentation

The Photo-isomerisation experiments were performed on degassed solutions in *N*,*N*-DMF and toluene using Oriel optical bench with a 200 W high pressure mercury lamp. The *trans to cis* photo-isomerisation of AZOC2 and RGO-AZOC2 hybrids was observed by irradiating samples using 354 nm ($\lambda_{\text{band pass}}$= 354± 20 nm) light. UV-Vis absorption measurements were recorded on a Cary 100 Bio. The isomerization was monitored through change in UV-Vis absorption spectra. The diffused reflectance Fourier transform infrared spectra of samples were taken on Perkin-Elmer Spectrum 100 FTIR Spectrophotometer at room temperature. Raman Spectra of the samples were measured using Renishaw Confocal Raman Microscope of 530 nm laser. ^{1}H NMR and ^{13}C NMR spectra were recorded using Bruker AV III 500 MHz FTNMR Spectrometer with toluene-d_8 and Acetone-d_6 as solvents. The TMS is used as internal standard. Mass spectra were recorded under HRMS-FAB. Small angle X-ray scattering measurements were performed by XEUSS SAXS System of Xenocs, operated at 50kV and 0.60 mA. The X-ray radiation was collimated with FOX2D mirror and two pairs of scatterless slits from Xenocs. The data were collected in the transmission mode geometry using Cu Kα radiation (wavelength λ =1.54 A°). The fiber diagrams were recorded using an image plate system (Mar 345 detector) and processed using Fit2D software.

TGA was carried out by TAQ50 instrument under nitrogen atmosphere at a heating rate of 5 °C per minute. The photo-current switching performance of the sample was studied by an advanced electrochemical system (Autolab, Metrohm, Switzerland). The Indium Tin Oxide (ITO) plate coated with the sample is used as

the working electrode. The Ag/AgCl was the reference electrode and platinum wire the counter electrode. The electrolyte solution used is 0.1M KCl. The ITO plates are washed by ultrasonicating with water, Extran, acetone and isopropyl alcohol. The plates are then covered with an insulation tape leaving 0.4 × 0.4 cm^2 active area. Then about 100 µL of bare azocompound AZOC2 is coated onto the plates. Further coating is done with covalent and non-covalent hybrid solution of RGO-AZOC2 in *N*,*N*-DMF and toluene. The plates are kept in vacuum oven at for 24 hours at 25 °C before making the measurements.

4.3. Results and Discussion

RGO-AZOC2 assemblies were prepared as mentioned in 4.2.7. These assemblies can be characterized by Ultraviolet Visible Spectroscopy (UV-Visible Spectroscopy) The UV-Visible absorption measurements in *N*,*N*-Dimethyl formamide (*N*,*N*-DMF) and toluene confirms the formation of assemblies of RGO-AZOC2. The appearance of the peak at 273 nm and the redshift in the π-π* band of AZOC2 from 365 nm to 394 nm indicate the covalent adduct formation (Figure 4.1.a). The non-covalent assembly formation is also supported by the bands at 269 nm and 371 nm.

The RGO-AZOC2 hybrid formation is further substantiated by Fourier transform infrared spectroscopic (FTIR) measurements (Figure 4.1.b). The covalent hybrid, RGO-AZOC2-C has stretching at 1573 cm^{-1} (-N=N-), 1765 cm^{-1} (-C=O-) corresponding to anhydride linkage, 2946 cm^{-1} & 2898 cm^{-1} of alkyl chain (-CH_2-). The absence of peak corresponding to the hydroxyl bond

in RGO-AZOC2-C brings out the bond formation between RGO and AZOC2. The non-covalent hybrid, RGO-AZOC2-NC retained the hydroxyl peak at 3440 cm^{-1} (-OH). The other peaks in the non-covalent hybrid include the carbonyl stretching at 1680 cm^{-1} (-C=O-), the azo stretching at 1479 cm^{-1} (-N=N-) and the alkyl stretching at 2910 & 2851 cm^{-1}(-CH_2-).

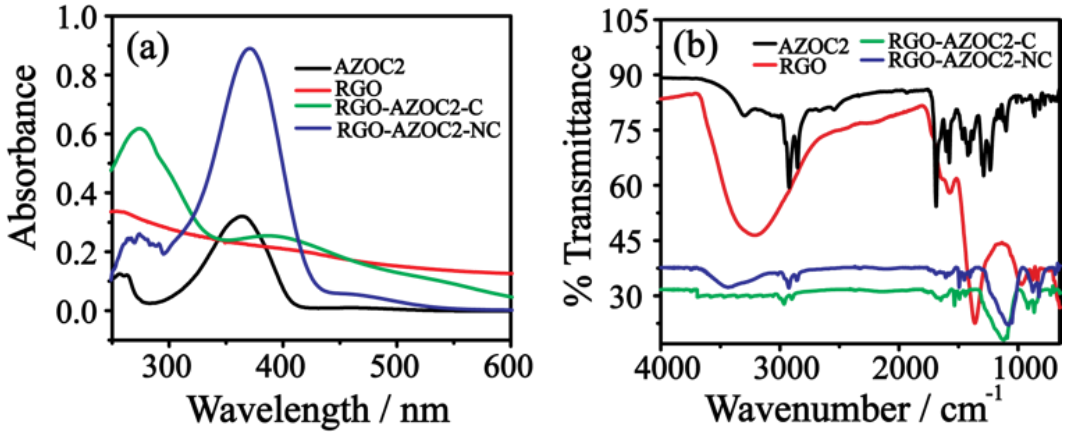

Figure 4.1: a) UV-Visible Spectrum of RGO, AZOC2, RGO-AZOC2-C, and RGO-AZOC2-NC b) Infrared Spectrum of RGO, AZOC2, RGO-AZOC2-C, and RGO-AZOC2-NC.

The crystal structure of RGO and assemblies of RGO-AZOC2 are determined by X-ray Diffraction experiment (XRD) (Figure 4.2 a). The RGO shows peak 2θ at 25.2˚ corresponding to (002) plane. In the case of RGO-AZOC2-C, there is a shift of peak to 24.4˚ compared to RGO. Similarly, in RGO-AZOC2-NC the peak is shifted to 26.12˚. Both the hybrids show other peaks including strong broader peaks around 19˚.

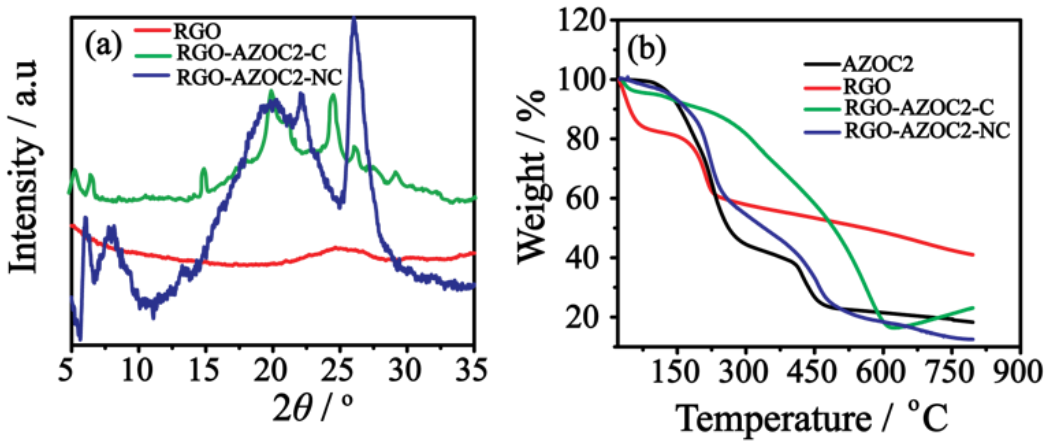

Figure 4.2: a) XRD patterns of RGO, RGO-AZOC2-C, and RGO-AZOC2-NC. b) TGA analysis of RGO, AZOC2, RGO-AZOC2-C, and RGO-AZOC2-NC.

Thermogravimmetric analysis (TGA) also supports the formation of covalent and non-covalent RGO-AZOC2 (RGO-AZOC2-C & RGO-AZOC2-NC) (Figure 4.2 b). The RGO shows main mass loss from 140 to 250 ˚C due the loss of carboxylic acid groups. Upon assembly formation with AZOC2, there occurs a comparatively lower rate of mass loss, which clearly points to the interaction of AZOC2 with RGO. The AZOC2 shows a two-step weight loss because of the larger rupture of the azobenzene backbone as well as the elimination of carboxylic acid groups. The covalent and non-covalent assemblies formed between RGO and AZOC2 are relatively stable as evident from their lower decomposition rates (Chen et al. 2015).

The covalent hybrid RGO-AZOC2-C is further characterized by scanning electron microscopy (SEM) with EDAX. The EDAX spectra shows the atomic percentage of nitrogen in covalent RGO-AZOC2-C as 14.26 (Figure 4.3).

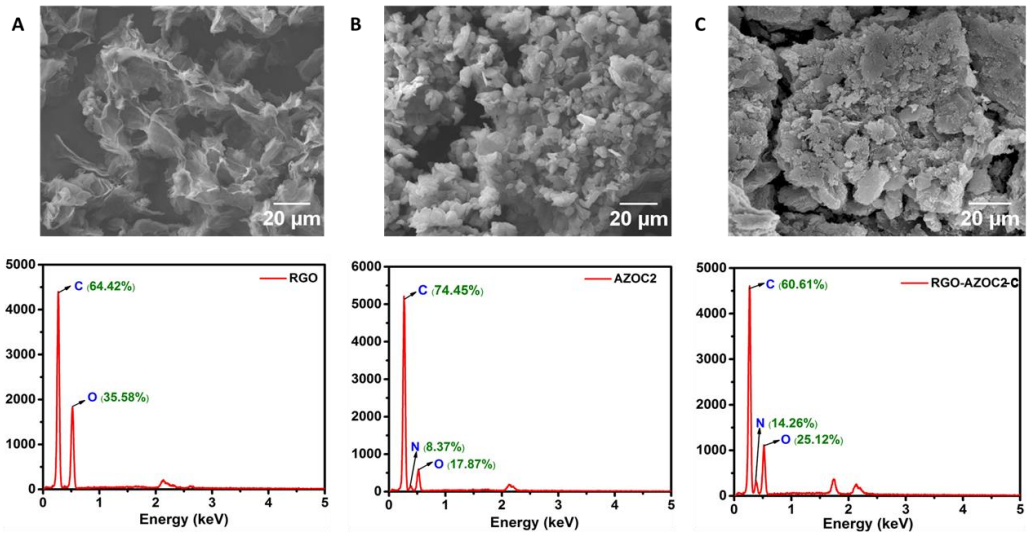

Figure 4.3: SEM with EDAX analysis of A) RGO, B) AZOC2 C) RGO-AZOC2-C.

Both covalent and non-covalent hybrid formation is again supported by transmission electron microscopy analysis (TEM) (Figure 4.4).

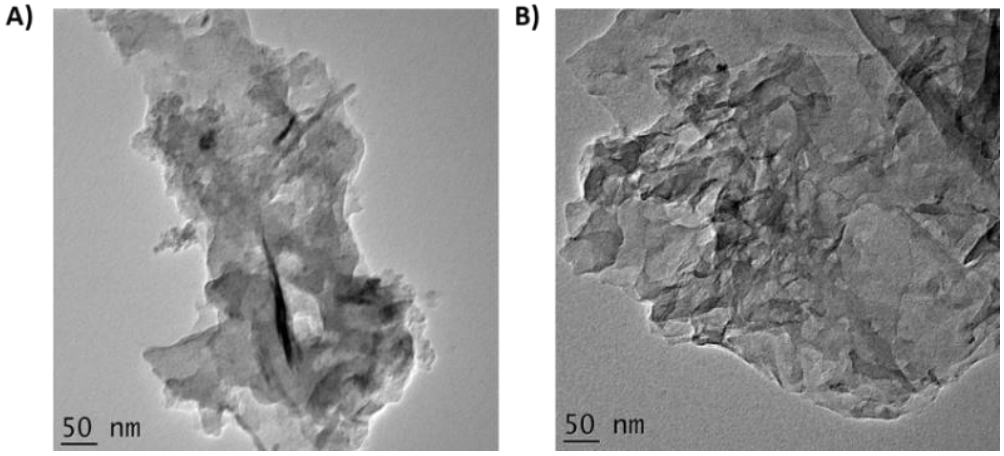

Figure 4.4: TEM of A) RGO-AZOC2-C B) RGO-AZOC2-NC. In both the hybrids the crystalline nature of RGO-AZOC2 is lost. The AZOC2 forms a layer over RGO in the case of RGO-AZOC2-NC through hydrogen bonding and π-π stacking interaction. In RGO-AZOC2-C, the AZOC2 is almost incorporated into the layers of RGO through anhydride linkage.

The photoisomerization behavior of AZOC2, covalent and non-covalent assemblies of RGO-AZOC2 are studied by photo irradiation using band pass at 360 nm by LOT Oriel 200W high pressure mercury lamp. The photostationery state (PSS) is reached around 25 min and 50 min respectively for AZOC2 and RGO-AZOC2-C. The non-covalent hybrid RGO-AZOC2-NC reached the PSS after 35 minutes. The yield of the *cis* isomer at PSS for AZOC2, RGO-AZOC2-C and RGO-AZOC2-NC are 27 %, 8.8 % and 25.2 %, respectively (Mahesh et al. 2012). The rate constant for the photoisomerisation of AZOC2 is 0.04829 min^{-1} and that for covalent RGO-AZOC2-C is 0.04259 min^{-1}. The non-covalent hybrid RGO-AZOC2-NC has a value 0.04687 min^{-1} (Airinei et al. 2011).

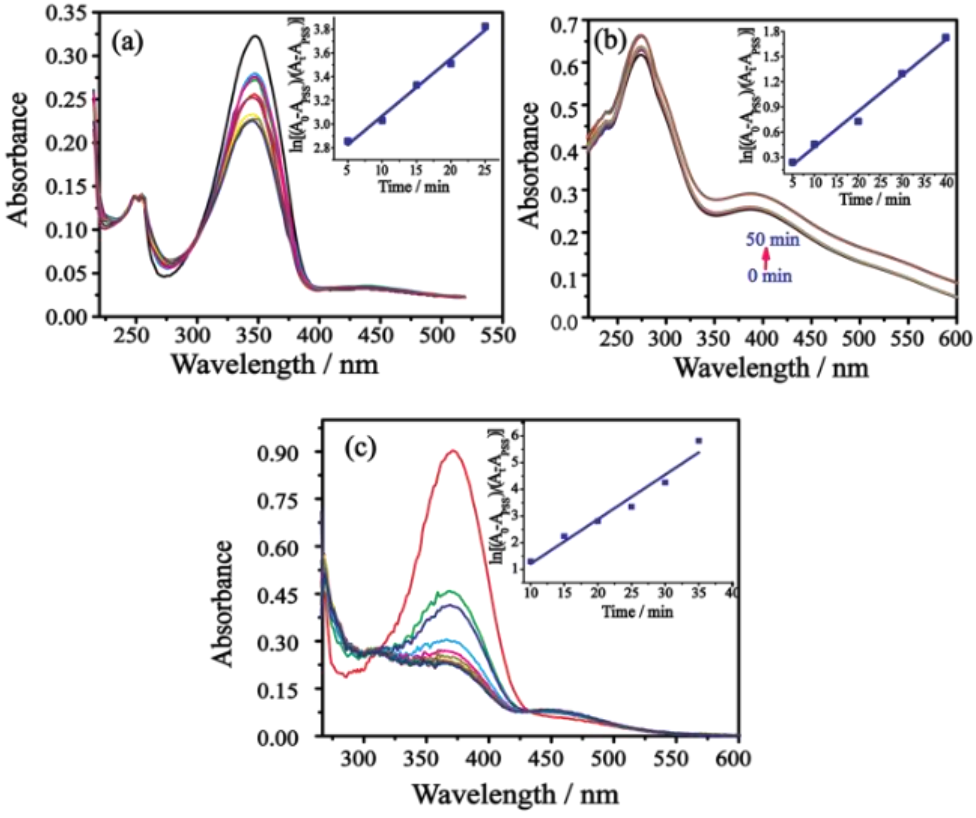

Figure 4.5: a), b) &c) Photoirradiation experiments of (a) AZOC2, (b) RGO-AZOC2-C, and (c) RGO-AZOC2-NC using bandpass light of 354 nm. The inset plot gives the rate constant (K) for *trans-cis* isomerisation.

The low value of rate constant as well as the reduced yield of *cis* isomer at photostationery state (PSS) for assemblies RGO-AZOC2 clearly indicates the restriction in the photoisomerisation capacity of AZOC2 upon functionalization with RGO (Feng et al. 2012; Luo et al. 2015). The steric hindrance offered by the RGO to the photoisomerization is the main reason for this (Figure 3a, 3b & 3c). From the values of rate constants it is clear that the hybrid formed through covalent linkage has relatively low rate of isomerization in comparison with the non-covalent hybrid.

The photomodulation of electrical conductance in the covalent and non-covalent hybrids RGO-AZOC2 is then monitored by chronoamperometric measurement (Figure 4.6). The molecule AZOC2 being an insulating material is not capable of showing any significant conductance whereas both the hybrids RGO-AZOC2 show a reasonable conductance value.

The photoresponsiveness of assemblies are studied by subjecting them to UV illumination at definite intervals. When the UV light is switched on there is an upswing in the value of photocurrent and upon removing the UV source the current subsides. The photoresponse ratio calculated for the covalent hybrid RGO-AZOC2-C is 0.178 and the same for the non-covalent hybrid RGO-AZOC2-NC is 0.571 (Fouda et al. 2014). The photoresponse ratio is calculated using the equation 4.1,

$$I_{Ph}/I_d \quad (4.1)$$

Where I_{Ph} is the response current, I_d is the current in dark and I_{UV} is the current under UV illumination condition. The response current is calculated using the equation 4.2,

$$I_{Ph}=I_{UV}-I_d \quad (4.2)$$

The current variation in the hybrids with UV illumination and non-illumination is directly connected to the photoisomerisation behavior of AZOC2 which is the azobenzene counterpart of the hybrids. The photoirradiation experiments clearly support the conversion of *trans*-AZOC2 to the *cis*-AZOC2 upon UV irradiation. The *trans* form of azobenzene systems are planar and generally possess larger molecular length compared to the *cis* isomer (Zhang et al. 2010). That means the tunneling distance for the current transport gets reduced when AZOC2 isomerizes to *cis* form upon UV irradiation (Del Valle et al. 2007). Thus the hybrids RGO-AZOC2 show a higher current upon UV illumination due to the isomerisation of AZOC2 in them to the *cis* form. On the other hand when the UV source is removed the current declines. This is because of the reverse isomerisation of AZOC2 to the *trans* form under dark condition (Zhang et al. 2010).

The chronoamperometric measurements (Figure 4.6) also provide a distinction in the behavior of covalent and non-covalent hybrids RGO-AZOC2 with regard to the conductance switching. In the case of covalent assembly there is a slight decrease in current after each cycle. On the other side the non-covalent hybrid exhibits uniform current switching in all the cycles. This current decrease in the covalent RGO-AZOC2-C can be attributed to the steric hindrance offered to AZOC2. In RGO-AZOC2-C, there is a direct bond formation between RGO and azobenzene system. So, the photoisomerisation rate of this hybrid decreases with time due the steric effect caused by the direct linkage. The direct linkage will restrict the freedom of AZOC2 to switch between the two conformational states. As a result the *trans-cis* isomerisation rate of the hybrid RGO-AZOC2 decreases after each

illumination cycle. As a result of this there is a decay in current with greater illumination time (Viero et al. 2015; Li et al. 2017).

The samples are expected to give more uniform cycles if the experiment is carried out under high vacuum conditions or in closed conditions. Still 100% percent isomerisation cannot be guaranteed (van der Molen et al. 2009).The measurements are done at different time intervals and same behavior is observed throughout. The UV illumination time is then fixed in order to avoid photodegradation leading to device failure.

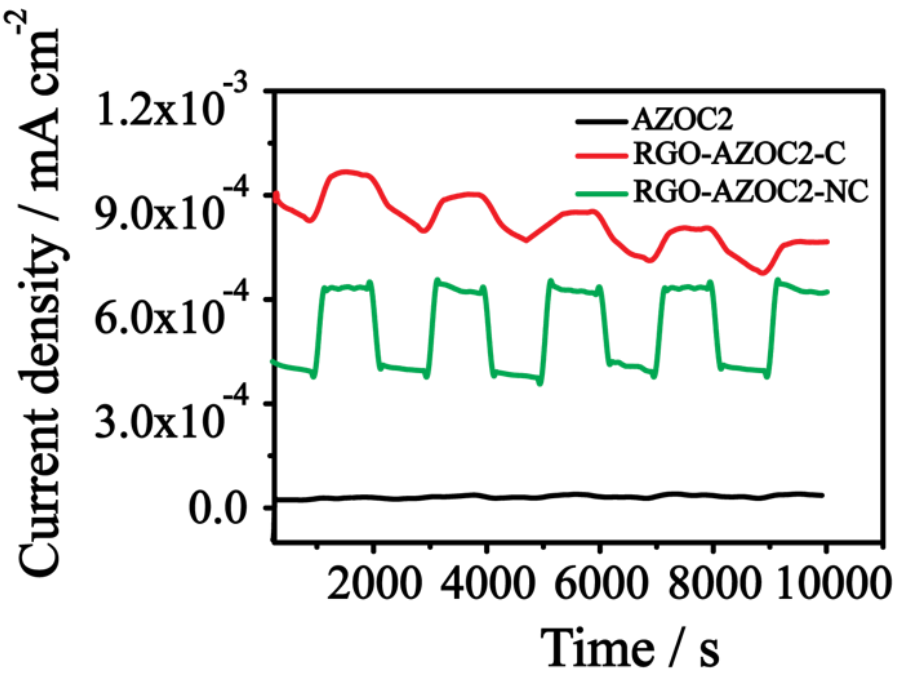

Figure 4.6: Photocurrent measurement of AZOC2, RGO-AZOC2-C, and RGO-AZOC2-NC as a function of time with alternate On/Off UV illumination at 0.45 V in 0.1 M KCl.

The non-covalent hybrid RGO-AZOC2-NC shows a steady current throughout the illumination cycles. Here there is no direct bondage between RGO and AZOC2. The interaction between the components is non-covalent like hydrogen bonding between the carboxylic acid functional groups and π-π stacking

of the carbon backbones. In RGO-AZOC2- NC the two bulkier alkyl chains of AZOC2 facilitate formation of dispersion with RGO. The flexibility of movement of AZOC2 is not much restricted in the non-covalent hybrid in comparison with the covalent one. So, the rate of photo-induced *trans-cis* isomerisation remains more or less the same throughout the illumination cycles. The cycles were repeated 100 times and the current/conductance behavior showed steady response.

The insulating azobenzene system AZOC2 possesses a remarkable ability in phototuning the conductance/current behaviour of RGO. The AZOC2 influences the conductance property of RGO with and without a direct linkage. Both the hybrids with phototunable behaviour are promising candidates especially in the field of sustainable molecular electronics. In the case of covalent assembly RGO-AZOC2, there is a damping of current value with time during the UV exposure. This may be due to the restricted rate of photoisomerisation of azomoiety in it, as a result of steric hindrance caused by the covalent linkage between the counterparts. The phototunability is there for about 50 cycles.

No doubt this kind of systems can be employed in developing chemresistors which form a suitable sensor configuration for targeting various analytes like gases (Zhang et al. 2008; Perreault et al. 2015). The non-covalent hybrid shows a lesser value of current compared to covalent hybrid but offers better phototunability of current than the latter. The current value remains steady with multiple cycles. This system can be employed in developing optoelectronic devices like field effect transistors (FETs) etc. The low cost of production with easy and facile synthetic method is an added advantage in the construction of both covalent and non-covalent assemblies.

4.4. Conclusion

In this work reduced graphene oxide (RGO) is coupled with a photochromic azobenzene molecule developed from cardanol (AZOC2). The interactions between both the components are studied using covalent and non-covalent approaches. Even though AZOC2 is an insulator, it modulates the conductance/current behaviour of RGO. The hybrids show enhanced current value upon UV illumination due to the *trans-cis* isomerisation of the azobenzene system. The current value in the case of covalent hybrid RGO-AZOC2-C decays significantly after prolonged UV irradiation. This is due to the steric effect which causes a restriction to the photoisomerisation ability of AZOC2. Unlike RGO-AZOC2-C, the RGO-AZOC2-NC exhibits a steadiness in the photo-induced conductance switching. The flexibility of the non-covalent hybrid removes the possibility of steric hindrance to the azobenzene system AZOC2 to a large extent, since there is no direct bondage of the former with RGO. Thus the non-covalent hybrid gives a better phototuned conductance than the covalent one. Both the hybrids can be utilized as potential candidates for developing optoelectronic devices like FETs, Chemresistors, Memory devices etc.

******

Chapter 5

Phototunable Hybrid Materials from cardanol derived photochromic molecule implanted with Single-walled Carbon Nanohorn

Single-walled carbon nanohorns are one of the most interesting new members of carbon nanomaterial family due to their peculiar properties. Though these materials are employed for fabricating a large number of smart materials. But their hybrids with photochromic molecules are rarely used. In this work, an azobenzene system derived from cardanol, a bioresource is integrated with nanohorns. The hybrids are developed in two ways- the covalent and non-covalent linkage between the components. The ability of an azo molecule of this hybrid system to modulate the current/conductance behavior of the single-walled nanohorn component is observed.

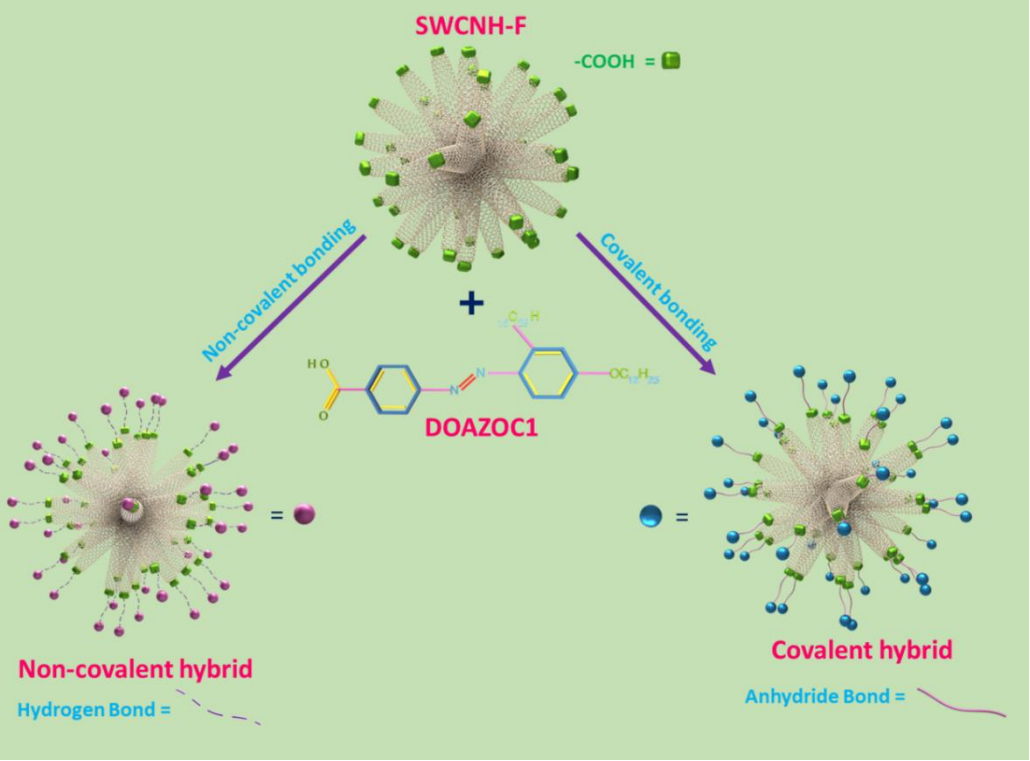

5.1. Introduction

Single-walled carbon nanohorns are a class of carbon nanocones belonging to the family of carbon nanomaterials. They are similar to single-walled carbon nanotubes but superior to them in many aspects. For example, the SWCNHs have high surface area, mechanical and thermal stability than carbon nanotubes. The SWCNHs are generally synthesized by two different methods: arc discharge (Yamaguchi et al. 2004) and CO_2 Laser Ablation method (Iijima et al. 1999). The most important advantage associated with their synthesis is that during the entire process metal catalyst can be excluded. The nanohorns are obtained in higher yields with greater purity around 95%. The morphology of SWCNHs formed is dependent on the type of inert gas employed as atmosphere during their synthesis. Under argon atmosphere the nanohorns assume dahlia-like morphology (95 %). With helium/nitrogen, nanohorns is in the form of budlike morphology (Zhu et al. 2010).With neon, *'Ne-dahlia'* is formed (Azami et al. 2007*).* Compared with the ablation method, arc discharge process is more cost-effective. The other popular strategies are simple pulsed arc discharge (Yamaguchi et al. 2004), welding arc torch in open air (Takikawa et al. 2002) and cavity arc jet methods under open air condition (Ikeda et al. 2002). Moreover an arc in liquid method is used to prepare metal encapsulated SWCNHs(Sano 2004; Sano et al. 2004).

The SWCNHs also have very peculiar structural properties making them distinct from other carbon nanomaterials. The individual nanohorns have an average diameter of 4 nm and tubular length of 30-50 nm. The horn tip is composed of pentagons and the cone opening angle is around 20° (Yudasaka et al. 2007). More

than 2000 such nanohorns combine to form aggregates with spherical morphology with diameter 80-100 nm. It is reported that carbon synthesized nanohorns normally consist of 70% tubular, 15% defective (on tips),12% graphitic and 2.5% amorphous carbon (Murata et al. 2001).

The unique structure of SWCNHs imparts them a variety of properties. They possess good thermal conductivity. The heat treatment of single-walled carbon nanohorns at 1200-1400 °C results in the formation of double-walled carbon nanohorns, whereas at 1960 °C yields multi-walled carbon nanohorns (Yudasaka et al. 2003).Other interesting properties of SWCNHs are high porosity and high specific surface area. The investigation of the porous nature of SWCNHs reveals the presence of two different types of micropores in them. The first type is the inter-nanohorn pores which are open and show size variation with temperature. The second type is the intra-nanohorn pore, the closed ones remaining unaffected on heat treatment (Figure 5.1)(Yang et al. 2005). The porosity, as well as the surface area of the molecules, can be increased by chemical modification (Murata et al. 2000; Bekyarova et al. 2002; Ohba et al. 2004).

The chemical modification can be done in a number of ways; the major method is through oxidation. The pristine SWCNHs have a surface area around 300 m^2g^{-1}. The heat treatment results in the creation of nano windows over the surface and opening of internal pores leading to an increased surface area (Murata et al. 2001). For example, the heat treatment at 693K resulted in increased surface area of 1010 m^2g^{-1} and an increased micropore volume of 0.47 ml/g. The oxidation at different temperatures provided the control over number as well as the size of these nano windows (Bekyarova et al. 2002). The fast rise in temperature during the

oxidation process always results in C-dust contamination. So always a slow increase of temperature, usually 1 °C or less, and low oxygen concentration is more advantageous in the hole opening of SWCNHs (Fan et al. 2006).

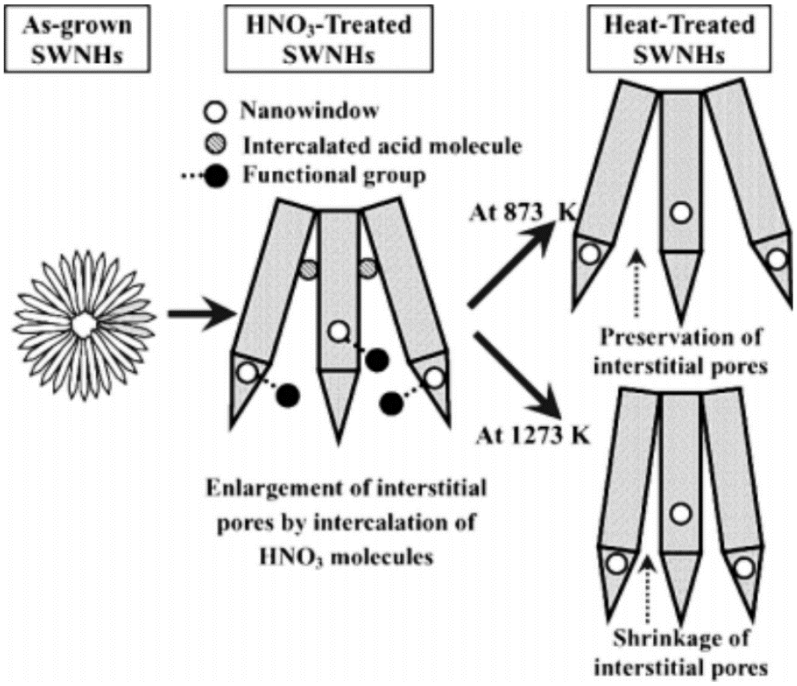

Figure 5.1: Schematic representation of different types of pore generation during functionalization. (Reprinted with permission from reference [298] Copyright 2005 WILEY-VCH Verlag GmbH & Co.KGaA,Weinheim.

The oxidation also results in an increase of oxygen containing functional groups.(Bekyarova et al. 2002). The oxidized nanohorns on heat treatment under H_2 condition developed more opened pores but with less oxygen functionalities (Miyawaki et al. 2004). The heat treatment under CO_2 atmosphere also resulted in the opening of pores; but this was less effective compared to oxygen condition (Bekyarova et al. 2002; Bekyarova et al. 2003). The treatment with strong acids like H_2SO_4, HNO_3 or mixture H_2SO_4/H_2O_2 also resulted in both inter and intra pore opening (Yang et al. 2004; Yang et al. 2005). The microwave irradiation methods

are now widely popular and have replaced for oxidation of SWCNHs (Yoshida et al. 2006).

The SWCNHs also exhibit magnetic character. The investigation with electron spin resonance (ESR) and static magnetic susceptibility measurements brings out the presence of at least one unpaired electron and a weak diamagnetic susceptibility nature (Bandow et al. 2001). The studies with high-resolution ^{13}C NMR spectroscopy revealed the presence of two components in SWCNHs. The first component appearing at 124 ppm corresponds to the fast spin-lattice relaxation behaviour indicating that the surface nanohorns show carbon nanotube like character. The other component at 116 ppm with much slower relaxation indicates the graphite-like core structure (Imai et al. 2006). The SWCNHs also show good field emitting character, with low turn-on field and good long-term stability (Bonard et al. 2002). SWCNHs also have good mechanical stability and high dispersibility(Casillas et al. 2014; Lodermeyer et al. 2016).

The SWCNHs also have unique electronic properties due to the presence of the conical apex of pentagons(Garaj et al. 2000; Yudasaka et al. 2007). Many scientists applied theoretical calculations to derive the electronic nature of SWCNHs. Berber et al. in 2000 employed parametrized linear combination of atomic orbitals calculations to study the stability, optimum geometry and electronic properties of SWCNHs. In their study, they considered distinct morphological SWCNHs with varying relative location of five terminating pentagons. The conclusion is that there is a net flow of electrons towards the pentagonal conical cap of nanohorns (Berber et al. 2000). This finding is again backed up by simulated scanning tunneling microscopy. Kolesnikov et al. in 2004 further investigated the

effect of pentagonal defects on the electronic structure near the tip of carbon nanohorns within the continuum gauge field-theory model. According to them, the more intense charge density near the tip is due to the existence of a localized electron state at the Fermi level (a true zero mode state)(Kolesnikov et al. 2004).

Generally, pristine SWCNHs exhibit an n-type semiconducting behavior. The oxidized SWCNHs behave as a p-type semiconductor. The CO_2 and O_2 adsorption studies provide evidence for this shift from the n-type to p-type behavior. (Urita et al. 2006). The CO_2 is an electron donor with electron affinity values -2.1 to -1.1 eV (Tang et al. 1974). The electron donors enhance the electrical conductivity of n-type semiconductors. Therefore, the adsorption of CO_2 causes an increased electrical conductivity of SWCNH. On the other hand, the oxidized SWCNHs show decreased electrical conductivity as a result of CO_2 adsorption. This is due to the annihilation of holes present in oxidized SWCNH by the electron donation from CO_2. After the initial drop, the conductivity increases because of the continued electron transfer from CO_2.

The O_2 molecule is a potential electron donor with electron affinity value ranging from 0.4-0.5 eV (Gutsev et al. 1998). The O_2 adsorption by n-type pristine SWCNH decreases its conductivity due to the combination of electron and hole carriers. But the O_2 adsorption does not explain the electrical π-conductivity behavior of oxidized SWCNHs. The dissimilarities in gas adsorption exhibited by pristine as well as oxidized SWCNHs are due to differences in pentagon concentration.

The functionalization of carbon nanohorns is done through both covalent and non-covalent modes (Zhu and Xu 2010). In the covalent functionalization, the foreign moieties are attached to the nanohorn surface through a stable bond formation between the components. This can be done in two different ways, i) by the oxidation of the conical apex which creates oxygen-containing functionalities at the apex (Sandanayaka et al. 2007; Mountrichas et al. 2009; Rubio et al. 2009), ii) imparting sidewall functionalization (Isobe et al. 2006; Rubio et al. 2009). The non-covalent functionalization is mediated by supramolecular interactions like π-π stacking, electrostatic interactions, hydrogen bonding (Pagona et al. 2007; Pagona et al. 2007; Mountrichas et al. 2009).

The multifunctional properties of SWCNH make them useful in different fields. They are widely employed as storage materials of hydrogen(Tanaka et al. 2004; Tanaka et al. 2005) and methane (Murata et al. 2004; Murata et al. 2005). SWCNHs act as good catalyst support (Karousis et al. 2009) (Kosaka et al. 2009) as well as efficient carriers in drug delivery system (Ajima et al. 2008). They are also utilized for magnetic resonance imaging(Miyawaki et al. 2006) and as sensor materials (Liu et al. 2010).

There is a plethora of reports, which deals with the functionalization of SWCNHs with various moieties like polymers (Kausar 2018), dendrimers (Guerra et al. 2012) and porphyrin (Pagona et al. 2012) through covalent and non-covalent approaches. For the first time we integrate an azo moiety of bio-origin with SWCNH through covalent as well as non-covalent functionalization. A comparative study of the conductance switching performance of the hybrids is also

conducted by us. This comparative study also includes the influence of azomolecule in the process.

5.2. Experimental Section

5.2.1. Materials and Methods

Pristine Single-walled carbon nanohorns are purchased from Global nanotech. India. Hydrogen peroxide (30%) is purchased from Merck Life Science Private Limited. Toluene is purchased from Spectrochem India Pvt Ltd. *N*,*N*-Dimethyl formamide(DMF) is purchased from spectrochem India Pvt Ltd.

5.2.2. Synthesis

5.2.2.1 Synthesis of functionalized single-walled carbon nanohorn (SWCNH-F)

The single-walled carbon nanohorn is stirred in methanol solution to remove its puffiness. The solution is then filtered and the carbon nanohorns are kept in the vacuum oven at a temperature of 65 °C for 12 h to ensure the complete removal of methanol. Around 500mg of SWCNH is added to 100 mL of hydrogen peroxide (30%) and the solution is refluxed at a temperature of 60 °C for 5 h. Then the solution is filtered and then repeatedly washed with deionized water to remove residual hydrogen peroxide. The sample is then kept in the vacuum oven for 24 h at a temperature of 65 °C (Scheme 5.1).

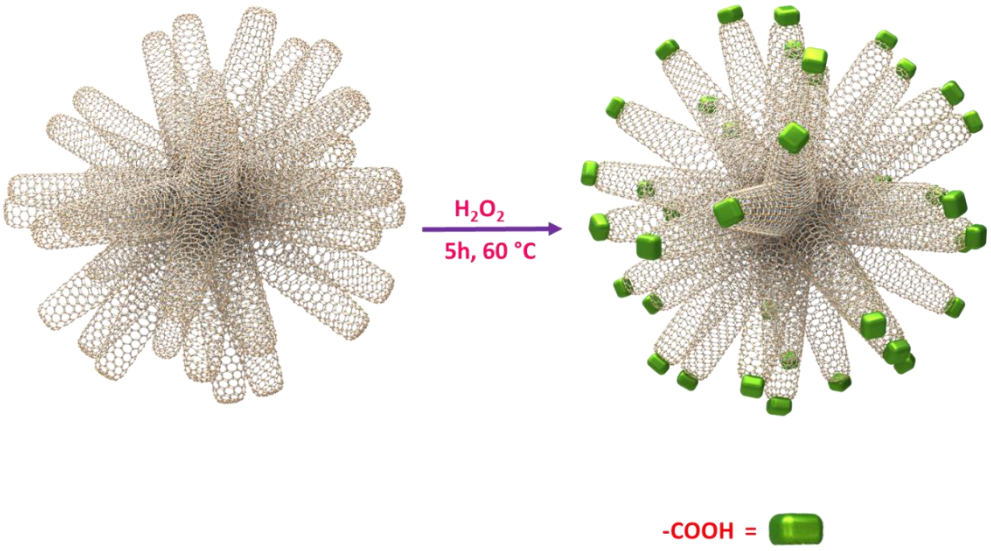

Scheme 5.1: Functionalization of SWCNH.

5.2.2.2. Synthesis of 4-[(4-cardanyl)azo]benzoic acid (AZOC1)

The synthesis of molecule AZOC1 is already explained in detail in chapter 2.

5.2.2.3. Synthesis of 4-[4-dodecyloxycarbonyl-2-pentadecylphenylazo] benzoic acid (DOAZOC1)

The Synthesis of molecule DOAZOC1 is already described in chapter 2.

5.2.2.4. Synthesis of SWCNH-F-DOAZOC1 Covalent Hybrid

A stock solution of SWCNH-F is prepared at a concentration of 0.5mg/ml in toluene. DOAZOC1 is converted to the acid chloride by refluxing with thionyl chloride for 24 h. After removing the excess thionyl chloride by vacuum distillation, the compound is mixed with SWCNH-F in the ratio 1:3 in 150 mL of toluene solution. The mixture is then kept for refluxing at 120 °C for 120 h under nitrogen atmosphere. The resulting SWCNH-F-DOAZOC1 covalent hybrid is filtered and washed repeatedly with ethanol. The complete removal of the reactants is made sure

by washing till the filtrate become colourless. The sample is then kept in vacuum oven for 6 h (Scheme 5.2).

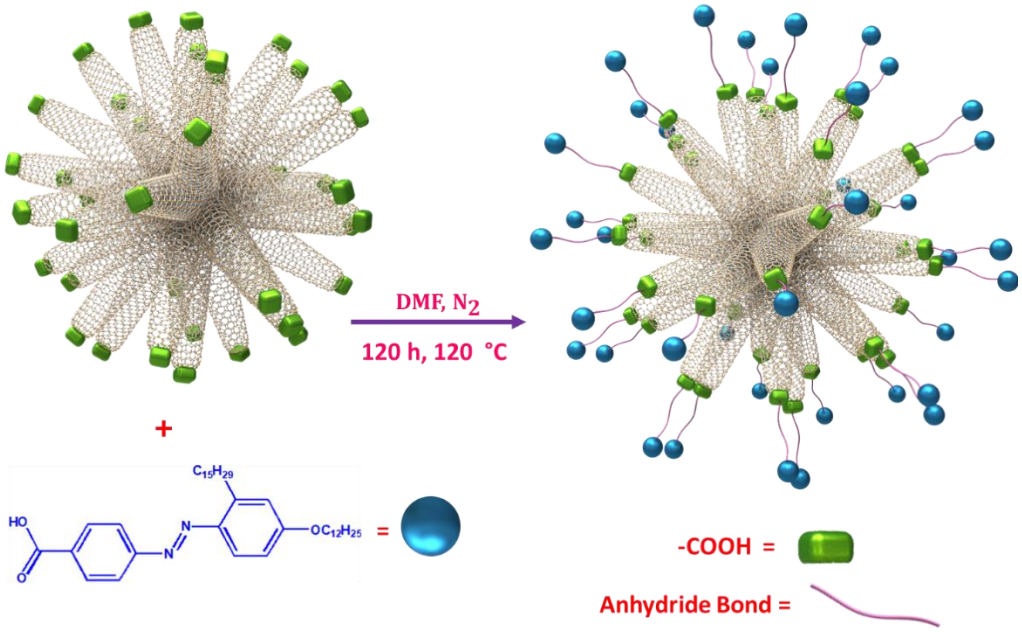

Scheme 5.2: Synthesis of SWCNH-F-DOAZOC1 Covalent Hybrid.

5.2.2.5. Synthesis of SWCNH-F-DOAZOC1 Non-Covalent Hybrid

To a 10 mL solution of 1×10^{-4} M solution of DOAZOC1 in toluene, 10 mL stock solution of SWCNH-F is added. The mixture is then subjected to probe sonication for 30 minutes. The solution is then kept for drying in a 100 mL beaker in vacuum oven for 4 h (Scheme 5.3).

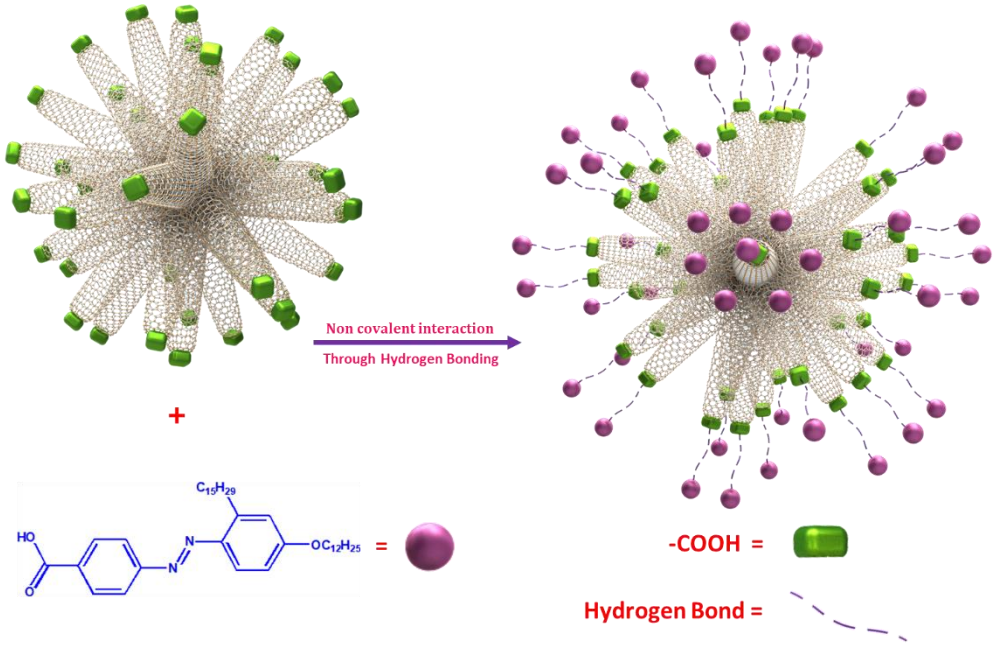

Scheme 5.3: Synthesis of SWCNH-F-DOAZOC1 Non-covalent Hybrid.

5.2.3. Instrumentation

The Fourier Transform Infrared studies are carried out using Perkin-Elmer spectrum 100 FTIR spectrophotometer at room temperature. The Raman analysis is carried out using a Renishaw Confocal Raman Microscope with 530 nm laser. X-ray diffraction analysis of all the samples is done using a PANalytical X'pert Pro instrument having a scan rate of 0.5 °C per min using Cu Kα radiation (1.5418 A°). The thermogravimetric measurements (TGA) are done using TAQ50 instrument under nitrogen condition with a heating rate of 5 °C per minute. The transmission electron microscopy (TEM) imaging of the sample is done with JEOL-JEM2100 microscope with acceleration voltage 200kV. Scanning electron microscopy (SEM) images are done with Gemini 500 FESEM. The photoirradiation experiments are done using Oriel Optical Bench fitted with a 200W high-pressure mercury lamp with 354 nm band pass and 600 nm long pass. The UV-Visible absorption spectra

are recorded using Cary Bio 100. The conductivity measurements are done using Keithly 6221A 4-probe station. The thickness of the films is measured using DEXTAK profilometer. The linear current-voltage (I-V) characteristics are done with EVERBEING INT'I CORP 2-probe station with Quick IV computer GUI interface (Keysight). The light-induced current switching characteristics are studied through chronoamperometry method are done using three electrode cell PGSTAT302N electrochemical workstation (Autolab, Metrohm, Switzerland)

5.3. Results and Discussion

SWCNH-F-DOAZOC1 Hybrid formation can be characterized by various spectroscopic and microscopic techniques. The infrared spectra (IR) support the hybrid formation between SWCNH-F and DOAZOC1(Figure 5.2). The important peaks in DOAZOC1 are 3461 (Ar-COOH), 2920,2847 (-CH_2), 1726 (Ar-COOH), 3012 & 777 (-CH=CH-), 1594 (-N=N-),1212(Ar-C-O),1113 (R-C-O-Ar) cm^{-1}.

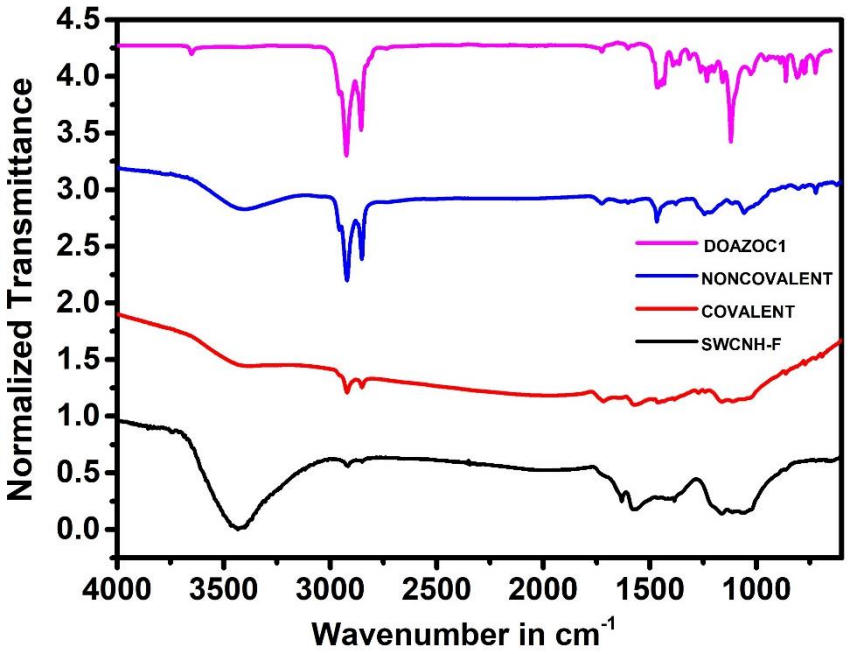

Figure 5.2: IR spectra of samples

The SWCNH-F has IR peaks at 3438 (Ar-COOH), 1552 (Ar-C=C-), 1100 (Ar-C-C-), 1635 (Ar-COOH) cm^{-1}. The evidence for the covalent hybrid formation is the appearance of IR peak at 1740 & 1800 cm^{-1} which corresponds to anhydride carbonyl stretch. Also, the hydroxyl peak is almost disappeared. Similarly, in the non-covalent hybrid, the hydroxyl peak at 3414 cm^{-1} is broader and the value is decreased when compared to that in SWCNH-F and DOAZOC1. This clearly indicates the hydrogen bond formation between SWCNH-F and DOAZOC1.

Further characterization of these hybrids were done by Raman Spectroscopy (Figure 5.3). The Raman spectra of SWCNH show D-band at 1323 cm^{-1} and G-band at 1582 cm^{-1}. Compared to other carbon nanomaterials, the D-band of SWCNH shows a slightly higher intensity due to the larger number of sp^3 atoms present (Utsumi et al. 2007). Upon oxidation, with hydrogen peroxide, the G-band shifts to a larger wavenumber of 1589 cm^{-1}. The carboxylic groups which are electron withdrawing in nature are responsible for this shift in wavenumber. The 2D peak also shows a shift from 2646 cm^{-1} to 2660 cm^{-1} due to the increase in the defect level.

In the covalent hybrid between SWCNH-F and DOAZOC1, the D-band is at 1339cm^{-1} and G-band at 1593 cm^{-1}. These shifts ($\Delta\lambda_D$ & $\Delta\lambda_{G)}$ are due to the direct linkage of DOAZOC1 with SWCNH-F which alter the defect site number. Similarly, in non-covalent hybrid, the values of D-band and G-band are 1338 cm^{-1} and 1586 cm^{-1} respectively. The I_D/I_G ratio of SWCNH-F, Covalent hybrid and non-covalent hybrid are 1.09, 1.21 and 1.29 respectively and this indicated the formation of respective hybrids

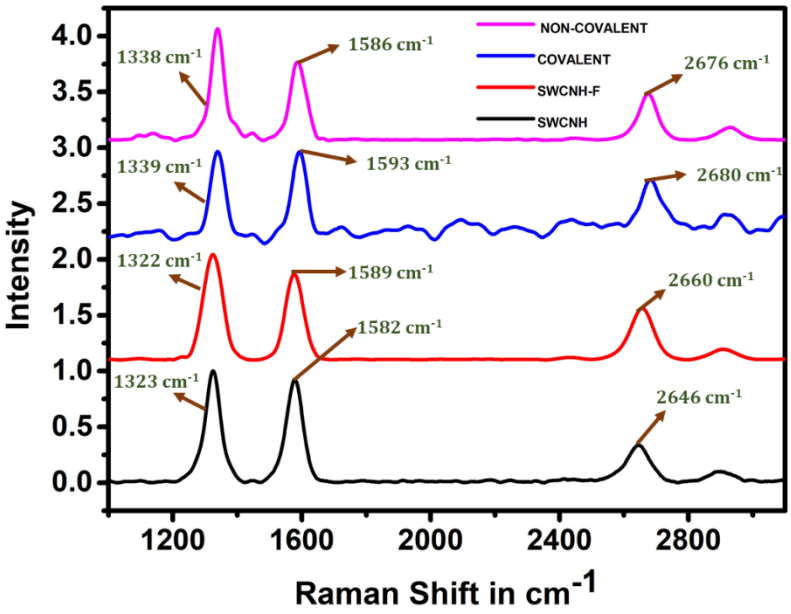

Figure 5.3: Raman Spectra of samples

Pristine SWCNH is an n-type semiconductor in nature which modify to p-type upon functionalization. Further functionalization with the electron donating DOAZOC1, regenerates the n-type behavior of SWCNH (Urita et al. 2006). As reported by Urita et al. in 2006 the electron donor species on SWCNHs improve the its electrical conductivity. Since the azobenzene part of DOAZOC1 is an electron donor, the doping with it can modify the electrical conductivity of SWCNH. This indicates that the electronic structure of SWCNH depends on the mode of interaction of azocompound with SWCNHs. That is both covalent and non-covalent interaction of azocompound with SWCNH can tune its electronic property which in turn reflects the phototunability property of the hybrid material. The 2D band of covalent and non-covalent hybrids appear at positions 2680 cm^{-1} and 2676 cm^{-1}. This indicates the improved graphitization of graphene layers after functionalization.(Wu et al. 2018).

We have investigated the formation and stability of these hybrids by thermal analysis techniques. The thermogravimetric and its derivative curves imply the stability of hybrids (Figure 5.4). The molecule DOAZOC1 starts decomposing around 75 °C, due to the removal of carboxylic acid molecules. Mass loss at 151 °C is due to the rupture of alkyl groups; that at and 295 °C is due to decomposition of azo compounds respectively. The SWCNH-F is relatively stable, but with increasing temperature, it shows mass loss, due to the decomposition of functional groups.

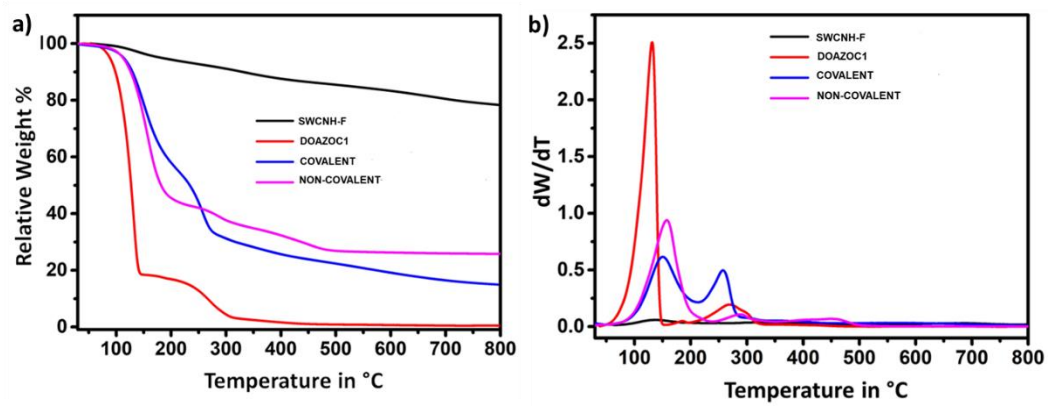

Figure 5.4: a) & b) TGA and DTG Spectra of samples

The covalent hybrid shows a mass loss at 106 °C, 186 °C and 271 °C due to the breaking of anhydride bonds and alkyl backbone (Zhang et al. 2010). The non-covalent hybrid exhibits mass loss at 115 °C and 204°C (Figure 5.4: a)(Chen et al. 2015). From the derivative plot Figure 5.4: b) the thermal stability of carbonyl group is improved in hybrids due to the interaction of DOAZOC1 with SWCNH-F.

In covalent hybrid the peak at 186 °C is less intense than the peak at 151°C in DOAZOC1. This difference arises due to the bonding of DOAZOC1 with SWCNH-F through the anhydride linkage. But in the case of non-covalent hybrid

the peak at 115 °C is more intense than covalent hybrid as the components are connected through supramolecular interactions like hydrogen bonding and π-π stacking. After covalent and non-covalent functionalization of SWCNH-F with DOAZOC1, the stability of DOAZOC1 is improved. The covalent hybrid is more stable compared to the non-covalent one as evident from the decomposition patterns.

SWCNH-F -DOAZOC1 hybridas can be characterized by microscopic techniques. We have characterized the hybrids by Transmission Electron Microscopy (TEM). The morphological study of samples by TEM shows that the pristine SWCNHs (Figure 5.5 a & b) resemble dahlia-like morphology with aggregate size ranging from 50-80 nm. Upon oxidation with hydrogen peroxide, there is no significant change in the morphology of SWCNH bundles. However a slight variation in the morphology of each nanohorn may occur due to the porosity creation during chemical oxidation (Figure 5.5 c & d)(Unni et al. 2015).

The morphology of covalent and non-covalent hybrid does not differ much from SWCNH-F (Figure 5.6). However, the presence of DOAZOC1 aggregates can be observed in the nanohorn surface. The process of such aggregation is comparatively less in covalent hybrid due to the effective bond formation between SWCNH-F and DOAZOC1. Since there is direct bond between SWCNH-F and DOAZOC1 the covalent hybrid assumes much well-defined bundle arrangement as well as petal distribution compared to the non-covalent hybrid.(Buback et al. 2010)

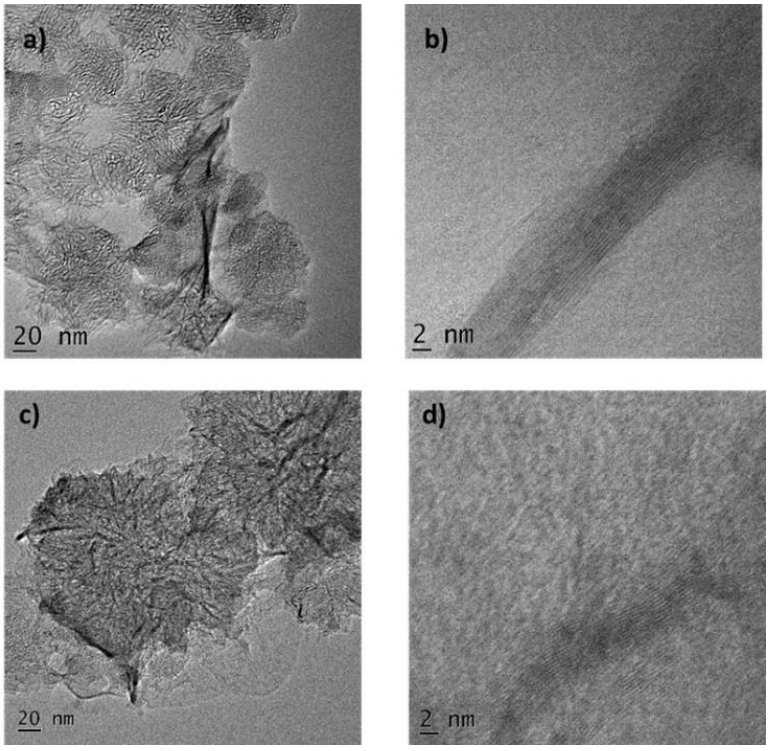

Figure 5.5: TEM images of a) & b) SWCNH, c) & d) SWCNH-F

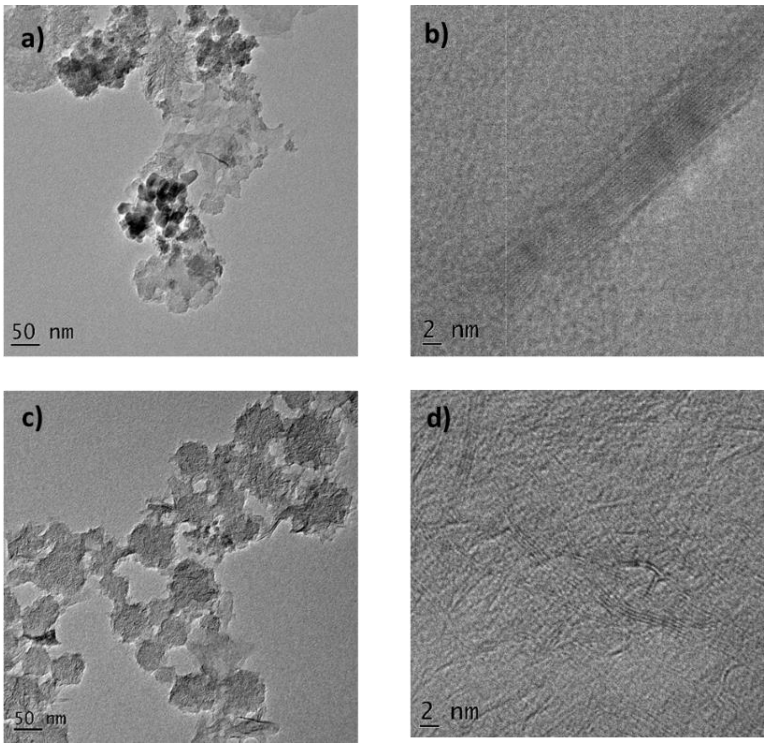

Figure 5.6: TEM images of a) & b) Non-covalent SWCNH-F-DOAZOC1, c) & d) Covalent SWCNH-F-DOAZOC1

Spectroscopic characterization of these hybrids were done by Ultraviolet Visible absorption Spectroscopy (UV-Visible). The UV-Visible absorption studies clearly indicate the hybrid development between SWCNH-F and DOAZOC1 in both covalent and non-covalent route.

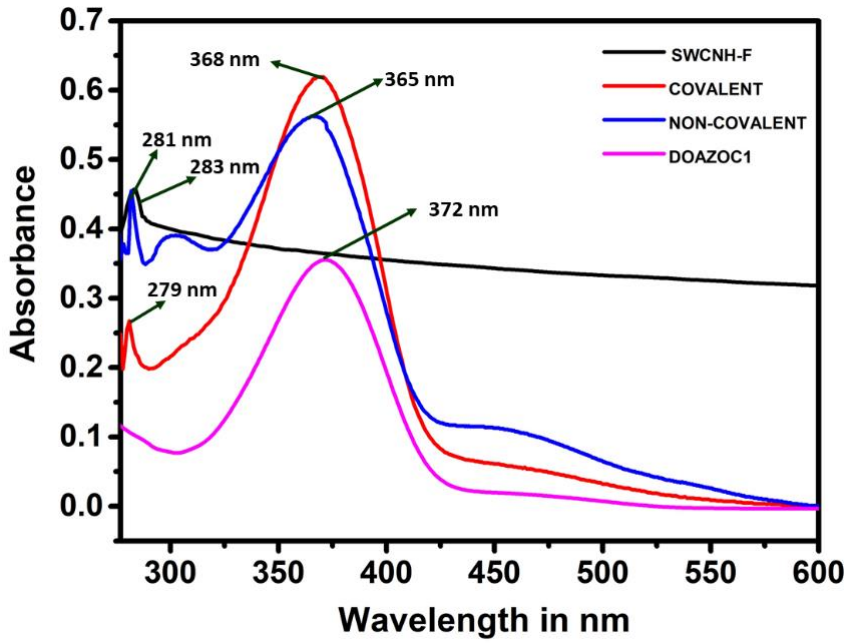

Figure 5.7: UV-Visible absorption spectra of samples

In toluene, SWCNH-F shows a peak around 281 nm corresponding to the π-π* transition. The DOAZOC1 molecule shows π-π* band at 372 nm. In the case of the covalent hybrid, the π-π* band appears at 368 nm. Another peak appears at 279 nm because of SWCNH-F. On the other hand, in non-covalent hybrid, the π-π* band appears at 365nm and the peak corresponding to SWCNH-F counterpart appears at 283 nm. The enhanced intensity of the π-π* band of DOAZOC1 in the hybrids is due to the hyperchromic effect induced by the auxochrome SWCNH-F (Figure 5.7).

On UV irradiation of covalent hybrid at 354 nm, the photostationary state (PSS) is reached after 80 minutes with 47 % yield of cis isomer. The rate constant

for the *trans-cis* photoisomerization is calculated as 0.04923 min^{-1}. Upon visible light irradiation at 600 nm the covalent hybrid recovers its decreased absorption after 220 minutes with a rate constant of 0.01751 min^{-1}(Figure 5.8).

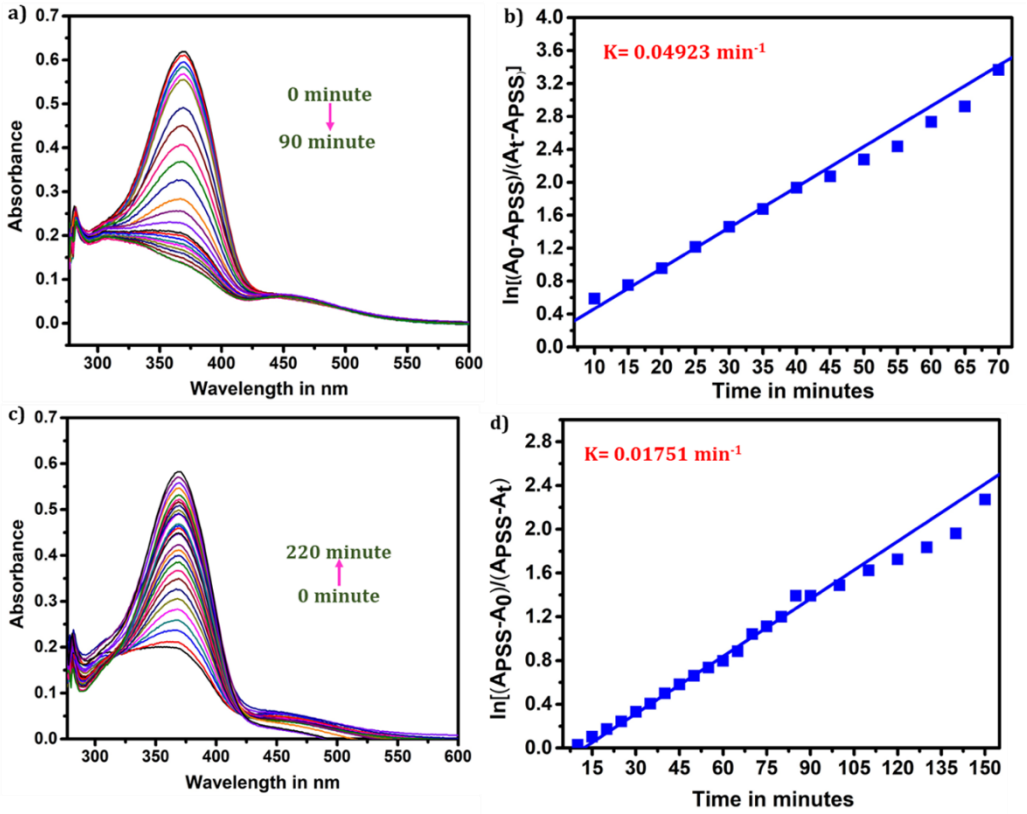

Figure 5.8: UV-Visible Photoirradiation experiments of Covalent SWCNH-F-DOAZOC1 a) at 354 nm, c) at 600 nm b) &d) corresponding rate constants at irradiation wavelength 354 nm and 600nm.

Compared to DOAZOC1 the rate constant as well as yield of cis isomer at PSS of covalent hybrid is significantly reduced (For DOAZOC1 yield of cis isomer is 70 % and rate constant for *trans-cis* photo-isomerisation is 0.34298 min^{-1}) (Devi et al. 2016). In the case of non-covalent hybrid, UV light irradiation at 354 nm reduces the absorption intensity due to the *trans-cis* photoisomerization of DOAZOC1(Figure 5.9). Compared to the covalent hybrid the photostationary state (PSS) of non-covalent hybrid is reached in 45 minutes.

The yield of cis isomer obtained for non-covalent hybrid at PSS is 62%, which is comparable with the 70% yield of DOAZOC1 and better than that of the covalent hybrid which is only 47%.

The rate constant for the *trans-cis* photoisomerization of non-covalent hybrid is 0.08684 min^{-1}. Photoirradiation with visible light of 600 nm of non-covalent hybrid resulted in *cis-trans* isomerization. The absorption intensity recovered after 160 minutes with a rate constant value of 0.03381 min^{-1}.

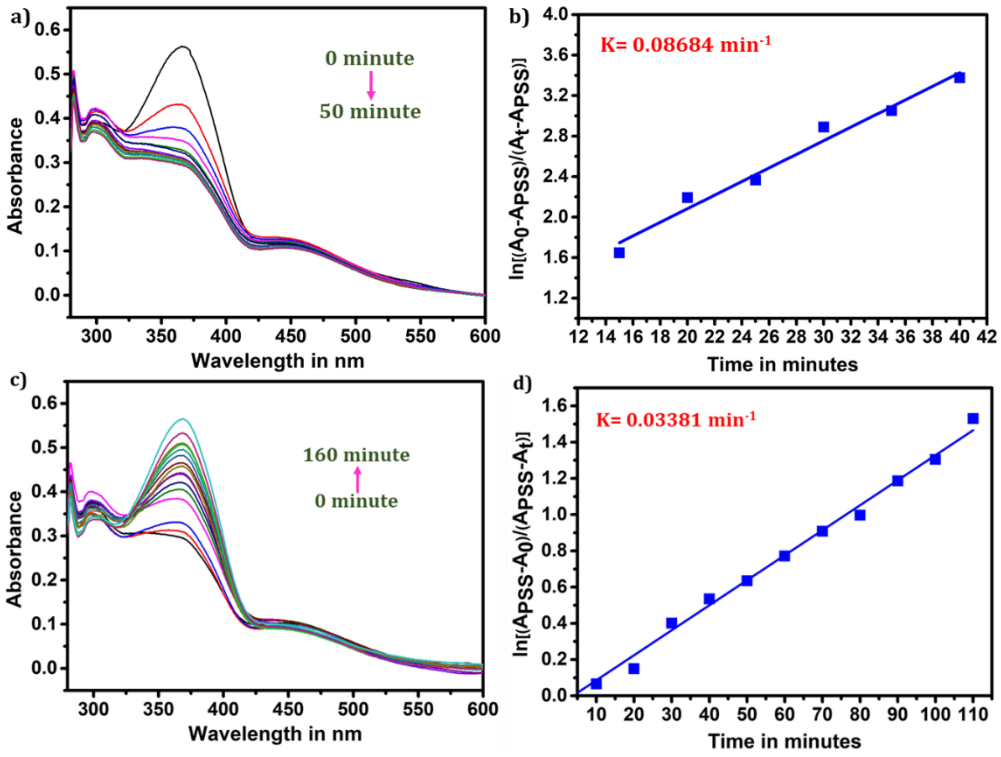

Figure 5.9: UV-Visible Photoirradiation experiments of Non-covalent SWCNH-F-DOAZOC1 a) at 354 nm, c) at 600 nm b) &d) corresponding rate constants at irradiation wavelength 354 nm and 600nm.

Among the hybrids, the non-covalent shows faster photoisomerization than the covalent. In, non-covalent hybrid the components are bonded through hydrogen bonding and π-π stacking. It makes the system more flexible and offers less

hindrance to the photoisomerization capability of the azo moiety. But in the covalent hybrid, the components are connected through covalent bonding and this makes the system more rigid. It hinders the photoisomerization ability of azocompound during irradiation experiments. Thus, the rate of photoisomerization reaction is slower compared to non-covalent hybrid.

The four probe conductivity measurements of hybrids in its *cis* and *trans* forms is measured by coating a thin film of thickness 1µm of samples over a glass plate. The electrical conductivity of non-covalent hybrid in its cis form is 104.4 S/cm which is higher than that of *trans* form (100.1 S/cm).

Compound	conductivity
SWCNH	**108.6 S/cm**
SWCNH-DOAZOC1 NON-COVALENT TRANS	**100.1 S/cm**
SWCNH-DOAZOC1 NON-COVALENT CIS	**104.4 S/cm**
SWCNH-DOAZOC1 COVALENT TRANS	**92.5 S/cm**
SWCNH-DOAZOC1 COVALENT CIS	**96.6 S/cm**

Table 5.1: Conductivity studies in 4-probe station

It is interesting to note that the electrical conductivity of SWCNHs (108.6 S/cm) is reduced after covalent and non-covalent functionalization. However covalent hybrid shows less conductivity compared to non-covalent hybrid and SWCNHs. In its *trans* and *cis* form, covalent hybrid displays an electrical

conductivity of 92.5 S/cm and 96.6 S/cm respectively. Low electrical conductivity of covalent hybrid is due to the rigidity of the system (Table 5.1).

A comparison of the linear current-voltage (I-V) characteristics of covalent and non-covalent hybrids is then made using 2-probe measurements (Figure 5.10). The voltage window is set from -40 to +40 V. The measurements are done with and without UV illumination. It is seen from the Figure 5.10 that in the case of the covalent hybrid, there is no noticeable increase in current with UV illumination time. But in the non-covalent hybrid there is an increase in current with the increased duration of UV irradiation. The insets of both graphs give the log value of current against voltage which shows that the current behaviour is the same irrespective of the positive or negative value of the voltage.

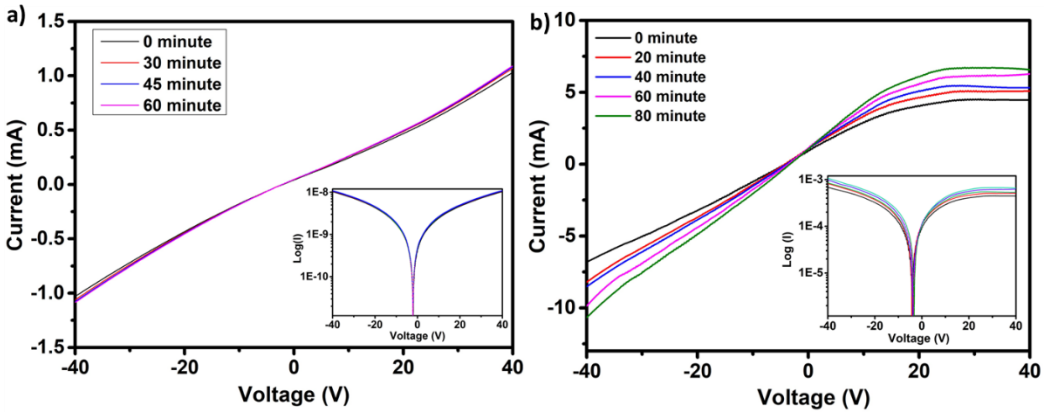

Figure 5.10: Linear current-voltage characteristics of a) Covalent SWCNH-F-DOAZOC1 & b) Non-covalent SWCNH-F-DOAZOC1. The inset shows the plot of the logarithm of current against voltage.

The photoresponse behaviour of the samples is measured as a function of time using chronoamperometric measurement. A three-electrode configuration setup is used for the same. The Ag/AgCl electrode is used as the reference

electrode and platinum wire and is used as the counter electrode. A thin film of hybrid samples spin coated over ITO plates is used as a working electrode.

It is seen from the figure 5.11 that when the UV light falls over the hybrids, the current shots up and on removing the source the current jumps down. In the case of the non-covalent hybrid, the reversible switching of current takes place for multiple cycles without any damping in the current value. The photoresponse ratio calculated for non-covalent hybrid is 151.89%. On the other hand, in covalent hybrid the photoresponse behaviour slowly dampens over time.

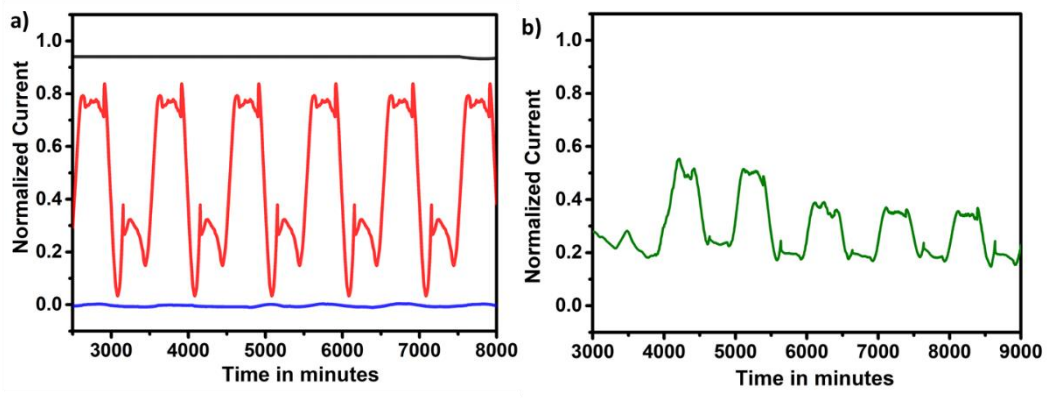

Figure 5.11: a) Photocurrent response of SWCNH-F (black), DOAZOC1 (blue) & Non-covalent SWCNH-F-DOAZOC1 (red) b) Covalent SWCNH-F-DOAZOC1 (green) as a function of time at alternate On/Off cycle of UV irradiation at +0.45 bias in 0.1M KCl solution.

Since the photoresponse behaviour of hybrid material strongly depends on the *cis*/*trans* isomeric form of DOAZOC1, the covalent and non-covalent functionalization of DOAZOC1 on SWCNHs influences the conductivity switching of the hybrids. Generally, *trans* azobenzene molecules are planar at room temperature. The theoretical calculations have proved that *trans* isomer possesses greater molecular length than *cis* isomer (Del Valle et al. 2007). The current flow between the photoresponsive molecules and carbon nanostructure is mainly due to

the tunneling of electrons. If the distance for the tunneling is less, more electron flow will occur and hence more current will be produced in the hybrid. With the cis isomer of the azo molecule, the tunneling distance is smaller as it is non-planar and this allows more current flow upon UV illumination (Feng et al. 2010). When the UV light is cut off, the back *cis-trans* isomerization of DOAZOC1 occurs and the current is decreased. It clearly indicates that the *cis* hybrid shows more conductance than the *trans* hybrid.

In the case of the covalent hybrid, both SWCNH-F and DOAZOC1 are linked through strong anhydride bond. So the system is highly rigid and intact. This greatly influence the photoisomerization ability of azobenzene counterpart in the hybrid. As evident from the UV-Visible irradiation studies the yield of cis isomer at PSS is less for covalent hybrid than for the non-covalent hybrid. Thus, the rate of *cis-trans* photoisomerization is faster in non-covalent hybrid which in turn improves its conductance switching behavior. It clearly suggests that the non-covalent SWCNH-F-DOAZOC1 hybrid is more photoresponsive than the covalent hybrid. This accounts for the improved conductance switching performance of the former.

5.4. Conclusion

To sum up, the study was focused on the photoinduced conductance switching properties of carbon nanohorn functionalized with cardanol derived azobenzene (DOAZOC1). Two different modes of coupling were used in the functionalization of DOAZOC1 on carbon nanohorns. One is the covalent approach through anhydride bond formation and the other one is non-

covalent/supramolecular approach through hydrogen bonding and π-π stacking interaction.

Then the covalent and non-covalent hybrids are characterized through techniques like IR, RAMAN, TGA, TEM. The UV-Visible photo-irradiation experiments illustrated the isomerization capability of both covalent and non-covalent hybrids. The rate of photoisomerisation exhibited by covalent hybrid is less than that of non-covalent hybrid. It is observed that upon UV illumination the conductance increases. The original value is restored when the UV source is removed. This is due to the *trans-cis* photoisomerization ability of azo molecule in the hybrids. The cis molecule offers shorter tunneling distance to the electron flow than the *trans* one. Thus, current increases with UV illumination. Upon removing the source, the isomerization shifts back to *cis-trans.* This increases the tunneling distance causing a fall in conduction.

The non-covalent hybrid shows more conductance than the covalent one. It is mainly due to the difference in the flexibility of the two systems. In the covalent hybrid, the SWCNH-F and DOAZOC1 are connected through anhydride linkage. Due to the stronger bonding, the rate of photoisomerization of DOAZOC1 in covalent hybrid is less as proved by photoirradiation experiments. The yield of cis isomer is also less for covalent hybrid compared to non-covalent one. Altogether this account for the lower conductance for covalent hybrid. It is evident that hybrids are typical candidates in the field of sustainable molecular electronic materials. Among them the non-covalent SWCNH-F-DOAZOC1 hybrid stands out with its distinct features.

Chapter 6

Conclusion and Future Perspectives

This chapter is an overall summary of the previous chapters and the conclusion of the entire research work performed on bioresource derived stimuli responsive molecules, and their hybrid materials with different carbon nanomaterials. Entire thesis is focused on development of optically responsive fluorescence switch and conductance switch from bioresource derived stimuli responsive molecules by both covalent and non-covalent approaches. Nature of substitution (Covalent, Non-covalent) and nature of carbon nanomaterial (1D, 2D, 3D) in the performance of conductance/flourescence switch also summarised in this chapter. The future perspectives of these optically responsive smart materials as sustainable molecular electronic devices are also analysed in this chapter.

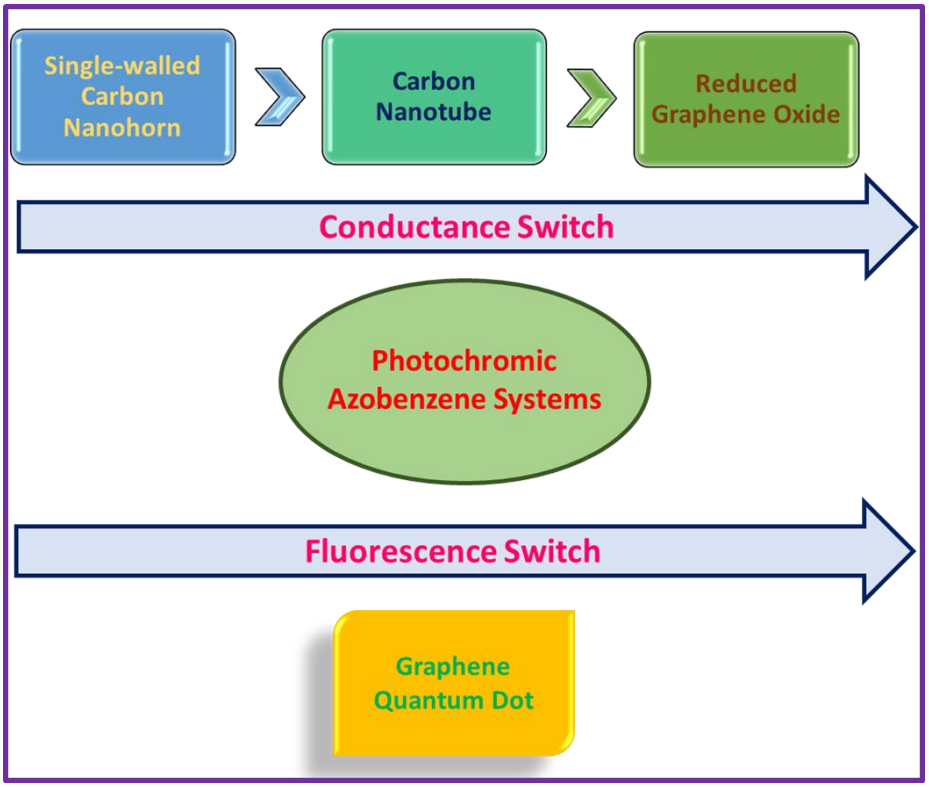

6.1 Conclusion

The present world is shaped largely by a revolution in the electronic field. The growing urbanization leads to an upgradation in the technology at the root levels. The human life is engulfed within the world of electronics in such a way that devices like mobiles, laptops, memory gadgets have become an integral part of the daily chore. Apart from this, devices like diodes, circuits, solar cells, LCDs play important role in running the society in its fast pace. Concept of smart home, smart devices, smart phones etc. is discussed by the scientific community for the last few years. Thus, the electronic industry always remains as a fertile land for new innovations and technology. The inorganic materials, mostly metals are widely used in the fabrication of various devices. But the extensive use of inorganic materials eventually affected the environment in a most hazardous way. The problems like increased energy demand for the construction of devices, their functioning and difficulty in used/damaged device disposal urged the scientists to look for alternate resources.

The organic molecules became an alternative choice and the field called ‘organic electronics’ emerged. Within the organic molecules the photochromic molecules gained prominent attention due to their ability to respond to light as an external stimulus. The attempt of scientists for the construction of materials/devices with organic molecules faced difficulties in terms of the performance, life-time, and resistance to withstand drastic conditions like heat, temperature etc. These hurdles were removed when they explored further and the carbon nanomaterials became the core materials for electronics. Thus the combination of organic molecules with

carbon nanomaterial offered a promising way for the future electronic materials. This combination envisages the synergistic effect in terms of properties and applications of these hybrid materials. As a step further, the carbon nanomaterials are combined with different organic molecules to prepare stimuli-responsive smart materials. The coupling of carbon nanomaterials with photochromic molecules culminated in an optimum level of success in the world of opto-electronics. The green/sustainable chemistry makes an impact over the electronic industry. Now the researchers are focussing on developing molecular devices from bioderived materials. Thus, the synthesis of molecules/materials from bioresources for the construction of devices is on the runway. A new applied branch of science called 'sustainable molecular electronics' to ensure the benign integration of electronics with nature made its presence felt in the electronic world. Thus, the present research work focuses on developing molecular electronic switches from sustainable materials.

As mentioned above, in this thesis we have utilized the concept of hybrid materials/ sustainable materials, using molecules DOAZOC1 and AZOC2, synthesized from cardanol, a fraction of cashewnut shell liquid through easy and facile synthetic routes. The synthesized (DOAZOC1 and AZOC2) azobenzene systems are then coupled with carbon nanomaterials in different dimensions for developing molecular switches, mainly fluorescence switch and conductance switch.

The molecule DOAZOC1 is coupled with a zero-dimensional carbon nanomaterial graphene quantum dot derived from honey and pesticide carbofuran to develop a sustainable fluorescence switch. The fluorescent switch performed

three useful functions as a molecular logic gate, a molecular keypad lock and a molecular fluorescent probe. The sustainable conductance switches are fabricated by coupling DOAZOC1 with one-dimensional multi-walled carbon nanotube and three-dimensional single-walled carbon nanohorn. Another conductance switch is prepared by coupling molecule AZOC2 with two-dimensional reduced graphene oxide. The conductance switches are fabricated through both covalent and non-covalent functionalization methods.

An efficient photo-tuned conductance switching is observed when the components of the conductance switch are connected through non-covalent interactions like hydrogen bonding and π-π stacking. The result is same in the case of all conductance switches fabricated from carbon nanotube, reduced graphene oxide and single-walled carbon nanohorn. This is due to a less steric hindrance offered to the photoisomerization ability of azobenzene systems on hybrid formation with carbon nanomaterials through non-covalent interactions.

We have also investigated the nature of carbon nanomaterials (0D, 1D, 2D) and mode of hybrid preparation (Covalent & Noncovalent) on the switching properties of hybrids. Among various hybrids, reduced graphene oxide based hybrid shows low conductivity switching in comparison to the other two carbon nanomaterial based hybrids. The yield of cis isomer of DOAZOC1 molecule at photostationary state is 70 % and that for the non-covalent hybrid of carbon nanotubes and single walled carbon nanohorns are 53% and 62% respectively. The higher yield for carbon nanohorns clearly indicates that the phototuning of conductance take place in an efficient manner in its non-covalent hybrid with azomolecules DOAZOC1. The peculiar morphology and three-dimensional

aggregate structure of carbon nanohorns allow the interaction with a larger number of azomolecules in comparison with one dimensional carbon nanotubes. Altogether this establishes that, for more efficient conductance switch the non-covalent hybrid prepared by coupling single walled carbon nanohorns with azobenzene system is a better one compared to other carbon morphologies.

6.2 Future Perspectives

The present research work resulted in the development of sustainable molecular devices in the laboratory level in an efficient and exclusive manner. All the hybrids are promising candidates in molecular electronics. The fluorescence switches developed in the present research work open a way for the construction of molecular keypad locks, logic gates and probes by using bioderived molecules/materials. By properly designing the synthetic strategy these fluorescent switches can also show simultaneous multifunctionality.

The conductance switches fabricated through non-covalent mode of functionalization exhibit stable performance. They can be employed for developing optically active smart materials like field effect transistors, diodes, molecular junctions, detectors and sensors. By incorporating photochromic molecules which can withstand drastic conditions like heat and higher temperature, it is also able to develop photothermal fuels by combining with various carbon nanomaterials. These kinds of hybrids can also find applications in the biomedical field, especially in designing drug carriers and also for bio imaging. The covalent conductance switches are not much efficient compared to the non-covalent ones. Still their optical response can be explored for developing devices like chem resistors. The

phototunability of the conductance switches also make them a good choice for the construction of memory devices.

In this way, the present research work, is a stepping stone in the construction of photo-responsive smart materials by sticking to the principles of sustainable molecular electronics. This can bring a revolution in the organic/carbon-based technology by making the synthetic routes more green and economic. These kind of hybrid materials can definitely be used in the de novo concept of smart home in the years to come.

******

REFERENCES

1. Abourashed, E. A. (2017). "Review of Stilbenes: Applications in Chemistry, Life Sciences and Materials Science." Journal of Natural Products 80(2): 577-577.
2. Agranovich, V., Y. N. Gartstein, et al. (2011). "Hybrid resonant organic–inorganic nanostructures for optoelectronic applications." Chemical Reviews 111(9): 5179-5214.
3. Ahn, H., J. Hong, et al. (2015). "A pH-Responsive Molecular Switch with Tricolor Luminescence." ACS Applied Materials & Interfaces 7(1): 704-712.
4. Airinei, A., N. Fifere, et al. (2011). "Optical properties of some new azo photoisomerizable bismaleimide derivatives." International journal of molecular sciences 12(9): 6176-6193.
5. Ajayan, P. M. and O. Z. Zhou (2001). Applications of carbon nanotubes. Carbon nanotubes, Springer: 391-425.
6. Ajima, K., T. Murakami, et al. (2008). "Enhancement of in vivo anticancer effects of cisplatin by incorporation inside single-wall carbon nanohorns." ACS nano 2(10): 2057-2064.
7. Allen, M. J., V. C. Tung, et al. (2009). "Honeycomb carbon: a review of graphene." Chemical Reviews 110(1): 132-145.
8. Allwood, J. M., M. F. Ashby, et al. (2011). "Material efficiency: A white paper." Resources, Conservation and Recycling 55(3): 362-381.
9. Andréasson, J. and U. Pischel (2015). "Molecules with a sense of logic: a progress report." Chemical Society Reviews 44(5): 1053-1069.
10. Andréasson, J., S. D. Straight, et al. (2009). "An All-Photonic Molecular Keypad Lock." Chemistry – A European Journal 15(16): 3936-3939.
11. Ante, F., D. Kälblein, et al. (2012). "Contact resistance and megahertz operation of aggressively scaled organic transistors." Small 8(1): 73-79.
12. Awasthi, K., A. Srivastava, et al. (2005). "Synthesis of carbon nanotubes." Journal of nanoscience and nanotechnology 5(10): 1616-1636.
13. Azami, T., D. Kasuya, et al. (2007). "Production of small single-wall carbon nanohorns by CO_2 laser ablation of graphite in Ne-gas atmosphere." carbon 6(45): 1364-1367.
14. Bak, S., D. Kim, et al. (2016). "Graphene quantum dots and their possible energy applications: A review." Current Applied Physics 16(9): 1192-1201.
15. Balachandran, V. S., S. R. Jadhav, et al. (2013). "Recent advances in cardanol chemistry in a nutshell: from a nut to nanomaterials." Chemical Society Reviews 42(2): 427-438.

16. Bandara, H. M. D. and S. C. Burdette (2012). "Photoisomerization in different classes of azobenzene." Chemical Society Reviews 41(5): 1809-1825.
17. Bandow, S., F. Kokai, et al. (2001). "Unique magnetism observed in single-wall carbon nanohorns." Applied Physics A 73(3): 281-285.
18. Basuki, S. W., V. Schneider, et al. (2015). "Light-controlled conductance switching in azobenzene-containing MWCNT–polymer nanocomposites." ACS applied materials & interfaces 7(21): 11257-11262.
19. Becerril, H. A., J. Mao, et al. (2008). "Evaluation of Solution-Processed Reduced Graphene Oxide Films as Transparent Conductors." ACS Nano 2(3): 463-470.
20. Bekyarova, E., Y. Hanzawa, et al. (2002). "Cluster-mediated filling of water vapor in intratube and interstitial nanospaces of single-wall carbon nanohorns." Chemical Physics Letters 366(5-6): 463-468.
21. Bekyarova, E., K. Kaneko, et al. (2002). "Oxidation and porosity evaluation of budlike single-wall carbon nanohorn aggregates." Langmuir 18(10): 4138-4141.
22. Bekyarova, E., K. Kaneko, et al. (2002). "Pore structure and adsorption properties of single-walled carbon nanohorn bud-like aggregates treated in different atmospheres." Physica B: Condensed Matter 323(1-4): 143-145.
23. Bekyarova, E., K. Kaneko, et al. (2003). "Controlled opening of single-wall carbon nanohorns by heat treatment in carbon dioxide." The Journal of Physical Chemistry B 107(19): 4479-4484.
24. Bekyarova, E., K. Kaneko, et al. (2002). "Micropore development and structure rearrangement of single-wall carbon nanohorn assemblies by compression." Advanced Materials 14(13-14): 973-975.
25. Berber, S., Y.-K. Kwon, et al. (2000). "Electronic and structural properties of carbon nanohorns." Physical Review B 62(4): R2291.
26. Beveridge, D. L. and H. H. Jaffé (1966). "The Electronic Structure and Spectra of cis- and trans-Azobenzene1." Journal of the American Chemical Society 88(9): 1948-1953.
27. Bhunia, S. K., A. Saha, et al. (2013). "Carbon nanoparticle-based fluorescent bioimaging probes." Scientific reports 3: 1473.
28. Bletz, M., U. Pfeifer-Fukumura, et al. (2002). "Ground-and first-excited-singlet-state electric dipole moments of some photochromic spirobenzopyrans in their spiropyran and merocyanine form." The Journal of Physical Chemistry A 106(10): 2232-2236.
29. Bluemmel, P., A. Setaro, et al. (2010). "Dispersion of carbon nanotubes using an azobenzene derivative." physica status solidi (b) 247(11-12): 2891-2894.
30. Boiko, Y. (2009). "Improvement of thermal stability in photochromic holograms." Optics Letters 34(8): 1279-1281.

31. Bonard, J.-M., R. Gaal, et al. (2002). "Field emission properties of carbon nanohorn films." Journal of applied physics 91(12): 10107-10109.
32. Bouas-Laurent, H. and H. Dürr (2001). "Organic photochromism (IUPAC technical report)." Pure and Applied Chemistry 73(4): 639-665.
33. Breuer, O. and U. Sundararaj (2004). "Big returns from small fibers: a review of polymer/carbon nanotube composites." Polymer composites 25(6): 630-645.
34. Browne, W. R. and B. L. Feringa (2006). "Making molecular machines work." Nature nanotechnology 1(1): 25-35.
35. Brundtland, G. H. (1987). "What is sustainable development." Our common future: 8-9.
36. Buback, J., M. Kullmann, et al. (2010). "Ultrafast Bidirectional Photoswitching of a Spiropyran." Journal of the American Chemical Society 132(46): 16510-16519.
37. Buruiana, E. C., M. Zamfir, et al. (2010). "Photo-polymers containing (S)-phenylalanine and stilbene pendants: synthesis and properties of ionic polyacrylates." Designed Monomers and Polymers 13(1): 21-32.
38. Cao, Y., S. Dong, et al. (2013). "Toward functional molecular devices based on graphene–molecule junctions." Angewandte Chemie 125(14): 3998-4002.
39. Carvalho, C. P., Z. Dominguez, et al. (2015). "A supramolecular keypad lock." Chemical Communications 51(13): 2698-2701.
40. Casillas, R., F. Lodermeyer, et al. (2014). "Substituting $TiCl_4$–Carbon Nanohorn Interfaces for Dye-Sensitized Solar Cells." Advanced Energy Materials 4(6): 1301577.
41. Chen, J., F. Zeng, et al. (2010). "Construction of energy transfer systems within nanosized polymer micelles and their fluorescence modulation properties." ChemPhysChem 11(5): 1036-1043.
42. Chen, S., L. Bao, et al. (2015). "A cationic azobenzene-surfactant-modified graphene hybrid: unique photoresponse and electrochemical behavior." Nanoscale 7(46): 19673-19686.
43. Corredor, C. C., Z.-L. Huang, et al. (2007). "Photochromic polymer composites for two-photon 3D optical data storage." Chemistry of Materials 19(21): 5165-5173.
44. Curtin, D. Y., E. J. Grubbs, et al. (1966). "Uncatalyzed syn-anti Isomerization of Imines, Oxime Ethers, and Haloimines1." Journal of the American Chemical Society 88(12): 2775-2786.
45. de Silva, P. A., N. H. Gunaratne, et al. (1993). "A molecular photoionic AND gate based on fluorescent signalling." Nature 364(6432): 42-44.
46. De Sousa, F. B., J. D. T. Guerreiro, et al. (2010). "Photo-response behavior of electrospun nanofibers based on spiropyran-cyclodextrin modified polymer." Journal of Materials Chemistry 20(44): 9910-9917.

47. De Volder, M. F., S. H. Tawfick, et al. (2013). "Carbon nanotubes: present and future commercial applications." science 339(6119): 535-539.
48. Deka, M. J. and D. Chowdhury (2017). "Chiral carbon dots and their effect on the optical properties of photosensitizers." RSC Advances 7(84): 53057-53063.
49. Del Valle, M., R. Gutiérrez, et al. (2007). "Tuning the conductance of a molecular switch." Nature nanotechnology 2(3): 176.
50. Devi, K. R., C. L. Lekshmi, et al. (2016). "Sustainable Electronic Materials: Reversible Phototuning of Conductance in a non-Covalent assembly of MWCNT and Bioresource Derived Photochromic molecule." ACS applied materials & interfaces 9(2): 1167-1172.
51. Devi, R., G. Prabhavathi, et al. (2014). "Synthesis, characterization and photoluminescence properties of graphene oxide functionalized with azo molecules." Journal of Chemical Sciences 126(1): 75-83.
52. Dhenadhayalan, N. and C. Selvaraju (2012). "Role of photoionization on the dynamics and mechanism of photoinduced electron transfer reaction of coumarin 307 in micelles." The Journal of Physical Chemistry B 116(16): 4908-4920.
53. Di Florio, G., E. Bründermann, et al. (2014). "Graphene Multilayer as Nanosized Optical Strain Gauge for Polymer Surface Relief Gratings." Nano letters 14(10): 5754-5760.
54. Doistau, B., L. Benda, et al. (2017). "Six States Switching of Redox-Active Molecular Tweezers by Three Orthogonal Stimuli." Journal of the American Chemical Society 139(27): 9213-9220.
55. Dong, Y., J. Shao, et al. (2012). "Blue luminescent graphene quantum dots and graphene oxide prepared by tuning the carbonization degree of citric acid." Carbon 50(12): 4738-4743.
56. Dulić, D., S. J. van der Molen, et al. (2003). "One-Way Optoelectronic Switching of Photochromic Molecules on Gold." Physical Review Letters 91(20): 207402.
57. Dürr, H. and H. Bouas-Laurent (2003). Photochromism: molecules and systems, Elsevier.
58. Emsley, J. (1980). "Very strong hydrogen bonding." Chemical Society Reviews 9(1): 91-124.
59. Endo, M., M. S. Strano, et al. (2007). Potential applications of carbon nanotubes. Carbon nanotubes, Springer: 13-62.
60. Esposito, B., Y. Kaschuck, et al. (2004). "Digital pulse shape discrimination in organic scintillators for fusion applications." Nuclear Instruments and Methods in Physics Research Section A: Accelerators, Spectrometers, Detectors and Associated Equipment 518(1): 626-628.

61. Fan, J., M. Yudasaka, et al. (2006). "Control of hole opening in single-wall carbon nanotubes and single-wall carbon nanohorns using oxygen." The Journal of Physical Chemistry B 110(4): 1587-1591.
62. Feng, W., W. Luo, et al. (2012). "Photo-responsive carbon nanomaterials functionalized by azobenzene moieties: structures, properties and application." Nanoscale 4(20): 6118-6134.
63. Feng, Y., W. Feng, et al. (2007). "Photoinduced anisotropic response of azobenzene chromophore functionalized multiwalled carbon nanotubes." Journal of applied physics 102(5): 053102.
64. Feng, Y., W. Feng, et al. (2007). "Synthesis of photoresponsive azobenzene chromophore-modified multi-walled carbon nanotubes." carbon 12(45): 2445-2448.
65. Feng, Y., Y. Yan, et al. (2006). "Photochromic thiophene oligomers based on bisthienylethene: syntheses, photochromic and two-photon properties." Journal of Materials Chemistry 16(37): 3685-3692.
66. Feng, Y., X. Zhang, et al. (2010). "A light-driven reversible conductance switch based on a few-walled carbon nanotube/azobenzene hybrid linked by a flexible spacer." Carbon 48(11): 3091-3096.
67. Feringa, B. L. and W. R. Browne (2001). Molecular switches, Wiley Online Library.
68. Feringa, B. L. and W. R. Browne (2011). Molecular switches, John Wiley & Sons.
69. Florea, L., A. Hennart, et al. (2012). "Synthesis and characterisation of spiropyran-polymer brushes in micro-capillaries: Towards an integrated optical sensor for continuous flow analysis." Sensors and Actuators B: Chemical 175: 92-99.
70. Fouda, A. N., E.-S. M. Duraia, et al. (2014). "Ultra-smooth and lattice relaxed ZnO thin films." Superlattice Microstruct 73.
71. Frolova, L. A., A. A. Rezvanova, et al. (2015). "Design of rewritable and read-only non-volatile optical memory elements using photochromic spiropyran-based salts as light-sensitive materials." Journal of Materials Chemistry C 3(44): 11675-11680.
72. Frolova, L. A., P. A. Troshin, et al. (2015). "Photoswitchable organic field-effect transistors and memory elements comprising an interfacial photochromic layer." Chemical Communications 51(28): 6130-6132.
73. Fu, L.-N., B. Leng, et al. (2016). "Photoresponsive organic field-effect transistors involving photochromic molecules." Chinese Chemical Letters 27(8): 1319-1329.
74. Fukaminato, T., T. Sasaki, et al. (2004). "Digital Photoswitching of Fluorescence Based on the Photochromism of Diarylethene Derivatives at a Single-Molecule Level." Journal of the American Chemical Society 126(45): 14843-14849.

75. Garaj, S., L. Thien-Nga, et al. (2000). "Electronic properties of carbon nanohorns studied by ESR." Physical Review B 62(24): 17115-17119.
76. Ghosh, T., S. Chatterjee, et al. (2015). "Photoinduced Electron Transfer from Various Aniline Derivatives to Graphene Quantum Dots." The Journal of Physical Chemistry A 119(49): 11783-11790.
77. Golovkova, T. A., D. V. Kozlov, et al. (2005). "Synthesis and properties of novel fluorescent switches." The Journal of Organic Chemistry 70(14): 5545-5549.
78. Griffiths, J. (1972). "II. Photochemistry of azobenzene and its derivatives." Chemical Society Reviews 1(4): 481-493.
79. Guerra, J., M. A. Herrero, et al. (2012). "Carbon nanohorns functionalized with polyamidoamine dendrimers as efficient biocarrier materials for gene therapy." Carbon 50(8): 2832-2844.
80. Guo, X., L. Huang, et al. (2005). "Directing and sensing changes in molecular conformation on individual carbon nanotube field effect transistors." Journal of the American Chemical Society 127(43): 15045-15047.
81. Guo, Z., W. Zhu, et al. (2007). "A fluorophore capable of crossword puzzles and logic memory." Angewandte Chemie 119(29): 5645-5649.
82. Gupta, P. and A. Raina (1988). "Reduction of geometric isomers of azobenzene at DME." Journal of the Indian Chemical Society 65(7): 495-497.
83. Gutowski, T. G., M. S. Branham, et al. (2009). "Thermodynamic analysis of resources used in manufacturing processes." Environmental science & technology 43(5): 1584-1590.
84. Gutsev, G. L., R. J. Bartlett, et al. (1998). "Electron affinities of CO_2, OCS, and CS_2." The Journal of Chemical Physics 108(16): 6756-6762.
85. Hall, R. A., P. J. Thistlethwaite, et al. (1994). "Acid-base equilibria of merocyanine air-water monolayers." Langmuir 10(10): 3743-3748.
86. Hariharan, P. S., J. Pitchaimani, et al. (2017). "A halochromic stimuli-responsive reversible fluorescence switching 3,4,9,10-perylene tetracarboxylic acid dye for fabricating rewritable platform." Optical Materials 64: 53-57.
87. Hartley, G. S. and R. J. W. Le Fèvre (1939). "119. The dipole moments of cis- and trans-azobenzenes and of some related compounds." Journal of the Chemical Society (Resumed)(0): 531-535.
88. Hauke, F. and A. Hirsch (2010). "Covalent functionalization of carbon nanotubes." Carbon Nanotubes and Related Structures: Synthesis, Characterization, Functionalization, and Applications: 135-198.
89. Herranz, M. Á. and N. Martín (2010). "Noncovalent functionalization of carbon nanotubes." Carbon Nanotubes and Related Structures: Synthesis, Characterization, Functionalization, and Applications: 103-134.

90. Hu, T., H. Xie, et al. (2011). "Preparation and orientation behavior of multi-walled carbon nanotubes grafted with a side-chain azobenzene liquid crystalline polymer." Polymer International 60(1): 93-101.
91. Huang, C., R. K. Wang, et al. (2011). "Spectroscopic properties of nanotube–chromophore hybrids." ACS nano 5(10): 7767-7774.
92. Hummers, W. S. and R. E. Offeman (1958). "Preparation of Graphitic Oxide." Journal of the American Chemical Society 80(6): 1339-1339.
93. Hwang, E., H. M. Hwang, et al. (2016). "Chemically modulated graphene quantum dot for tuning the photoluminescence as novel sensory probe." 6: 39448.
94. Iijima, S. (1991). "Helical microtubules of graphitic carbon." Nature 354: 56.
95. Iijima, S., M. Yudasaka, et al. (1999). "Nano-aggregates of single-walled graphitic carbon nano-horns." Chemical Physics Letters 309(3-4): 165-170.
96. Ikeda, M., H. Takikawa, et al. (2002). "Preparation of carbon nanohorn aggregates by cavity arc jet in open air." Japanese journal of applied physics 41(7B): L852.
97. Imai, H., P. K. Babu, et al. (2006). "C ^{13} NMR spectroscopy of carbon nanohorns." Physical Review B 73(12): 125405.
98. Imin, P., M. Imit, et al. (2012). "Supramolecular functionalization of single-walled carbon nanotubes (SWNTs) with a photoisomerizable conjugated polymer." Macromolecules 45(12): 5045-5050.
99. Ipe, B. I., S. Mahima, et al. (2003). "Light-induced modulation of self-assembly on spiropyran-capped gold nanoparticles: a potential system for the controlled release of amino acid derivatives." Journal of the American Chemical Society 125(24): 7174-7175.
100. Irie, M. (2010). "Photochromism of diarylethene molecules and crystals." Proceedings of the Japan Academy. Series B, Physical and biological sciences 86(5): 472-483.
101. Irie, M., T. Fukaminato, et al. (2014). "Photochromism of diarylethene molecules and crystals: memories, switches, and actuators." Chemical reviews 114(24): 12174-12277.
102. Irie, M., T. Fukaminato, et al. (2002). "A digital fluorescent molecular photoswitch." Nature 420: 759.
103. Irie, M., T. Lifka, et al. (2000). "Photochromism of 1, 2-bis (2-methyl-5-phenyl-3-thienyl) perfluorocyclopentene in a single-crystalline phase." Journal of the American Chemical Society 122(20): 4871-4876.
104. Irie, M., O. Miyatake, et al. (1992). "Blocked photochromism of diarylethenes." Journal of the American Chemical Society 114(22): 8715-8716.

105. Irie, M. and M. Mohri (1988). "Thermally irreversible photochromic systems. Reversible photocyclization of diarylethene derivatives." The Journal of Organic Chemistry 53(4): 803-808.
106. Irimia-Vladu, M. (2014). "“Green” electronics: biodegradable and biocompatible materials and devices for sustainable future." Chemical Society Reviews 43(2): 588-610.
107. Isobe, H., T. Tanaka, et al. (2006). "Preparation, purification, characterization, and cytotoxicity assessment of water-soluble, transition-metal-free carbon nanotube aggregates." Angewandte Chemie 118(40): 6828-6832.
108. Jaekel, S., A. Richter, et al. (2018). "Reversible and Efficient Light-Induced Molecular Switching on an Insulator Surface." ACS nano 12(2): 1821-1828.
109. Jang, A. R., E. K. Jeon, et al. (2012). "Reversibly Light-Modulated Dirac Point of Graphene Functionalized with Spiropyran." ACS nano 6(10): 9207-9213.
110. Jean-Ruel, H., R. R. Cooney, et al. (2011). "Femtosecond dynamics of the ring closing process of diarylethene: A case study of electrocyclic reactions in photochromic single crystals." The Journal of Physical Chemistry A 115(45): 13158-13168.
111. Jen, A. K.-Y., Y. Cai, et al. (1997). "Synthesis and characterization of highly efficient and thermally stable diphenylamino-substituted thiophene stilbene chromophores for nonlinear optical applications." Advanced Materials 9(2): 132-135.
112. Jenekhe, S. A. and D. J. Kiserow (2004). Chromogenic Phenomena in Polymers, American Chemical Society.
113. Ji, H.-F., Y. Feng, et al. (2004). "Photon-driven nanomechanical cyclic motion." Chemical Communications(22): 2532-2533.
114. Jia, C., J. Wang, et al. (2013). "Conductance Switching and Mechanisms in Single-Molecule Junctions." Angewandte Chemie International Edition 52(33): 8666-8670.
115. Jochum, F. D. and P. Theato (2013). "Temperature- and light-responsive smart polymer materials." Chemical Society Reviews 42(17): 7468-7483.
116. Joshi, G. K., K. N. Blodgett, et al. (2014). "Ultrasensitive Photoreversible Molecular Sensors of Azobenzene-Functionalized Plasmonic Nanoantennas." Nano letters 14(2): 532-540.
117. Kalita, H., J. Mohapatra, et al. (2016). "Efficient synthesis of rice based graphene quantum dots and their fluorescent properties." RSC Advances 6(28): 23518-23524.
118. Karousis, N., T. Ichihashi, et al. (2009). "Decoration of Carbon Nanohorns with Palladium and Platinum Nanoparticles." Journal of nanoscience and nanotechnology 9(10): 6047-6054.

119. Kassem, S., T. van Leeuwen, et al. (2017). "Artificial molecular motors." Chemical Society Reviews 46(9): 2592-2621.
120. Kausar, A. (2018). "Prevailing Research Trends in Carbon Nanohorn and Polymer-based Hybrids." Polymer-Plastics Technology and Engineering 57(2): 118-132.
121. Kawai, T., Y. Nakashima, et al. (2005). "Photon-mode modulation of fluorescence and electrical current with a photochromic conducting polymer." Current Applied Physics 5(2): 139-142.
122. Kay, K.-Y., K.-J. Han, et al. (2002). "Dendritic fullerenes (C60) with photoresponsive azobenzene groups." Tetrahedron Letters 43(29): 5053-5056.
123. Kim, D., J. E. Kwon, et al. (2018). "Fully Reversible Multistate Fluorescence Switching: Organogel System Consisting of Luminescent Cyanostilbene and Turn-On Diarylethene." Advanced Functional Materials 28(7): 1706213.
124. Kim, M., N. S. Safron, et al. (2011). "Light-driven reversible modulation of doping in graphene." Nano letters 12(1): 182-187.
125. Klajn, R. (2014). "Spiropyran-based dynamic materials." Chemical Society Reviews 43(1): 148-184.
126. Kobatake, S., Y. Terakawa, et al. (2009). "Solvent effect on photochromism of a dithienylperfluorocyclopentene having diethylamino group." Tetrahedron 65(31): 6104-6108.
127. Kolesnikov, D. V. and V. A. Osipov (2004). "Electronic structure of carbon nanohorns near the Fermi level." Journal of Experimental and Theoretical Physics Letters 79(11): 532-536.
128. Kördel, C., A. Setaro, et al. (2012). "Controlled reversible debundling of single-walled carbon nanotubes by photo-switchable dendritic surfactants." Nanoscale 4(10): 3029-3031.
129. Kosaka, M., S. Kuroshima, et al. (2009). "Single-wall carbon nanohorns supporting Pt catalyst in direct methanol fuel cells." The Journal of Physical Chemistry C 113(20): 8660-8667.
130. Kucharski, T. J., N. Ferralis, et al. (2014). "Templated assembly of photoswitches significantly increases the energy-storage capacity of solar thermal fuels." Nature chemistry 6(5): 441.
131. Kumar, K., C. Knie, et al. (2016). "A chaotic self-oscillating sunlight-driven polymer actuator." Nature Communications 7: 11975.
132. Kumar, K. S. and A. Patnaik (2011). "Solvent-Polarity-Tunable Dimeric Association of a Fullerene (C60)–N,N-Dimethylaminoazobenzene Dyad: Modulated Electronic Coupling of the Azo Chromophore with a Substituted 3D Fullerene." Chemistry – A European Journal 17(19): 5327-5343.
133. Kumar, K. S. and A. Patnaik (2011). "Tunable One-, Two-, and Three-Dimensional Self-Assemblies from an Acceptor–Donor Fullerene–N, N-

Dimethylaminoazobenzene Dyad: Interfacial Geometry and Temporal Evolution." Langmuir 27(17): 11017-11025.

134. Kumar, M., R. Kumar, et al. (2009). "A reversible fluorescent Hg $^{2+}$/K^{+} switch that works as keypad lock in the presence of F^{-} ion." Chemical Communications(47): 7384-7386.
135. Kume, S. and H. Nishihara (2008). "Photochrome-coupled metal complexes: molecular processing of photon stimuli." Dalton Transactions(25): 3260-3271.
136. Kwon, W., S. Do, et al. (2012). "Formation of highly luminescent nearly monodisperse carbon quantum dots via emulsion-templated carbonization of carbohydrates." RSC Advances 2(30): 11223-11226.
137. Larson, J. W. and T. B. McMahon (1984). "Gas-phase bihalide and pseudobihalide ions. An ion cyclotron resonance determination of hydrogen bond energies in XHY- species (X, Y = F, Cl, Br, CN)." Inorganic Chemistry 23(14): 2029-2033.
138. Lee, J. H., J. Jaworski, et al. (2013). "Luminescent metal-organic framework-functionalized graphene oxide nanocomposites and the reversible detection of high explosives." Nanoscale 5(18): 8533-8540.
139. Lennartson, A., A. Roffey, et al. (2015). "Designing photoswitches for molecular solar thermal energy storage." Tetrahedron Letters 56(12): 1457-1465.
140. Li, F., X. Jiang, et al. (2015). "Graphene oxide: A promising nanomaterial for energy and environmental applications." Nano Energy 16: 488-515.
141. Li, M., K. Deng, et al. (2008). "Site-selective fabrication of two-dimensional fullerene arrays by using a supramolecular template at the liquid-solid interface." Angewandte Chemie 120(35): 6819-6823.
142. Li, S., Y. Feng, et al. (2017). "The light-switching conductance of an anisotropic azobenzene-based polymer close-packed on horizontally aligned carbon nanotubes." Journal of Materials Chemistry C 5(21): 5068-5075.
143. Li, Y., Y. Duan, et al. (2013). "Self-assembly of graphene oxide with a silyl-appended spiropyran dye for rapid and sensitive colorimetric detection of fluoride ions." Analytical chemistry 85(23): 11456-11463.
144. Li, Y., Y. Hu, et al. (2011). "An Electrochemical Avenue to Green-Luminescent Graphene Quantum Dots as Potential Electron-Acceptors for Photovoltaics." Advanced Materials 23(6): 776-780.
145. Liang, Z., M. Kang, et al. (2016). "Probing Energy and Electron Transfer Mechanisms in Fluorescence Quenching of Biomass Carbon Quantum Dots." ACS Applied Materials & Interfaces 8(27): 17478-17488.
146. Liao, B., W. Wang, et al. (2015). "The carbon nanoparticles grafted with copolymers of styrene and spiropyran with reversibly photoswitchable fluorescence." Carbon 91: 30-37.

147. Liddell, P. A., G. Kodis, et al. (2002). "Photonic switching of photoinduced electron transfer in a dithienylethene− porphyrin− fullerene triad molecule." Journal of the American Chemical Society 124(26): 7668-7669.
148. Lin, C.-Y., C.-S. Chang, et al. (2013). "Optical controlled graphene-based nonvolatile ternary-logic transistor with azobenzene copolymer." Applied Physics Letters 102(1): 013505.
149. Liu, R., D. Wu, et al. (2011). "Bottom-Up Fabrication of Photoluminescent Graphene Quantum Dots with Uniform Morphology." Journal of the American Chemical Society 133(39): 15221-15223.
150. Liu, X., H. Li, et al. (2010). "Functionalized single-walled carbon nanohorns for electrochemical biosensing." Biosensors and Bioelectronics 25(10): 2194-2199.
151. Liu, Y., J. Ren, et al. (2012). "An aptamer-based keypad lock system." Chemical Communications 48(6): 802-804.
152. Liu, Z., S. Tabakman, et al. (2009). "Carbon nanotubes in biology and medicine: In vitro and in vivo detection, imaging and drug delivery." Nano Research 2(2): 85-120.
153. Lodermeyer, F., M. Prato, et al. (2016). "Facile and quick preparation of carbon nanohorn-based counter electrodes for efficient dye-sensitized solar cells." Nanoscale 8(14): 7556-7561.
154. Lovley, D. R. (2017). "e-Biologics: Fabrication of Sustainable Electronics with “Green” Biological Materials." mBio 8(3): e00695-00617.
155. Luo, W., Y. Feng, et al. (2015). "A high energy density azobenzene/graphene hybrid: a nano-templated platform for solar thermal storage." Journal of Materials Chemistry A 3(22): 11787-11795.
156. Luo, W., Y. Feng, et al. (2015). "High-energy, stable and recycled molecular solar thermal storage materials using AZO/graphene hybrids by optimizing hydrogen bonds." Nanoscale 7(39): 16214-16221.
157. Ma, L., Q. Wang, et al. (2009). "Photochromic nanostructures based on diarylethenes with perylene diimide." Langmuir 26(9): 6702-6707.
158. Magee, J. L., W. Shand Jr, et al. (1941). "Non-adiabatic reactions. Rotation about the double bond." Journal of the American Chemical Society 63(3): 677-688.
159. Maggini, L., T. Marangoni, et al. (2013). "Azobenzene-based supramolecular polymers for processing MWCNTs." Nanoscale 5(2): 634-645.
160. Mahesh, S., A. Gopal, et al. (2012). "Light-induced Ostwald ripening of organic nanodots to rods." Journal of the American Chemical Society 134(17): 7227-7230.
161. Mahesh, S., C. L. Lekshmi, et al. (2017). "New paradigms for the synthesis of graphene quantum dots from sustainable bioresources." New Journal of Chemistry 41(17): 8706-8710.

162. Mahesh, S., C. L. Lekshmi, et al. (2016). "Simple and Cost-Effective Synthesis of Fluorescent Graphene Quantum Dots from Honey: Application as Stable Security Ink and White-Light Emission." Particle & Particle Systems Characterization 33(2): 70-74.
163. Mahesh, S., D. Raju, et al. (2014). "Self-assembly of cardanol based supramolecular synthons to photoresponsive nanospheres: light induced size variation at the nanoscale." RSC Advances 4(80): 42747-42750.
164. Makarova, N., P. Levchenko, et al. (2011). "Synthesis and photochromic properties of new nonsymmetric dihetarylethenes—indole and thiophene derivatives." Russian Chemical Bulletin 60(9): 1899-1905.
165. Malic, E., C. Weber, et al. (2011). "Microscopic model of the optical absorption of carbon nanotubes functionalized with molecular spiropyran photoswitches." Physical review letters 106(9): 097401.
166. Margapoti, E., P. Strobel, et al. (2014). "Emergence of Photoswitchable States in a Graphene–Azobenzene–Au Platform." Nano letters 14(12): 6823-6827.
167. Margulies, D., C. E. Felder, et al. (2007). "A Molecular Keypad Lock: A Photochemical Device Capable of Authorizing Password Entries." Journal of the American Chemical Society 129(2): 347-354.
168. Mativetsky, J. M., G. Pace, et al. (2008). "Azobenzenes as Light-Controlled Molecular Electronic Switches in Nanoscale Metal−Molecule−Metal Junctions." Journal of the American Chemical Society 130(29): 9192-9193.
169. McArdle, C. B., H. Blair, et al. (1983). "Positive and negative photochromism in thin organic Langmuir-Blodgett films." Thin Solid Films 99(1-3): 181-188.
170. McGee, D. J., C. Huang, et al. (2012). "Molecular orientation and photoswitching kinetics on single-walled carbon nanotubes by optical second harmonic generation." Applied Physics Letters 101(26): 264101.
171. Min, M., S. Seo, et al. (2013). "Voltage-Controlled Nonvolatile Molecular Memory of an Azobenzene Monolayer through Solution-Processed Reduced Graphene Oxide Contacts." Advanced materials 25(48): 7045-7050.
172. Minkin, V. I. (2004). "Photo-, thermo-, solvato-, and electrochromic spiroheterocyclic compounds." Chemical Reviews 104(5): 2751-2776.
173. Misra, A., P. Srivastava, et al. (2012). "Fluorescent probe mimicking multiple logic gates and a molecular keypad lock upon interaction with Hg^{2+} and bovine serum albumin." Analyst 137(15): 3470-3478.
174. Miyawaki, J., M. Yudasaka, et al. (2004). "Solvent effects on hole-edge structure for single-wall carbon nanotubes and single-wall carbon nanohorns." The Journal of Physical Chemistry B 108(30): 10732-10735.

175. Miyawaki, J., M. Yudasaka, et al. (2006). "In vivo magnetic resonance imaging of single-walled carbon nanohorns by labeling with magnetite nanoparticles." Advanced Materials 18(8): 1010-1014.
176. Moniruzzaman, M., C. Sabey, et al. (2007). "Photoresponsive polymers: an investigation of their photoinduced temperature changes during photoviscosity measurements." Polymer 48(1): 255-263.
177. Morimitsu, K., S. Kobatake, et al. (2003). "Efficient photocycloreversion reaction of diarylethenes by introduction of cyano subsutituents to the reactive carbons." Chemistry letters 32(9): 858-859.
178. Morimitsu, K., K. Shibata, et al. (2002). "Thermal cycloreversion reaction of a photochromic dithienylperfluorocyclopentene with tert-butoxy substituents at the reactive carbons." Chemistry letters 31(6): 572-573.
179. Mountrichas, G., T. Ichihashi, et al. (2009). "Solubilization of carbon nanohorns by block polyelectrolyte wrapping and templated formation of gold nanoparticles." The Journal of Physical Chemistry C 113(14): 5444-5449.
180. Mountrichas, G., N. Tagmatarchis, et al. (2009). "Functionalization of carbon nanohorns with polyethylene oxide: synthesis and incorporation in a polymer matrix." Journal of nanoscience and nanotechnology 9(6): 3775-3779.
181. Murata, K., A. Hashimoto, et al. (2004). "The Use of Charge Transfer to Enhance the Methane-Storage Capacity of Single-Walled, Nanostructured Carbon." Advanced Materials 16(17): 1520-1522.
182. Murata, K., K. Kaneko, et al. (2000). "Pore structure of single-wall carbon nanohorn aggregates." Chemical Physics Letters 331(1): 14-20.
183. Murata, K., K. Kaneko, et al. (2001). "Molecular potential structures of heat-treated single-wall carbon nanohorn assemblies." The Journal of Physical Chemistry B 105(42): 10210-10216.
184. Murata, K., J. Miyawaki, et al. (2005). "High-density of methane confined in internal nanospace of single-wall carbon nanohorns." Carbon 43(13): 2826-2830.
185. Myeong-Suk, K., S. Tadafumi, et al. (2003). "Amorphous Photochromic Films for Near-field Optical Recording." Japanese journal of applied physics 42(6R): 3676.
186. Myles, A. J. and N. R. Branda (2001). "Controlling Photoinduced Electron Transfer within a Hydrogen-Bonded Porphyrin− Phenoxynaphthacenequinone Photochromic System." Journal of the American Chemical Society 123(1): 177-178.
187. Nakano, H., R. Ichikawa, et al. (2013). "Photomechanical Bending of Azobenzene-Based Photochromic Molecular Fibers." Micromachines 4(2): 128.

188. Nguyen, P., J. Li, et al. (2013). "Covalent Functionalization of Dipole-Modulating Molecules on Trilayer Graphene: An Avenue for Graphene-Interfaced Molecular Machines." Small 9(22): 3823-3828.
189. Nie, K., B. Dong, et al. (2017). "Thienyl diketopyrrolopyrrole as a robust sensing platform for multiple ions and its application in molecular logic system." Sensors and Actuators B: Chemical 244(Supplement C): 849-853.
190. Notarianni, M., J. Liu, et al. (2016). "Synthesis and applications of carbon nanomaterials for energy generation and storage." Beilstein journal of nanotechnology 7: 149.
191. Nurbawono, A. and C. Zhang (2013). "Reversible magnetism switching in graphene-based systems via the decoration of photochromic molecules." Applied Physics Letters 103(20): 203110.
192. Ohba, T., T. Omori, et al. (2004). "Interstitial nanopore change of single wall carbon nanohorn assemblies with high temperature treatment." Chemical Physics Letters 389(4-6): 332-336.
193. Ohsumi, M., M. Hazama, et al. (2008). "Photocyclization reaction of a diarylmaleimide derivative in polar solvents." Chemical Communications(28): 3281-3283.
194. Ortíz-Palacios, J., G. Zaragoza-Galán, et al. (2017). "Synthesis, characterization and optical properties of novel dendronized azo-dyes containing a fullerene C 60 unit and well-defined oligo (ethylene glycol) segments." RSC Advances 7(27): 16751-16762.
195. Oudar, J. d. (1977). "Optical nonlinearities of conjugated molecules. Stilbene derivatives and highly polar aromatic compounds." The Journal of Chemical Physics 67(2): 446-457.
196. Pagona, G., J. Fan, et al. (2007). "Aqueous carbon nanohorn–pyrene–porphyrin nanoensembles: controlling charge-transfer interactions." Diamond and related materials 16(4-7): 1150-1153.
197. Pagona, G., A. S. Sandanayaka, et al. (2007). "Photoinduced electron transfer on aqueous carbon nanohorn–pyrene–tetrathiafulvalene architectures." Chemistry–A European Journal 13(27): 7600-7607.
198. Pagona, G., G. E. Zervaki, et al. (2012). "Carbon Nanohorn–Porphyrin Dimer Hybrid Material for Enhancing Light-Energy Conversion." The Journal of Physical Chemistry C 116(17): 9439-9449.
199. Pardo, R., M. Zayat, et al. (2011). "Photochromic organic–inorganic hybrid materials." Chemical Society Reviews 40(2): 672-687.
200. Peimyoo, N., J. Li, et al. (2012). "Photocontrolled Molecular Structural Transition and Doping in Graphene." ACS nano 6(10): 8878-8886.
201. Peng, J., W. Gao, et al. (2012). "Graphene Quantum Dots Derived from Carbon Fibers." Nano letters 12(2): 844-849.

202. Perreault, F., A. F. De Faria, et al. (2015). "Environmental applications of graphene-based nanomaterials." Chemical Society Reviews 44(16): 5861-5896.
203. Perry, A., S. J. Green, et al. (2015). "A pyrene-appended spiropyran for selective photo-switchable binding of Zn (II): UV–visible and fluorescence spectroscopy studies of binding and non-covalent attachment to graphene, graphene oxide and carbon nanotubes." Tetrahedron 71(38): 6776-6783.
204. Petriashvili, G., M. P. De Santo, et al. (2016). "Rewritable Optical Storage with a Spiropyran Doped Liquid Crystal Polymer Film." Macromolecular Rapid Communications 37(6): 500-505.
205. Ponnamma, D., K. K. Sadasivuni, et al. (2013). "Interrelated shape memory and Payne effect in polyurethane/graphene oxide nanocomposites." RSC Advances 3(36): 16068-16079.
206. Poon, C.-T., W. H. Lam, et al. (2011). "Gated photochromism in triarylborane-containing dithienylethenes: a new approach to a “lock–unlock” system." Journal of the American Chemical Society 133(49): 19622-19625.
207. Pu, S., G. Liu, et al. (2007). "Efficient synthesis and properties of isomeric photochromic diarylethenes having a pyrrole unit." Organic Letters 9(11): 2139-2142.
208. Pu, S., R. Wang, et al. (2012). "Photochromism of new unsymmetrical diarylethene derivatives bearing both benzofuran and thiophene moieties." Dyes and Pigments 94(2): 195-206.
209. Pu, S., T. Yang, et al. (2006). "Syntheses and properties of new photochromic diarylethene derivatives having a pyrazole unit." Tetrahedron Letters 47(36): 6473-6477.
210. Radoi, A., M. Dragoman, et al. (2011). "Memristor device based on carbon nanotubes decorated with gold nanoislands." Applied Physics Letters 99(9): 093102.
211. Rau, H. (1990). Photoisomerization of azobenzenes, CRC Press: Boca Raton, FL.
212. Ritchie, C., G. Vamvounis, et al. (2017). "Photochrome-doped organic films for photonic keypad locks and multi-state fluorescence." Physical Chemistry Chemical Physics 19(30): 19984-19991.
213. Rosca, I. D., F. Watari, et al. (2005). "Oxidation of multiwalled carbon nanotubes by nitric acid." Carbon 43(15): 3124-3131.
214. Rowell, M. W., M. A. Topinka, et al. (2006). "Organic solar cells with carbon nanotube network electrodes." Applied Physics Letters 88(23): 233506.
215. Roy, P., A. P. Periasamy, et al. (2014). "Plant leaf-derived graphene quantum dots and applications for white LEDs." New Journal of Chemistry 38(10): 4946-4951.

216. Roy, P., A. P. Periasamy, et al. (2015). "Photoluminescent graphene quantum dots for in vivo imaging of apoptotic cells." Nanoscale 7(6): 2504-2510.
217. Rubio, N., M. A. Herrero, et al. (2009). "Efficient functionalization of carbon nanohorns via microwave irradiation." Journal of Materials Chemistry 19(25): 4407-4413.
218. Sadowska, K., K. P. Roberts, et al. (2009). "Synthesis, characterization, and electrochemical testing of carbon nanotubes derivatized with azobenzene and anthraquinone." Carbon 47(6): 1501-1510.
219. Saminathan, M. and C. Pillai (2000). "Synthesis of novel liquid crystalline polymers with cross-linked network structures." Polymer 41(8): 3103-3108.
220. Sandanayaka, A. S., G. Pagona, et al. (2007). "Photoinduced electron-transfer processes of carbon nanohorns with covalently linked pyrene chromophores: Charge-separation and electron-migration systems." Journal of Materials Chemistry 17(24): 2540-2546.
221. Sano, N. (2004). "Low-cost synthesis of single-walled carbon nanohorns using the arc in water method with gas injection." Journal of Physics D: Applied Physics 37(8): L17.
222. Sano, N., J. Nakano, et al. (2004). "Synthesis of single-walled carbon nanotubes with nanohorns by arc in liquid nitrogen." Carbon 3(42): 686-688.
223. Sasaki, T. and J. M. Tour (2008). "Synthesis of a new photoactive nanovehicle: a nanoworm." Organic Letters 10(5): 897-900.
224. Schindler, F., J. M. Lupton, et al. (2006). "How single conjugated polymer molecules respond to electric fields." Nat Mater 5(2): 141-146.
225. Schneider, V., O. Polonskyi, et al. (2017). "Light-induced Conductance Switching in Photomechanically Active Carbon Nanotube-Polymer Composites." Scientific Reports 7(1): 9648.
226. Schneider, V., T. Strunskus, et al. (2015). "Light-induced conductance switching in azobenzene based near-percolated single wall carbon nanotube/polymer composites." Carbon 90: 94-101.
227. Schnorr, J. M. and T. M. Swager (2010). "Emerging applications of carbon nanotubes." Chemistry of Materials 23(3): 646-657.
228. Schuster, D. I., K. Li, et al. (2007). "Azobenzene-Linked Porphyrin−Fullerene Dyads." Journal of the American Chemical Society 129(51): 15973-15982.
229. Schuster, D. I., B. Nuber, et al. (2003). "Synthesis, photochemistry and photophysics of stilbene-derivatized fullerenes." Photochemical & Photobiological Sciences 2(3): 315-321.
230. Sciascia, C., R. Castagna, et al. (2012). "Light-Controlled Resistance Modulation in a Photochromic Diarylethene–Carbon Nanotube Blend." The Journal of Physical Chemistry C 116(36): 19483-19489.

231. Setaro, A., P. Bluemmel, et al. (2012). "Non-Covalent Functionalization of Individual Nanotubes with Spiropyran-Based Molecular Switches." Advanced Functional Materials 22(11): 2425-2431.
232. Shen, Q., Y. Cao, et al. (2009). "Conformation-induced electrostatic gating of the conduction of spiropyran-coated organic thin-film transistors." The Journal of Physical Chemistry C 113(24): 10807-10812.
233. Shen, Y. (1989). "Optical second harmonic generation at interfaces." Annual Review of Physical Chemistry 40(1): 327-350.
234. Shim, S., I. Eom, et al. (2007). "Ring closure reaction dynamics of diarylethene derivatives in solution." The Journal of Physical Chemistry A 111(37): 8910-8917.
235. Shirota, Y., H. Nakano, et al. (2004). Synthesis, Properties, and Applications of Photochromic Amorphous Molecular Materials and Electrochromic Polymers. Chromogenic Phenomena in Polymers, American Chemical Society. 888: 173-186.
236. Simmons, J. M., I. In, et al. (2007). "Optically Modulated Conduction in Chromophore-Functionalized Single-Wall Carbon Nanotubes." Physical Review Letters 98(8): 086802.
237. Simpson, G. J. and K. L. Rowlen (2000). "Measurement of orientation in organic thin films." Accounts of chemical research 33(11): 781-789.
238. Sliwa, M., S. Létard, et al. (2005). "Design, synthesis, structural and nonlinear optical properties of photochromic crystals: Toward reversible molecular switches." Chemistry of Materials 17(18): 4727-4735.
239. Soh, N., K. Yoshida, et al. (2007). "A fluorescent photochromic compound for labeling biomolecules." Chemical Communications(48): 5206-5208.
240. Song, P.-S. and W. M. Horspool (2004). CRC Handbook of Organic Photochemistry and Photobiology, CRC press.
241. Song, X., J. Zhou, et al. (1995). "Correlations between solvatochromism, Lewis acid-base equilibrium and photochromism of an indoline spiropyran." Journal of Photochemistry and Photobiology A: Chemistry 92(1-2): 99-103.
242. Sreejith, S. and A. Ajayaghosh (2012). "Molecular logic gates: Recent advances and perspectives." Retrieved from http://nopr.niscair.res.in/handle/123456789/13362.
243. Stranius, K. and K. Börjesson (2017). "Determining the Photoisomerization Quantum Yield of Photoswitchable Molecules in Solution and in the Solid State." Scientific reports 7: 41145.
244. Sun, H., L. Wu, et al. (2013). "Recent advances in graphene quantum dots for sensing." Materials Today 16(11): 433-442.
245. Suresh, M., A. Ghosh, et al. (2008). "A simple chemosensor for Hg^{2+} and Cu^{2+} that works as a molecular keypad lock." Chemical Communications(33): 3906-3908.

246. Suryawanshi, A., M. Biswal, et al. (2014). "Large scale synthesis of graphene quantum dots (GQDs) from waste biomass and their use as an efficient and selective photoluminescence on–off–on probe for Ag^{+} ions." Nanoscale 6(20): 11664-11670.
247. Swansburg, S., E. Buncel, et al. (2000). "Thermal racemization of substituted indolinobenzospiropyrans: Evidence of competing polar and nonpolar mechanisms." Journal of the American Chemical Society 122(28): 6594-6600.
248. Takikawa, H., M. Ikeda, et al. (2002). "Fabrication of single-walled carbon nanotubes and nanohorns by means of a torch arc in open air." Physica B: Condensed Matter 323(1-4): 277-279.
249. Tanaka, H., H. Kanoh, et al. (2004). "Quantum effects on hydrogen adsorption in internal nanospaces of single-wall carbon nanohorns." The Journal of Physical Chemistry B 108(45): 17457-17465.
250. Tanaka, H., H. Kanoh, et al. (2005). "Quantum effects on hydrogen isotope adsorption on single-wall carbon nanohorns." Journal of the American Chemical Society 127(20): 7511-7516.
251. Tang, S., E. W. Rothe, et al. (1974). "Negative ion formation from energetic collisions of cesium with CO_2, CS_2, and COS." The Journal of Chemical Physics 61(7): 2592-2595.
252. Tetsuka, H., A. Nagoya, et al. (2016). "Molecularly Designed, Nitrogen-Functionalized Graphene Quantum Dots for Optoelectronic Devices." Advanced Materials 28(23): 4632-4638.
253. Tian, H. and S. Yang (2004). "Recent progresses on diarylethene based photochromic switches." Chemical Society Reviews 33(2): 85-97.
254. Tian, X., B. Wang, et al. (2016). "Surface Grafting of Paper with Photochromic Spiropyran Ether Methacrylate." BioResources 11(4): 8627-8637.
255. Tian, X., B. Wang, et al. (2017). "Photochromic paper from wood pulp modification via layer-by-layer assembly of pulp fiber/chitosan/spiropyran." Carbohydrate Polymers 157: 704-710.
256. Tournus, F., S. Latil, et al. (2005). "π-stacking interaction between carbon nanotubes and organic molecules." Physical Review B 72(7): 075431.
257. Traven, V. F., A. Y. Bochkov, et al. (2010). "Novel photochromic 3-(3-coumarinyl)-4-(3-thienyl) maleic acid cyclic derivatives." Mendeleev Communications 1(20): 22-24.
258. Tsivgoulis, G. (1995). "New Photochromic Materials." Human Capital and Mobility (European).
259. Tyer, N. W. and R. S. Becker (1970). "Photochromic spiropyrans. I. Absorption spectra and evaluation of the pi.-electron orthogonality of the constituent halves." Journal of the American Chemical Society 92(5): 1289-1294.

260. Uchida, K., E. Tsuchida, et al. (1999). "Substitution effect on the coloration quantum yield of a photochromic bisbenzothienylethene." Chemistry letters 28(1): 63-64.
261. Umeyama, T., K. Kawabata, et al. (2010). "Dispersion of carbon nanotubes by photo-and thermal-responsive polymers containing azobenzene unit in the backbone." Chemical Communications 46(32): 5969-5971.
262. Unni, S. M., S. N. Bhange, et al. (2015). "Nitrogen-Induced Surface Area and Conductivity Modulation of Carbon Nanohorn and Its Function as an Efficient Metal-Free Oxygen Reduction Electrocatalyst for Anion-Exchange Membrane Fuel Cells." Small 11(3): 352-360.
263. Urita, K., S. Seki, et al. (2006). "Effects of gas adsorption on the electrical conductivity of single-wall carbon nanohorns." Nano letters 6(7): 1325-1328.
264. Utsumi, S., H. Honda, et al. (2007). "Direct evidence on C− C single bonding in single-wall carbon nanohorn aggregates." The Journal of Physical Chemistry C 111(15): 5572-5575.
265. Valeur, B. and I. Leray (2000). "Design principles of fluorescent molecular sensors for cation recognition." Coordination Chemistry Reviews 205(1): 3-40.
266. Van Amersfoort, E. S. and J. A. G. Van Strijp (1994). "Evaluation of a flow cytometric fluorescence quenching assay of phagocytosis of sensitized sheep erythrocytes by polymorphonuclear leukocytes." Cytometry 17(4): 294-301.
267. van der Molen, S. J., J. Liao, et al. (2009). "Light-controlled conductance switching of ordered metal-molecule-metal devices." Nano Lett 9(1): 76-80.
268. van der Molen, S. J., J. Liao, et al. (2009). "Light-Controlled Conductance Switching of Ordered Metal−Molecule−Metal Devices." Nano letters 9(1): 76-80.
269. Viero, Y., G. Copie, et al. (2015). "High Conductance Ratio in Molecular Optical Switching of Functionalized Nanoparticle Self-Assembled Nanodevices." The Journal of Physical Chemistry C 119(36): 21173-21183.
270. Vijayakumar, C., B. Balan, et al. (2011). "Noncovalent functionalization of SWNTs with azobenzene-containing polymers: solubility, stability, and enhancement of photoresponsive properties." The Journal of Physical Chemistry C 115(11): 4533-4539.
271. Vilanove, R., H. Hervet, et al. (1983). "Photochromism of monolayers of poly (methylmethacrylate) having spirobenzopyran side groups." Macromolecules 16(5): 825-831.
272. Wagner, K., R. Byrne, et al. (2011). "A multiswitchable poly (terthiophene) bearing a spiropyran functionality: understanding photo-and electrochemical control." Journal of the American Chemical Society 133(14): 5453-5462.

273. Wan, S., Y. Zheng, et al. (2014). "“On–off–on” Switchable Sensor: A Fluorescent Spiropyran Responds to Extreme pH Conditions and Its Bioimaging Applications." ACS Applied Materials & Interfaces 6(22): 19515-19519.
274. Wang, D. and X. Wang (2011). "Self-assembled graphene/azo polyelectrolyte multilayer film and its application in electrochemical energy storage device." Langmuir 27(5): 2007-2013.
275. Wang, D., G. Ye, et al. (2011). "Graphene functionalized with azo polymer brushes: surface-initiated polymerization and photoresponsive properties." Advanced Materials 23(9): 1122-1125.
276. Wang, J. and C.-S. Ha (2010). "Azobenzene-based system for fluorimetric sensing of H_2PO_4- (Pi) that works as a molecular keypad lock." Analyst 135(6): 1214-1218.
277. Wang, L. and Q. Li (2018). "Photochromism into nanosystems: towards lighting up the future nanoworld." Chemical Society Reviews 47(3): 1044-1097.
278. Wang, L., W. Li, et al. (2016). "Facile synthesis of fluorescent graphene quantum dots from coffee grounds for bioimaging and sensing." Chemical Engineering Journal 300: 75-82.
279. Wang, Q., S.-F. Lee, et al. (2014). "Azobenzene dendronized carbon nanoparticles: the effect of light antenna." RSC Advances 4(35): 18193-18197.
280. Wang, Z., Z.-x. Li, et al. (2009). "Photostimulated reversible attachment of gold nanoparticles on multiwalled carbon nanotubes." The Journal of Physical Chemistry C 113(10): 3899-3902.
281. Wang, Z., H. Zeng, et al. (2015). "Graphene quantum dots: versatile photoluminescence for energy, biomedical, and environmental applications." Journal of Materials Chemistry C 3(6): 1157-1165.
282. WCED, S. W. S. (1987). World Commission on Environment and Development, Oxford University Press London.
283. Wei, M., Y. Gao, et al. (2017). "Stimuli-responsive polymers and their applications." Polymer Chemistry 8(1): 127-143.
284. Wei, Y. and C.-T. Chen (2007). "Doubly Ortho-Linked cis-4,4‘-Bis(diarylamino)stilbene/Fluorene Hybrids as Efficient Nondoped, Sky-Blue Fluorescent Materials for Optoelectronic Applications." Journal of the American Chemical Society 129(24): 7478-7479.
285. Wildgoose, G. G., C. E. Banks, et al. (2006). "Metal Nanoparticles and Related Materials Supported on Carbon Nanotubes: Methods and Applications." Small 2(2): 182-193.
286. Wu, J.-B., M.-L. Lin, et al. (2018). "Raman spectroscopy of graphene-based materials and its applications in related devices." Chemical Society Reviews 47(5): 1822-1873.

287. Wu, Y., S. Chen, et al. (2012). "A novel gated photochromic reactivity controlled by complexation/dissociation with BF_3." Chemical Communications 48(4): 528-530.
288. Xiang, D., X. Wang, et al. (2016). "Molecular-Scale Electronics: From Concept to Function." Chemical Reviews 116(7): 4318-4440.
289. Xu, B., B. Zhang, et al. (2018). "Tubular Micro/Nanomachines: From the Basics to Recent Advances." Advanced Functional Materials 28(25): 1705872.
290. Xu, L., F. Mou, et al. (2017). "Light-driven micro/nanomotors: from fundamentals to applications." Chemical Society Reviews 46(22): 6905-6926.
291. Yagai, S. and A. Kitamura (2008). "Recent advances in photoresponsive supramolecular self-assemblies." Chemical Society Reviews 37(8): 1520-1529.
292. Yagi, K. and M. Irie (2003). "Photochromic and fluorescent properties of a diarylethene dimer." Chemistry letters 32(9): 848-849.
293. Yamaguchi, T., S. Bandow, et al. (2004). "Synthesis of carbon nanohorn particles by simple pulsed arc discharge ignited between pre-heated carbon rods." Chemical Physics Letters 389(1-3): 181-185.
294. Yamaguchi, T. and M. Irie (2006). "Photochromism of diarylethene derivatives having n-alkylbenzothiophene and n-alkylbenzofuran units." Bulletin of the Chemical Society of Japan 79(7): 1100-1105.
295. Yan, H., L. Zhu, et al. (2012). "A photoswitchable [2] rotaxane array on graphene oxide." Asian Journal of Organic Chemistry 1(4): 314-318.
296. Yang, C.-M., D. Kasuya, et al. (2004). "Microporosity development of single-wall carbon nanohorn with chemically induced coalescence of the assembly structure." The Journal of Physical Chemistry B 108(46): 17775-17782.
297. Yang, C. M., H. Noguchi, et al. (2005). "Highly ultramicroporous single-walled carbon nanohorn assemblies." Advanced Materials 17(7): 866-870.
298. Yang, Y., X. Wang, et al. (2007). "Structure and photoresponsive behaviors of multiwalled carbon nanotubes grafted by polyurethanes containing azobenzene side chains." The Journal of Physical Chemistry C 111(30): 11231-11239.
299. Yao, X., T. Li, et al. (2016). "Recent Progress in Photoswitchable Supramolecular Self-Assembling Systems." Advanced Optical Materials 4(9): 1322-1349.
300. Yerushalmi, R., A. Scherz, et al. (2005). "Stimuli responsive materials: new avenues toward smart organic devices." Journal of Materials Chemistry 15(42): 4480-4487.

301. Yin, J., G. Ye, et al. (2010). "Self-Structured Surface Patterns on Molecular Azo Glass Films Induced by Laser Light Irradiation." Langmuir 26(9): 6755-6761.
302. Yoshida, S. and M. Sano (2006). "Microwave-assisted chemical modification of carbon nanohorns: Oxidation and Pt deposition." Chemical Physics Letters 433(1-3): 97-100.
303. Yu, Y. and T. Ikeda (2004). "Alignment modulation of azobenzene-containing liquid crystal systems by photochemical reactions." Journal of Photochemistry and Photobiology C: Photochemistry Reviews 5(3): 247-265.
304. Yudasaka, M., T. Ichihashi, et al. (2003). "Structure changes of single-wall carbon nanotubes and single-wall carbon nanohorns caused by heat treatment." carbon 41(6): 1273-1280.
305. Yudasaka, M., S. Iijima, et al. (2007). Single-wall carbon nanohorns and nanocones. Carbon nanotubes, Springer: 605-629.
306. Zhang, J., G. Wang, et al. (2003). "Interactions of Small Molecules and Au Nanoparticles with Solubilized Single-Wall Carbon Nanotubes." The Journal of Physical Chemistry B 107(16): 3726-3732.
307. Zhang, T., S. Mubeen, et al. (2008). "Recent progress in carbon nanotube-based gas sensors." Nanotechnology 19(33): 332001.
308. Zhang, X., P. Bauerle, et al. (2012). Organic electronics for a better tomorrow: Innovation, accessibility, sustainability. A White Pap. From Chem. Sci. Soc. Summit San Fr. California, United States.
309. Zhang, X., Y. Feng, et al. (2010). "Investigation of optical modulated conductance effects based on a graphene oxide–azobenzene hybrid." Carbon 48(11): 3236-3241.
310. Zhang, X., Y. Feng, et al. (2010). "Enhanced reversible photoswitching of azobenzene-functionalized graphene oxide hybrids." Langmuir 26(23): 18508-18511.
311. Zhang, X., L. Hou, et al. (2016). "Coupling carbon nanomaterials with photochromic molecules for the generation of optically responsive materials." Nature communications 7: 11118.
312. Zhao, X., Y. Feng, et al. (2017). "Controlling Heat Release from a Close-Packed Bisazobenzene–Reduced-Graphene-Oxide Assembly Film for High-Energy Solid-State Photothermal Fuels." ChemSusChem 10(7): 1395-1404.
313. Zhao, Y., C. Huang, et al. (2013). "Functionalization of single-wall carbon nanotubes with chromophores of opposite internal dipole orientation." ACS applied materials & interfaces 5(19): 9355-9361.
314. Zhou, X., T. Zifer, et al. (2009). "Color Detection Using Chromophore-Nanotube Hybrid Devices." Nano Letters 9(3): 1028-1033.

315. Zhu, L., H. Yan, et al. (2012). "Light-controllable cucurbit [7] uril-based molecular shuttle." The Journal of Organic Chemistry 77(22): 10168-10175.
316. Zhu, M.-Q., L. Zhu, et al. (2006). "Spiropyran-Based Photochromic Polymer Nanoparticles with Optically Switchable Luminescence." Journal of the American Chemical Society 128(13): 4303-4309.
317. Zhu, S. and G. Xu (2010). "Single-walled carbon nanohorns and their applications." Nanoscale 2(12): 2538-2549.

LIST OF PUBLICATIONS

1. **Devi Renuka K**, C. Lalitha Lekshmi, Kuruvilla Joseph, Sankarapillai Mahesh, "Photoresponse modulation of reduced graphene oxide by surface modification with cardanol derived azobenzene", ***New Journal of Chemistry.*****2018**, *42* , 18182-18188.

2. **Devi Renuka K**, C. Lalitha Lekshmi, Kuruvilla Joseph, Sankarapillai Mahesh, "Sustainable Bioresource-Derived Components for Molecular Keypad Lock and IMPLICATION Logic Gate Construction", ***Chemistry Select.*** **2017**, *2* , 11615-11619.

3. **Devi Renuka K**, C. Lalitha Lekshmi, Kuruvilla Joseph, Sankarapillai Mahesh, "Sustainable Electronic Materials: Reversible Phototuning of Conductance in a non-Covalent assembly of MWCNT and Bioresource Derived Photochromic molecule", ***ACS applied materials & interfaces.*** **2017**, *9* , 1167-1172.

4. C. Lalitha Lekshmi, **Devi Renuka K**, Kuruvilla Joseph, Sankarapillai Mahesh, Mahesh "New paradigms for the synthesis of graphene quantum dots from sustainable bioresources", ***New Journal of Chemistry***.2017,41,8706-8710.

5. C. Lalitha Lekshmi, **Devi Renuka K**, Kuruvilla Joseph, Sankarapillai Mahesh, "Simple and Cost-Effective Synthesis of Fluorescent Graphene Quantum Dots from Honey: Application as Stable Security Ink and White-Light Emission. ***Particle & Particle Systems Characterization.*** **2016,** *33* (2), 70-74.

LIST OF CONFERENCES ATTENDED/CONDUCTED/PAPERS PRESENTED

1. **Oral presentation** in Interanational Conference on Chemistry and Physics of Materials-2018 (ICCPM-18) organised by Dept of Chemistry, St Thomas' College, Thrissur during 19th-21st December 2018.

2. **Oral presentation** in 2nd Interanational Conference on Recent Trends in Materials Science and Technology – 2018 (ICMST-18) organised by Dept of Chemistry, Indian Institute of Space Science and Technology, Thiruvananthapuram during 10th-13th October 2018.

3. **Poster presentation** in 8th East Asian Symposium on Functional Dyes and Advanced Materials organized by CSIR-NIIST Thiruvananthapuram during September 20-22,2017.

4. **Poser presentation** in International Conference of Young Researchers on Advanced Materials (IUMRS-ICYRAM 2016) Organised by Indian Institute of Science (IISc) Bangalore during December 11-16, 2016, Bangalore.
5. **Poster presentation** in 1st Symposium on Advanced Functional Materials (FUNMAT-2016) Organized by CSIR-Central Electrochemical Research Institute (CECRI), Karaikudi during May 26-28, 2016, Karaikudi, Tamil Nadu.
6. **Poster presentation** in 17 th CRSI National Symposium On Chemistry Organised by CSIR-NCL Pune and IISER Pune during February 6-8,2015,Pune.
7. Participated in Seminar on Photoresponsive Soft materials on February 3rd 2015 Organized by CRSI-Local Chapter Thiruvananthapuram and CSIR-NIIST Thiruvananthapuram.

8. **Poster presentation** in 8th Asian Photochemistry Conference (APC) Organised by IISER Thiruvananthapuram and CSIR-NIIST Thiruvananthapuram during November 9-13,2014,Kovalam,Thiruvananthapuram.

9. **Poster presentation** in National Conference on Recent Trends in Materials Science and Technology – 2016 (NCMST-16) organised by Dept of Chemistry, Indian Institute of Space Science and Technology, Thiruvananthapuram during 12th-14thJuly 2016.

10. Participated/conducted in National Conference on Recent Trends in Materials Science and Technology – 2015 (NCMST-15) organised by Dept of Chemistry, Indian Institute of Space Science and Technology, Thiruvananthapuram during 6th-8thJuly 2015.

11. Participated/conducted in National Conference on Recent Trends in Materials Science and Technology – 2014 (NCMST-14) organised by Dept of Chemistry, Indian Institute of Space Science and Technology, Thiruvananthapuram during 28th-30thJuly 2014.

12. Participated/conducted in IIST Research Scholars' Day organized by Dept of Chemistry, Indian Institute of Space Science and Technology, Thiruvananthapuram during December, 16-17, 2013.